The Skerin ridge on Eyjafjallajökull, south Iceland: Morphology and magma-ice interaction in an ice-confined silicic fissure eruption

Birgir Vilhelm Óskarsson

Faculty of Earth Sciences
University of Iceland
2009

The Skerin ridge on Eyjafjallajökull, south Iceland: Morphology and magma-ice interaction in an ice-confined silicic fissure eruption

Birgir Vilhelm Óskarsson

90 ECTS thesis submitted in partial fulfillment of a
Magister Scientiarum degree in Geology

Supervisors:
Magnús Tumi Guðmundsson
Þorvaldur Þórðarson

Examiner:
Ármann Höskuldsson

Faculty of Earth Sciences
School of Engineering and Natural Sciences
University of Iceland
Reykjavík, September 2009

The Skerin ridge on Eyjafjallajökull, south Iceland: Morphology and magma-ice interaction in an ice-confined silicic fissure eruption

The Skerin ridge: an ice-confined silicic fissure eruption

90 ECTS thesis submitted in partial fulfillment of a *Magister Scientiarum* degree in Geology

Faculty of Earth Sciences
School of Engineering and Natural Sciences
University of Iceland
Sturlugata 7,
101 Reykjavík

Sími: 525 4600

This thesis can be referred as:
Óskarsson, B.V., 2009, The Skerin ridge on Eyjafjallajökull, south Iceland: Morphology and magma-ice interaction in an ice-confined silicic fissure eruption, Master´s thesis, Faculty of Earth Sciences, University of Iceland, pp. 111.

ISBN 978-9979-9914-3-4

Printed by Háskólaprent
Reykjavík, September 2009

Hér með lýsi ég því yfir að ritgerð þessi er samin af mér og að hún hefur hvorki að hluta né í heild verið lögð fram áður til hærri prófgráðu.

_____

Birgir Vilhelm Óskarsson

Abstract

Skerin ridge is a 4.5 km long and on average 100 m wide ridge, situated on a radial fissure trending NW from the summit caldera of the ice-capped central volcano Eyjafjallajökull, south Iceland. Results from previous studies on tephrochronological dating of deposits produced by jokulhlaups originating in the Skerin area indicate that the ridge was formed by an intraglacial (or within glacier) eruption in the 10th century. Recent glacial recession has exposed the Skerin ridge and thus enabled a detailed examination of the ridge structure and architecture, in particular features that indicate confinement and rapid cooling by meltwaters as expected for lava-ice interaction. In this study, the ridge and associated formations were mapped in detail, the petrographic and chemical characteristics documented and the thickness of ice surrounding the ridge measured with a mobile radio-echo sounder.

Skerin ridge is primarily constructed by trachytic lavas (volume $\approx$0.043 km^3) but also includes lesser mafic (basaltic icelandite/hawaiite) and intermediate (trachyandesite) tephra deposits (volume $\approx$0.012 km^3). Lithostratigraphy correlations indicate that the initial stage of the Skerin eruption was marked by a basaltic eruption creating a scoria cone on the NW end of the ice-free fissure with a phreatomagmatic eruption of same composition creating a tuff deposit on the SE ice-covered section of the fissure. At synchronous time an explosive eruption took place forming pumice deposits followed by an effusive eruption of trachyte lavas from a row of vents along the volcanic fissure. The lavas confined by wet cavities and canyons in the thin ice ($\approx$100 m) formed a marginal carapace of glassy columnar joints representing the area cooled by the meltwaters and a brecciated flow top being the subaerial expression of the flow as the lavas broke through the glacier. A massive microcrystalline flow interior with flow structures and fabrics formed within the crust typical for lavas cooled within an insulated environment. The eruption ended with a strombolian phase forming scoria deposits of intermediate composition on top of the trachyte lavas. Evidence is for at least one previous eruption episode to Skerin ridge of unknown age forming a glacio-confined lava flow field of basaltic composition north of the ridge. Petrographic examination shows that the erupted magma features numerous examples of disequilibrium textures confirming that magma mixing/mingling took place shortly before onset of eruption in which the silicic eruption appears to have been triggered by a mafic intrusion. The eruption products plot on the transitional line of the alkali versus silica diagram which is a characteristic trend for the south Iceland flank zone.

The products and related eruption styles at Skerin ridge provide important data for paleo-ice thicknesses as well as constraints on ice melting rates. Volume constrains on ice melting and the application of a simple modeling of meltwater generation gave meltwater volumes of 500-2500 m^3/s for the initial phreatomagmatic phase (<2 hrs) and 10-100 m^3/s for the effusive phase (5 to 50 days). Thus an eruption of this type although not large demands precaution by civil protection authorities since flooding may cause hazard for e.g. popular tourist routes and farmland by Markarfljót.

Ágrip

Skerin (Skerjahryggur) eru 4.5 km langur og 100-200 m breiður hryggur, sem stefnir í NNV út frá gíg Eyjafjallajökuls. Fyrri rannsóknir á gjóskulögum og jökulset frá jökulhlaupum í nágrenni Skerjahryggs benda til þess að hryggurinn sé myndaður í gosi í jökli á 10. öld. Vegna hops jökulsins undanfarna áratugi er hryggurinn nú að verulegu leyti íslaus og því hægt að kortleggja hraunin sem runnu, m.a. kólnunarfleti og önnur hugsanleg merki um hraðkælingu fyrir áhrif vatns og jökuls. Í þessari rannsókn var hryggurinn og tengdar myndanir kortlagðar og stuðlun og annar innri strúktúr hraunanna kannaður ásamt berg- og jarðefnafræðilegum einkennum. Íssjá var notuð til að kortleggja ísþykktina í nágrenni hryggjarins og til að áætla rúmmál hans.

Skerin eru aðallega mynduð úr trakít hraunum (rúmmál $\approx$0.043 km^3). Þar finnst einnig trakít vikur og gjall úr trakíandesíti og basalti ásamt basísku túffi. Rúmmál lausu gosefnanna er áætlað ($\approx$0.012 km^3). Innbyrðis lagskipting bendir til þess að gosið hafi byrjað með myndun gjallgígs í basísku strombólsku gosi á norðvesturenda hryggjarins sem á þeim tíma var að mestu íslaus. Uppi í jöklinum, á suðausturenda Skerjanna varð sprengigos sem myndaði túfflag. Á sama tíma varð þeytigos sem myndaði vikurlag af trakíti og hraun sömu gerðar tók að renna frá gosopum eftir endilangri sprungunni. Hraunin bræddu sig leið gegnum u.þ.b. 100 m þykka ísþekjuna en jaðrar þeirra voru kældir af bræðsluvatni í holrýmum og opnum ísgljúfrum. Kælingin myndaði hraðkælda, glerjaða skorpu á hliðum hraunanna sem einnig einkennast af láréttri smástuðlun. Bendir þetta til náinnar snertingar við bræðsluvatn. Yfirborð hraunanna er yfirleitt kargi sem bendir til þess að hraunið hafi náð upp úr vatni í í jökulgljúfrinu. Innan kólnunarkápunnar á hliðunum sjást algengir flæðistrúktúrar auk þess sem kjarninn er vel kristallaður. Áhrif vatnskælingar virðast því einangruð við jaðra hraunsins. Ísgljúfrið skorðaði útbreiðslu hraunanna sem aðeins runnu mjög takmarkaða vegalengd eftir gljúfrinu en ekkert út fyrir það. Gosinu lauk með strombólskum fasa á suðausturhluta sprungunnar þar sem ísúrt gjall lagðist ofan á trakít hraunin. Vísbendingar eru um að áður hafi gosið á sömu sprungu (aldur óþekktur) en það gos myndaði hraun sem flætt hefur beint niður hlíðina norðan við Skerin. Það hraun sýnir einnig ummerki um að hafa verið bundin við ísgljúfur í jöklinum. Bergfræðilegar athuganir benda til þess að kvikublöndun hafi átti sér stað stuttu fyrir gosið og að basískt innskot hafi orðið til þess að súra kvikan leitaði til yfirborðs. Gosefnin (frá basalti til trakíts) raðast á línu millibergraðarinnar á hliðstæðan hátt og önnur gosefni frá Eyjafjallajökli og suðurhluta eystra gosbeltisins norðan Vestmannaeyja.

Hæð hryggjarins sem myndaðist í gosinu gefur vísbendingar um þykkt jökulsins

á þeim tíma sem gosið átti sér stað og einnig hversu mikið bræðsluvatn myndaðist í gosinu. Rúmmál hryggsins og íssins sem bráðnaði ásamt einföldu líkani sem gefur vísbendingar um bræðsluhraða íss í slíku gosi benda til vatnsrennslis 500-2500 m^3/s meðan sprengivirkni var á gossprungunni í byrjun gossins (áætlaður tími 2 klst.) og 10-100 m^3/s fyrir flæðigosfasann þegar trakít hraunin urðu til (áætlaður myndunartími 5 til 50 dagar). Þessar niðurstöður benda til þess að þó gos af þessu tagi sé ekki stórt, gæti það valdið umtalsverðum hlaupum sem skapað gætu hættu fyrir vegfarendur og land við Markarfljót.

Acknowledgments

I first want to express my gratitude to Magnús Tumi Guðmundsson for innumerable advices and encouragement. I also want to give special thanks to Þorvaldur Þórðarson for valuable instructions and fruitful discussion and for hosting me in my trip to Edinburgh.

My gratitude goes also to all that accompanied me in the field: Ronni Grapenthin, Snævar Guðmundsson, Eyjólfur Magnússon, Brynjar, Melanie and Baltó.

People that helped in one way or another: Sveinn Jakobsson, Níels Óskarsson, Björn Oddson, Ingibjörg Jónsdóttir, Guðrún Larsen, Nikolas Odling, Benedikt Ófeigsson and so many more, thanks a lot.

My dear wife and family for great inspiration and always present support, life is so much fun with you all on my side.

To Viðlagatrygging Íslands and the University of Iceland that provided funding for this project, my sincere gratitude.

Contents

List of Figures

List of Tables

Chapter 1

Introduction

Studies on intraglacial volcanism are very significant for paleoenvironment reconstruction and hazard assessment (e.g. Lescinsky and Fink, 2000; Smellie, 2002; Gudmundsson, 2005). Intraglacial volcanism (volcanoes that grow within a glacial setting) create products that reflect the multi-environment provided by the glacier (subglacial, subaquatic and subaerial) forming a wide range of lithofacies (Jones, 1969; Werner and Schmincke, 1999; Tuffen et al., 2001; Tuffen and Castro, 2008; McGarvie, 2009). These products bear useful clues about the paleoenvironment in which they erupted, the eruption intensity and size and volume of water released in the form of glacial floods (icelandic=jökulhlaup). Large volumes of meltwater drain in flooding events reflecting the high thermal exchange that occurs in intraglacial volcanism and can be a major hazard to neighboring areas (e.g. Smellie, 2002; Gudmundsson et al., 2008).

Intraglacial volcanic activity has been widely observed, nevertheless due to the extreme environment in which these events take place the knowledge of the operating processes is poorly constrained. On the other hand, studies on the products of pre-historical eruptions give significant additional insight into the operating mechanisms and help us to better understand present events (e.g. Jones, 1969).

In Iceland volcanoes and glaciers are abundant and interact on a regular basis. Basaltic intraglacial eruptions with their predominant tuya edifices and ridges are very common in the volcanic zones and thus the subject of several studies (e.g. Kjartansson, 1943; Jones, 1969, 1970; Werner and Schmincke, 1999; Gudmundsson et al., 2002; Gudmundsson, 2005; Jakobsson and Gudmundsson, submitted december 2007). Products of intermediate to silicic composition are less common, calculated to account for ≈20% of the volcanic rocks produced last 1100 years in Iceland and thus intraglacial edificies of this type are less studied although a

growing field (e.g. Tuffen et al., 2001; McGarvie et al., 2007; Tuffen and Castro, 2008; McGarvie, 2009).

In general intraglacial volcanic eruptions can be divided into three phases: the subglacial phase, the emergent explosive phase and the aerial effusive phase (Jones, 1970; Gudmundsson, 2005). Of these phases, the last of the effusive aerial phase appear to esteem less attention whereas their structural morphology may resemble ordinary subaerial lava flows. Lavas of intermediate to silicic composition have been studied at the flanks of ice covered stratovolcanos interpreted to have flowed into glacial canyons confined by the ice-walls. These hold an architecture supporting confinement and rapid cooling identified by their structural architecture, especially the lateral flow margins and the brecciated flow top (Lescinsky and Sisson, 1998; Lescinsky and Fink, 2000). The flow margins with subvertical walls of glassy polygonal columns growing inwards perpendicular to the margins into the flow interior reveal the ice-confined margin cooled rapidly by the meltwaters/ice and the brecciated flow top the subaerial expression of the flow in an open environment (Lescinsky and Sisson, 1998; Lescinsky and Fink, 2000). Other papers have described silicic rhyolitic lavas rising into open confinements in the glacier forming silicic tuyas or into cavities in effusive-dominated edifices which show meltwater/ice interaction characters in some cases mingled with subaerial facies (Tuffen and Castro, 2008; LaMoreaux, 2008; McGarvie, 2009). Thus for paleoenvironment reconstruction these parameters need to be addressed properly preventing "intra"glacial flows to be confounded with flows erupted in "inter"glacial periods.

The aim of this thesis is to describe the products and define the eruption environment of a relatively small fissure eruption of a complex multi-composition multi-environment volcano within a still-present ice cap at the central volcano Eyjafjallajökull in south Iceland. The eruption formed a 4.5 km long ridge named Skerin or Skerjahryggur (Figure 1.1). Glacial recession following present climate changes has exposed segments of the ridge with useful parameters for this research. In particular, the surface and internal structural morphology of lavas of trachyte composition reveal important constrains for paleoenvironment reconstruction and lava flow emplacement and in this case suggest confinement of glacial cavities and open ice canyons and enhanced cooling by meltwaters. Subsidiary tephra products at Skerin that are present as distinct lithofacies made up of tuff, scoria, spatter and pumice enable an assessment of the paleoenvironment in which the ridge was constructed and geochemical and petrographic analysis reveal an interesting magma mixing story immediately prior to the eruption.

In this thesis, systematic mapping of the lithofacies that make up the Skerin ridge along with observations describing the paleo-thickness and ice confinement during the eruption are presented, the volume of ice melted in the eruption is estimated and an order of magnitude estimate done of melting rates and discharge of glacial floods.

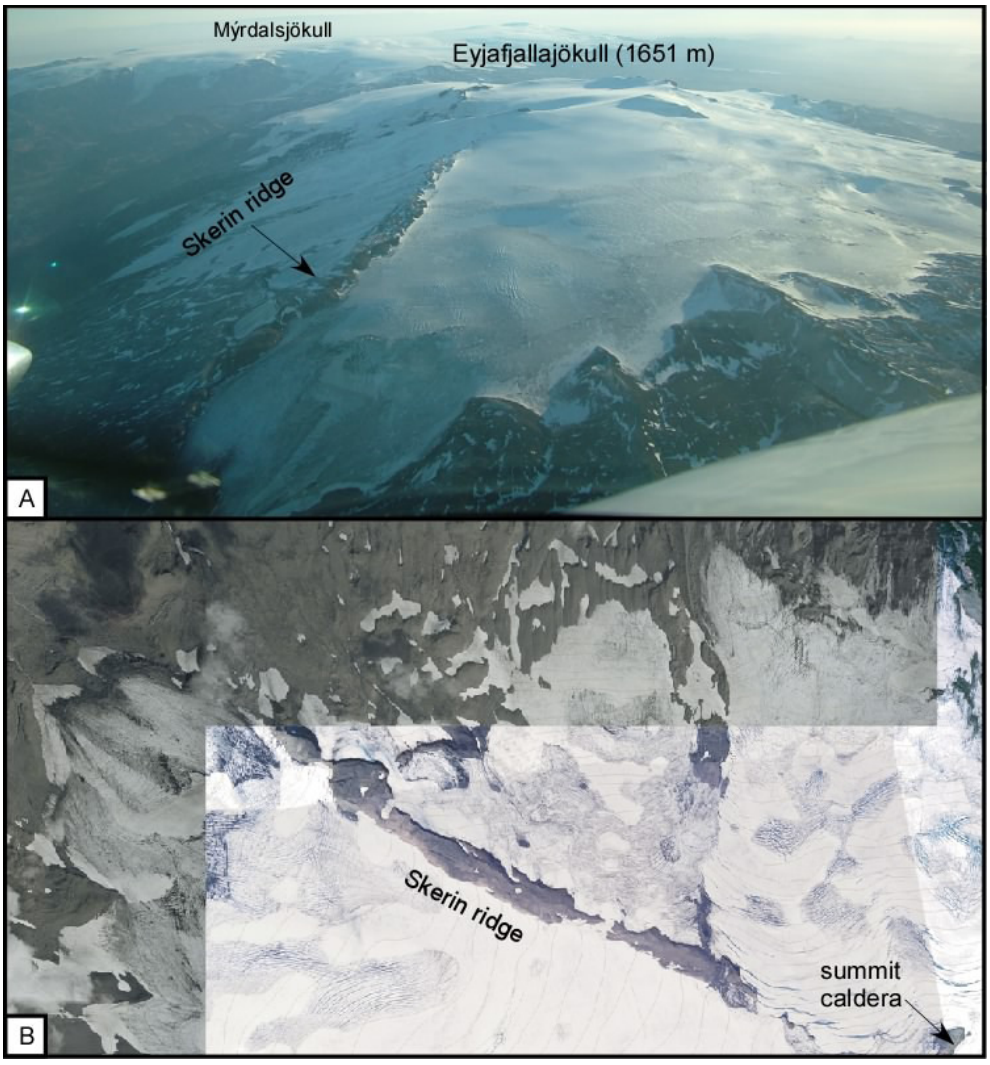

Figure 1.1: A) Aerial photograph showing the NW side of Eyjafjalljökull. Mýrdalsjökull glacier is in the background. Courtesy by Magnús T. Guðmundsson. B) Spot Images of Skerin ridge, from 16.7.2003 and 18.9.2003 provided by Landmælingar Íslands (Spot Image, 2003).

Chapter 2

Previous Studies

Studies on intraglacial volcanism is a rapidly expanding field with a growing number of papers being published every year. Studies of intraglacial volcanism involve past and present events as well as predictions of future eruption events (e.g Mathews, 1947; Jones, 1969, 1970; Werner and Schmincke, 1999; Gudmundsson et al., 1997; Tuffen et al., 2001; Edwards et al., 2002; Smellie, 2002; Gudmundsson et al., 2004; Tuffen and Castro, 2008). Observed eruptions have given scientists a glimpse into the effects, products and hazards related to this type of volcanism promoting more intense research in the field. Studies of the deposits of past intraglacial volcanism have grouped the eruptions on the basis of magma composition into mafic, intermediate and silicic eruptions. The differences in properties of each group leads to production of volcanic edifices with different morphology. These differences are related to magma rheology, but physical factors such as volume of erupted material, ice thickness, pre-eruption topography, behaviour of meltwater produced and stored at the eruption site also play a prominent role (e.g. McGarvie, 2009). This chapter briefly reviews previous studies on intraglacial volcanism that range from mafic to silicic but the main emphasis is on the products of silicic eruptions and emplacement mechanisms and lava-ice dynamics involving cooling structures and meltwater generation.

2.1 Past intraglacial eruption events

Basaltic intraglacial volcanic edifices were first described by Kjartansson (1943); Mathews (1947), as flat-topped, steep-sided volcanoes interpreted to originate within intraglacial lakes in Pleistocene ice-sheets. These edifices have been named "tuya" after the location in Tuya-Teslin, northern British Columbia but also table mountains and "stapi" (in Iceland). In this thesis I use the name tuya whereas

the term is more internationally recognized.

Mathews (1947) suggested that an active subglacial volcano goes through three phases as it grows in an eruption and becomes fully subaerial. This sequence of events begins with the aquatic effusive phase or the subglacial phase, moves to the emergent explosive phase where the volcano is situated in a stable lake of meltwater and ending with the subaerial effusive phase. The product of the effusive subglacial/subaquatic phase was interpreted to be pillow lava, the product of the emergent explosive phase fragmental material or hyaloclastites, the products of the subaerial phase compound lava flows forming the lava cap. Later studies suggested that at the subaerial phase lavas can flow from the top of the edifice into the glacial lake quenching and fragmenting and being deposited into the lake water by gravity flows forming layers of flow-foot breccia (Jones, 1969). All this material confined in the rims of the intraglacial lake would form roughly circular to elliptical edifices capped with flat laying flows of columnar basalt (Figure 2.3A) (Mathews, 1947). The contact between the lava and the fragmented magma/breccia is named the passage zone, which shows the paleo-water level and gives a rough indication about the paleo-ice thickness of the surrounding region at the time the edifice was formed (Jones, 1969; Gudmundsson et al., 2002).

Further studies conducted on several volcanic edifices in Iceland by (Jones, 1969, 1970; Sæmundsson, 1970; Werner and Schmincke, 1999; Gudmundsson, 2005), British Columbia (Allen et al., 1982; Edwards et al., 2002) and Antarctica (Skilling, 1994; Smellie and Skilling, 1994) combined similar observations as Mathews used in Tuya region, with additional insight into subglacial/subaquatic lava interaction processes during the formation of basaltic tuyas and their related volcanic products.

Tuyas are understood to be the fully developed volcanic edifices of an intraglacial mafic volcanic eruption. Nevertheless most volcanic eruptions do come to halt before the complete tuya is formed leaving partially formed edifices called mounds (Jakobsson and Gudmundsson, submitted december 2007).

This same concept of stepwise-growth eruption phases with a range of partially to fully formed edifices in intraglacial volcanism can be applied to volcanic edifices of more intermediate to silicic material (Lescinsky and Sisson, 1998; McGarvie, 2009; Stevenson et al., 2009). There is scarce data in the published literature on edifices built in stepwise intermediate-eruptions as described above. Papers dealing with intraglacial intermediate eruptions are mainly concerned with lava flows that have been interpreted to interact with thin ice or snow covers and valley glaciers during emplacement (Lescinsky and Sisson, 1998; Lescinsky and

Fink, 2000; Mee et al., 2006; Spörli and Rowland, 2006; Smellie, 2002). Characteristic structures for these lava flows are: highly hackly/columnar flow base and margins with a brecciated flow top (Lescinsky and Sisson, 1998); mixed zones of blocky subaerial lava with glassy clasts from snow-contact lava within autobreccia horizons and hackly, pseudopillowed bodies (Mee et al., 2006); and small secondary columns forming on the sides of larger primary cooling columns (Spörli and Rowland, 2006).

Lescinsky and Fink (2000) describe a four component structure for large (0.3-4 km^3) andesite and dacite lava flows erupted from stratovolcanoes in the Cascade Mountains and interpreted to have been emplaced within valley glaciers (Figure 2.3B). These are flow base, flow interior, flow sides and flow top. Flow bases are comprised of broad (30-40 cm in diameter) columns oriented perpendicular to the basal floor and commonly with flow bands lying parallel to the basal floor. Underlying breccia happens to be no thicker than 5 cm. 2-5 m above the basal contact is a sharp contact marking the transition to the flow interior. The flow interior is characterized by columns (50-80 cm in diameter) and a massive, well crystallized matrix. Within the interior flow structures as platy joints spaced 1-5 cm apart brake parallel to the flow base and become more irregularly oriented close to the flow margins. Flow sides have glassy columns (8-20 cm in diameter) extending perpendicular to the margins 2-4 m into the flow. On the flow front the glassy zone can be up to 12 m thick. The flow tops are composed of flow breccia and lava spines (Figure 2.3B).

Lescinsky and Fink (2000) suggest that the cooling pattern of the lava sides and front (glassy margin with columnar joints) is indicative of rapid quenching and cooling by water as the flow moved forward due to the confinement induced by the presence of ice/glacier walls (Figure 2.1 and 2.2). Carving of channels in the ice cap and valley glaciers is interpreted to have largely preceded the lavas, most likely by the action of running meltwaters during a likely initial explosive phase of the eruption (Figure 2.1). Cooling of the lateral margins added strength to the crust and insulated the interior enabling the lavas to be transported away from the erupted vents with minimal temperature loss similar to that in lava tubes. The lavas interacted with the meltwaters confined by the glacier and in instances were deflected to follow the pathway of the ice-channel (Lescinsky and Fink, 2000). The top of the flow which is exposed subaerially formed breccia and spines, products of fragmentation due to shear tearing and compression of the rigid crust during the advance of the flow. As the flow comes to a halt, the interior cools in an insulated and warmer environment forming vertical/subvertical joints that are larger than

the quenched columns on the margins. Platy jointing in the flow interior reflect tensional stresses at the end-stage of cooling and creeping of viscous-plastic lava (Spörli and Rowland, 2006). Thus lava flows with this architecture are good indicators of confinement and rapid cooling by water attributed in this case to ice caps at stratovolcanoes and valley glaciers.

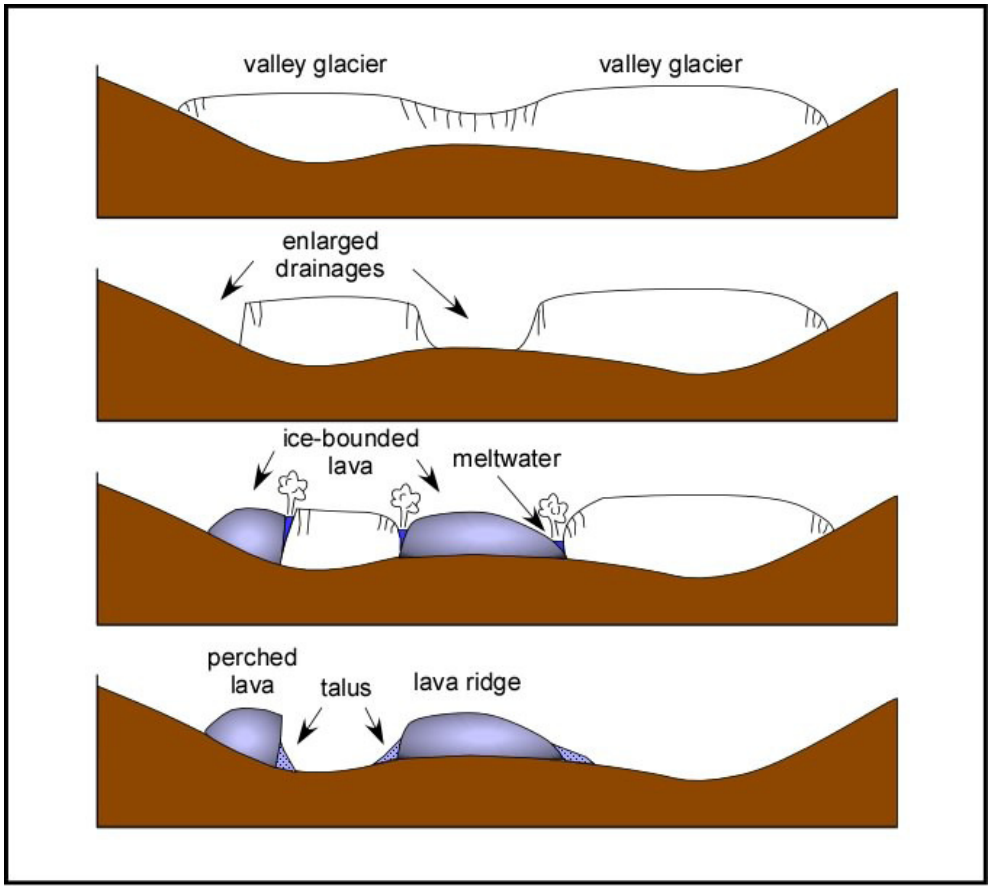

Figure 2.1: Cross sections showing sequential events of a proposed ice-marginal formation of ridge-forming and perched lava flows. Sketch adapted from Lescinsky and Sisson (1998).

Silicic intraglacial edifices are rare in comparison to mafic edifices. In Iceland nevertheless, silicic ice-volcano structures are abundant and it has bee suggested that at least 350 km^3 of rhyolite has erupted since the late Pleistocene under intraglacial conditions (McGarvie, 2009). Three main types of edifices have been described for silicic intraglacial eruptions - Effusion dominated edifices, tuyas and ice-capped central volcanoes (Tuffen et al., 2001, 2002a; Stevenson et al., 2006; McGarvie, 2009).

Effusion dominated edifices (Figure 2.3C) are characterized by products that show abundant evidence for quench fragmentation and water interaction while there is little evidence for magmatic fragmentation from explosive activity (i.e. volatile-driven) (McGarvie, 2009). Eruptions of this type are interpreted to be

sustained and substantial effusive episodes of lavas enclosed by the walls of a moderately thick glacier (observed examples are estimated to have occurred under a glacier <800 m thick). The products of this eruption environment are poorly sorted breccia and ash and graded matrix with extrusive conical-to-irregularly shaped lava lobes (5-10 m long with a crust of columnar joints). Only two examples located in Iceland have been studied in detail namely Bláhnúkur and Prestahnúkur with volumes <0.1 km^3 and 0.6 km^3 (DRE-dense rock equivalent) (Tuffen et al., 2001; McGarvie, 2009).

Rhyolitic tuyas (Figure 2.3C) are not unlike basaltic tuyas holding steep sided edifices with relatively flat tops. They differ being an order of magnitude smaller (Gudmundsson, 2005) and firm evidences of eruption within a lake of meltwater confined by the glacier is usually lacking (Tuffen et al., 2002b; Stevenson, 2005). Rhyolitic tuyas can form on fissures as well as from single vents (McGarvie, 1985) and observed examples reach heights of about 700 m with volumes up to 2 km^3 (McGarvie, 2009). The base of the edifice is composed of tephras produced in vigorous phreatomagmatic fragmentation within the subglacial phase of the eruption. As the eruption breaks through the glacier, less meltwater and ice interacts with the growing edifice and lavas extrude subaerially with non-explosive degassing forming a cap on top of the edifice (Tuffen et al., 2002b; Stevenson, 2005).

Central volcanoes are usually not associated with environmental conditions such as being formed in a glacial setting. Nevertheless many central volcanoes do hold ice caps which interact significantly with the volcanic products. Eyjafjallajökull has been classified as a stratovolcano (e.g. McGarvie, 2009) although recently the term shield-like volcano has been applied, considered being more descriptive for the large scale morphology of the Eyjafjöll complex (Thordarson and Larsen, 2007). Nevertheless we find silicic products in Eyjafjallajökull that have interacted with the ice cap and thus it is grouped with a central volcano in terms of ice-volcano interaction.

2.2 Present intraglacial eruption events

Presently active intraglacial volcanoes are in many areas well monitored and eruptions have enabled a better understanding of the mechanisms that operate under these harsh conditions although much is still to be contemplated. Much of the attention has been directed at the active volcanoes of Iceland (e.g. Grímsvötn in the glacier of Vatnajökull (Thorarinsson, 1974; Gudmundsson and Björnsson,

Figure 2.2: Trachydacite lava lobe at Öræfajökull volcano showing well developed glassy columnar joints. This lobe is interpreted to have formed with the lava perching against the ice wall of a valley glacier. Person for scale. Courtesy by David McGarvie.

1991) and Gjálp (Gudmundsson et al., 1997, 2004) and Katla in the glacier of Mýrdalsjökull (Thorarinsson, 1975; Larsen, 2000)), as well as the volcanoes of the Cascades and Antarctica (e.g. Smellie, 2002).

The eruption in Gjálp in 1996 (Gudmundsson et al., 2004) was of great significance for our understanding of intraglacial volcanism. The eruption was first detected with seismic activity but the volcano is located under an ice cap of thickness about 550 to 750 m. Extremely fast rates of heat transfer from magma to ice were observed to occur (5-6x10^5 Wm^{-2}) (Gudmundsson et al., 2004), forming two cauldrons about 2 km wide and 100 m deep after 16 hours of eruption. After 31 hours the eruption broke through the ice cap and a Surtseyan type of eruption took place. Other cauldrons formed to the north giving evidence of a 6 km active volcanic fissure. 15-20° C meltwater from the eruption carved southwards a 3.5 km long canyon with approximate depth of 150 m and then drained subglacially into the caldera lake of Grímsvötn (Gudmundsson et al., 1997; Gudmundsson, 2003). Three weeks after the eruption ceased, meltwater was released from the glacier in a sudden jökulhlaup with a volume of 3.6 km^3 having a great impact on the lowlands of Skeiðarásandur, carrying massive blocks of ice and destroying bridges.

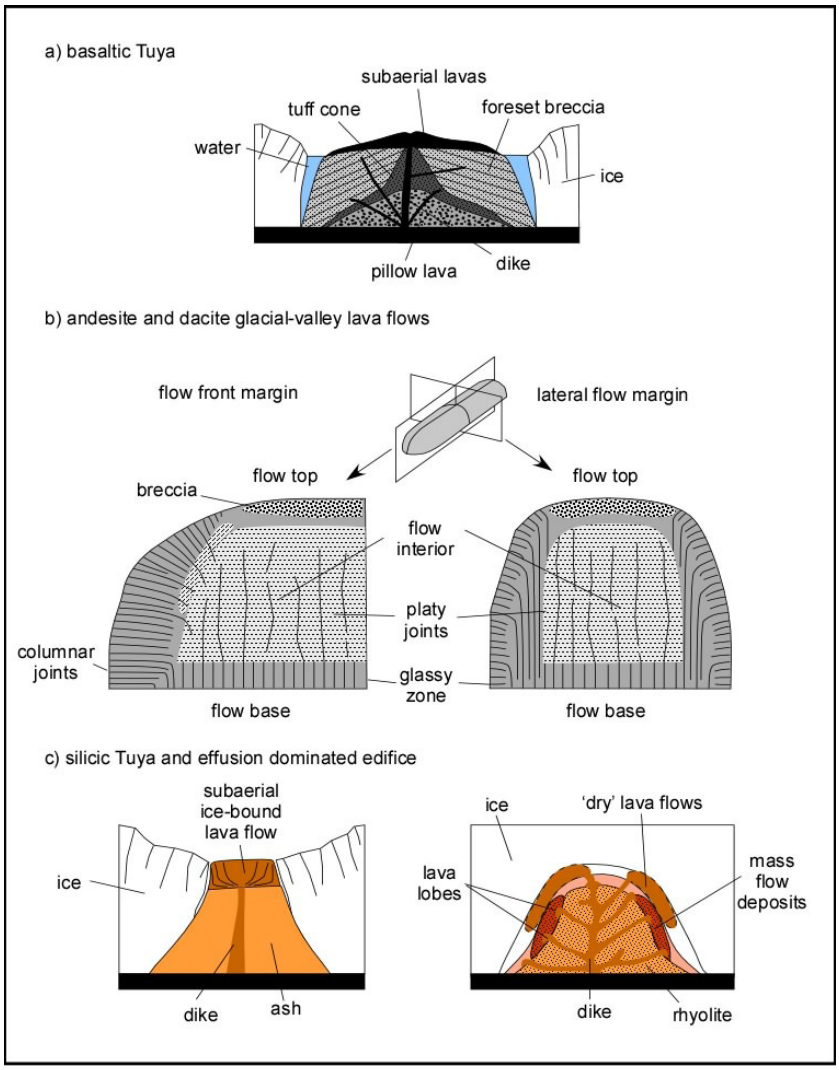

Figure 2.3: Types of volcanic edifices and structures that form within intraglacial environment varying from mafic to silicic. A) Basaltic tuya. B) Andesitic or dacitic lava flows interpreted to have been emplaced within the confinements of valley glaciers. C) A silicic tuya (left) and an effusive dominated edifice (right). Not to scale. Based on Lescinsky and Sisson (1998); Gudmundsson (2005); McGarvie (2009).

Post eruption geophysical surveys documented a 6 km long, 450 m high ridge mainly formed of basaltic andesitic hyaloclastites with volumes of about 0.7 km^3 (Gudmundsson et al., 2002). The total volume of material estimated for the Gjálp eruption was about 0.45 km^3 DRE and approximately 0.07 km^3 of material was washed into the Grímsvötn caldera. The flow of water along the bed of the glacier followed the predictions obtained from assuming that a static fluid potential controls the pathways of meltwater. This potential is mainly controlled by the ice overburden pressure and calculated from the pre-eruption ice surface and bedrock topography (Björnsson, 1988; Björnsson et al., 1992; Gudmundsson, 2003).

An eruption through relatively shallow ice took place in 1969 on Deception Island, Antarctica (Smellie, 2002). The eruption was of basaltic andesite composition within a thin glacier (<100 m). The eruption was short (<48 hours) and produced a jökulhlaup which drained both subglacially and supraglacially. The impact of the meltwaters extended the coast line of the island, modified the glacier and destroyed buildings at a British and a Chilean station. Although the eruption was subglacial the products created by the eruption where mainly tephras, pyroclastic cones and scoria cones (about 0.01 km^3), undistinguishable from those produced of dry strombolian eruptions, suggesting limited access of water to the vents during the latter stages of the eruption (Smellie, 2002).

2.3 Products of intraglacial silicic volcanism and emplacement mechanisms

As shown above, intraglacial volcanism has three main phases beginning with the subglacial phase, moving toward the emergent effusive phase and ending with the aerial phase (e.g. Gudmundsson, 2005). Thus products of this type of volcanism vary greatly ranging from lithofacies showing quenching and cooling by water/ice intermingled with lithofacies of subaerial exposure. Papers have described a number of lithofacies created in such environments: e.g. clasts of fragments and glass embedded in ash, beds of stratified lapilly-tuff, tuffaceous breccia, pumice-ash breccia, sandstone, gravel, lava lobes highly columnar (Tuffen et al., 2001; Stevenson et al., 2006; McGarvie et al., 2007). Due to the broad extent of this subject, the following is a short overview with main structures and emplacement mechanisms expected for silicic intraglacial volcanism with special attention to those relevant to this study.

Low effusive events as characteristic for many dome-forming silicic eruptions, when erupted under relatively thick glaciers may form fragmental deposits from rapid cooling, quenching and sporadic steam explosions (Tuffen et al., 2001). Fumaroles may induce the formation of cavities in the ice that may later be filled by conical lava lobes and poorly sorted breccia and ash (Tuffen et al., 2002b). Enlargement of these cavities with melting are interpreted to cause unstable piles of volcanic material to collapse and flow down to lower areas of the edifice (Tuffen et al., 2001). With even further melting of the ice roof, tunnels in the ice may form pathways for large coherent lava flows (observed examples range from 100-200 m in length and 20 m high (Tuffen et al., 2001)).

Phreatomagmatic eruptions will produce fragmented grains and shards that

can either flow unsorted down the sides of the edifice in gravity mass flows or in turbulent flows in small water bodies (Tuffen et al., 2001; Stevenson, 2005; McGarvie et al., 2007). Deposits from this type of activity form a complex mixtures of hyaloclastites, breccia, stratified lapilli-tuff, sandstone, gravel, very often in a tuffaceous ash based matrix (Zimanowski et al., 1991; Larsen, 2000; Branney and Kokelaar, 2002). In open air phreatomagmatic activity considerable tephra fall deposits are expected around the crater and the surface glacier (e.g. Houghton and Nairn, 1991).

Our lack of more in-depth ice-volcanic understanding does not permit a compilation of standard empirical relations between ice-thickness and the lithofacies produced. This factor is controlled by the confining pressure (ice-thickness/water depth), the size of the eruption, magma composition, energy dissipated and effusion rates (e.g. Zimanowski et al., 2003).

At the end of the subglacial phase, the eruption brakes through the overlying cauldron in the ice, subaerial explosive and effusive phases, sometimes with little meltwater interference can continue to deliver fine-grained volcaniclastics and ash and erupt lava flows (Fink and Bridges, 1995; Hoskuldsson and Sparks, 1997; Fink and Griffiths, 1998; Tuffen et al., 2002b). Explosive eruptions with high gas discharge, rapid decompression, ascent and crystallization will form products that are highly vesicular ($\approx$70-85% with sizes from $\approx$20 μmm-2 mm and density of $\leq$0.5 g cm^3) in a groundmass of devitrified glass (pumice) (Houghton and Wilson, 1989; Wright et al., 2003). The energy dissipated in such eruptions can be so excessive that even in the subaquatic environment and depths up to 1000 m (pressure of about 9 MPa), pyroclastic eruptions have been suggested to be able to prevent phreatomagmatic eruption, possibly by displacing the ambient water with an insulated eruption column and form vesiculated pumice deposits (Wright et al., 2003).

Subaerial silicic lava flows

Silicic subaerial effusive lava flows are usually associated with a dome, coulee or blocky lava. Subaerial flows confined by ice walls in a glacier are expected to hold surface structures of subaerial deposits although marginal facies may show water-ice interaction. An exception might be lava flows emplacement within cavities in the ice more likely to lack surface subaerial morphologies and only present cooling structures or hyaloclastites. Nevertheless, understanding subaerial lava flows will help in defining structures of intraglacial origin. For later comparison, two modern day examples of silicic lava flows are given below, one forming a well

developed channel on the slopes of a stratovolcano and the other erupted lavas from a point source forming a dome that interacts with shallow sea waters.

Harris et al. (2004) describes an active dacitic flow observed in 2000-2002 at Santiaguito volcano, Guatemala. Steep ground slopes (20-30°) enabled the lavas to overcome the yield strength and flow down, developing a flow structure and morphology resembling basaltic a'a lava flows (Lipman and Banks, 1987; Harris et al., 2004).

The 3.75 km long (0.066 km^3) flow can be divided into four zones, from vent to flow front: the stable channel, the transitional channel, the dispersed flow and flow toe (Lipman and Banks, 1987; Harris et al., 2004). The stable channel comprises a well delineated channel and marginal levees that make almost 40 % of the total length of the transport system. The levees formed by mainly rubble and massive intrusions can form steep outer angles (≈45°) and almost vertical inner walls. The flow in the channel is characterized by rubble and pressure ridges that extend with this morphology all the way to the next zone, the transitional channel. The transitional channel is marked by lower levees and in some sections a more blurred margin. The channel becomes less convex and merges gradually with the dispersal zone. This zone forms 10-40% of the total length of the transport system. The dispersal zone forms the broadest section of the flow (2-3 times wider than the channel) where the flow is no longer confined to a channel but disperses into the whole flow. Lobate features or toes mark the flanks of the dispersal zone that produce rubbly, rounded- to subangular blocks (1-3 m wide) steeply arranged at the front face (a normal coulee flows form larger smooth polyhedral blocks).

A key process that enabled the lavas at Santiaguito volcano to advance long distances from the vent, in spite of low extrusion rates (0.5-1.6 $m^3\ s^{-1}$) and high viscosity (10^{9-10} Pa S) was the formation of an insulated transport system in the channel path and flow front. This enabled the lava to effuse relatively quietly out of the vent into the channel and flow to the dispersal zone and flow front with minimal heat loss (0.03-0.09 °C h^{-1}), advancing with rates 2-13 m day^{-1} (Harris et al., 2004). Not unlike a'a lava flows, the dacite flow formed a rubbly/clinkery crust by viscous tearing induced by the friction along the margins and the pull of the faster moving liquid core (Rowland and Walker, 1990). This carapace was eventually dislodged toward the margins and added to the levees or rafted with the flow and piled at the flow front. And not unlike surface ropes on basaltic pahoehoe, pressure ridges of rubble aligned convex perpendicular to the flow in the channel, forming ogives that became more closely spaced at the dispersal

zone where the advance rates decreased. At the flow front the core extruded in the form of massive, large pillow-like lobes giving rise to very steep slopes leading to constant disruption and fall of debris that gathered in a talus in front of the moving lobe. Ash plumes were generated with each disruption and debris fall. Thus the flow moved in a caterpillar-track motion as described for a'a flows (Rowland and Walker, 1990).

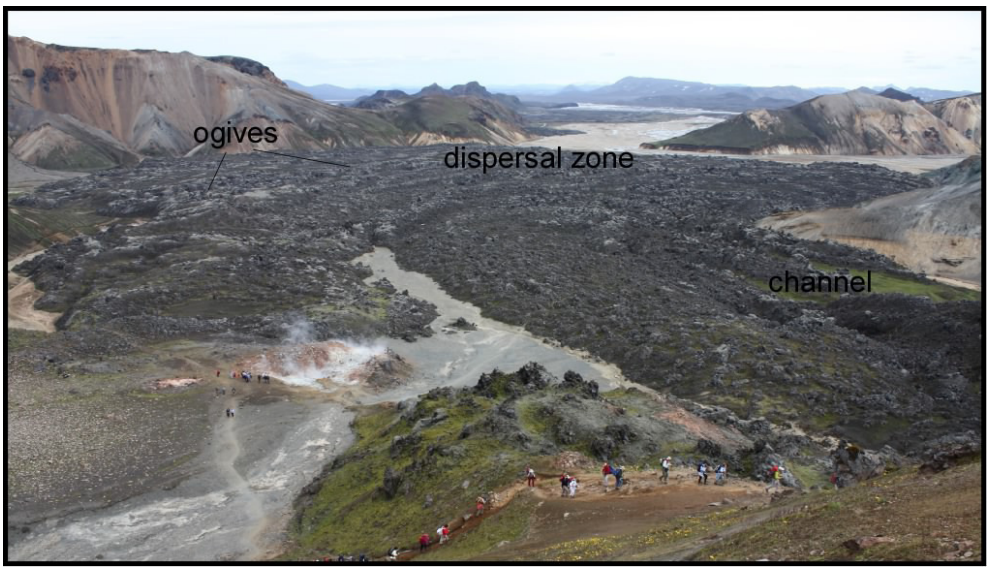

Figure 2.4: Laugahraun silicic lava field displaying the channel and the dispersal zone. Ogives form perpendicular to the flow head. Courtesy by Magnús Tumi Guðmundsson.

A silicic lava dome (SiO_2 67-73 wt.%, 0.062 km^3) that emerged from a subaquatic eruption at Showa Iwo, Japan in 1934-35 described by Maeno and Taniguchi (2006) shows a combination of a lava flow erupted from a point source with surface flow morphology of subaerial lavas and features of lava-water interaction. The eruption began subaquatically building a basement of pyroclastics and pumice with phreatomagmatic explosions. At the subaerial phase, lavas effused radially forming a dome with axisymmetric shape, that is, with rather low relief, regular outlines and fragmental crust. Two main parts characterize the dome, the margins formed by breccia and fractures and a central part formed by breccia and folded lava. The folding and wrinkles (pressure ridges similar to ogives) on the margins are aligned radially perpendicular to the flow (Maeno and Taniguchi, 2006). The dome reveals also two lavas with slightly different composition, one located at the margins with dacitic composition and the other forming the central part of rhyolitic composition. A cross section of the central part shows a microcystalline interior grading upward into finely vesicular lava with a crust of coarsely vesicular lava and pumice breccia at the top (Maeno and Taniguchi, 2006).

High temperature (830-990°C) dacitic lavas are interpreted to have erupted

first flowing to the shallow seafloor, brecciating and forming hyaloclastites. Elevated temperatures and consequently lower viscosities (10^{7-9} Pa S) explain the axisymmetric shape of the dome (indicative for viscous fluid behavior) rather than forming spiny shaped dome (bingham plastics behavior). With stretching, shearing and compression of the surface these fragments became brecciated and ramped and parts did trap in the extension cracks reheating and welding (Maeno and Taniguchi, 2006). In a later stage low temperature rhyolites were effused from the vent thrusting the colder margins causing fracturing, effective brecciation of the crust and ramping of breccia at the flow front. The vesicular pumice fragments at the central part are interpreted to have formed with folding of the crust extending and compressing as the flow advanced (Fink, 1980, 1983).

Internal structure of silicic lavas

Internal structures of lava flows as observed in open cross sections and thin sections give information on many features that are related to flowage (Smith, 2002). From basaltic lava flows to silicic domes, the internal arrangement of flow-related structures have been important diagnostics to determine growth by exogenous or endogenous processes (Fink, 1993; Goto and McPhie, 1998; Thordarson and Self, 1998). In the case of a dome growth, when lava is added to the outer surface of the dome, the style referred is exogenous. If lava is injected into the interior of the dome which grows by inflation the growth is referred as endogenous (Fink, 1993). Main features associated to the internal structure of silicic lavas that act as gauges for strain, vorticity, pressure, stress, temperature and rheology are e.g. vesicles, flow banding, folding, phenocrysts and jointing (Smith, 2002; LaMoreaux, 2008). Textural domains and fabrics give further support to flow-related structures (Smith, 2002).

In the absence of external water, degassing of a magma is the primary control on the mode of eruption of lava (Anderson et al., 1995). Vesicles rise by buoyancy through the liquid lava core to arrange inhomogeneously into planar and irregular zones in areas solidifying by thermal cooling (e.g Toramaru et al., 1996). Vesicularity has been a useful parameter for showing inflation in basaltic lavas (e.g. Thordarson and Self, 1998; Oskarsson, 2005) but little is known about silicic lavas in this respect although this emplacement mechanism may be important. Vapor bubbles migrating upwards through the magma will accrete into the ductile zone at the brittle-ductile boundary. Many will coalescence with adjacent bubbles into larger populations forming larger vesicles, pipes and macrovesicles (Thordarson and Self, 1998). With viscous-tearing these vesicles may deform forming stretched

or elongated domains. With incremental addition of lava to the brittle-ductile crust in the process of inflation and in instances lava drop, bands of vesicles may form marking each pulse. In lava drop episodes vesicles may connect to gaps at the boundary which later brake into sheets. Finally, both single identities or accretions will eventually be stretched and relax in the flowing body, some being recycled into the magma while others will be preserved in their state of stress giving evidence of the final stage of emplacement or initial stage of cooling as the lavas crept in a visco-elastic manner.

Crystal alignment both in the groundmass or of phenocrysts or both are common structural textures in volcanic products. For silicic rocks the terms pilotaxitic, trachytic, trachytoidal, banded and others have been used to describe flow-related textures (Smith, 2002). Notably, trachytic texture refers to subparallel arrangement of microcrystalline feldspar laths and pilotaxitix represents a groundmass of crudely aligned small crystals that swirl around larger phenocrysts. Flow banding is an expression of crystal arrangement and is a feature much observed in intermediate to silicic flows and the term is descriptive for both texture and structure (Smith, 2002). Banding consists of planar zones of crystal abundance formed by extreme stretching of ductile bodies of differing crystallinity (Smith, 2002). The thickness of each band may range from millimeters to meters. Microlites can be found oriented parallel to the axial plane of the folds but are perpendicular to the banding in the nose of the fold. Furthermore, the flow may develop folds and swirling (even boudins) in the banding due to different viscous properties in the outer chilled crust and the inner part (Smith, 2002).

Phenocrysts may be found evenly distributed in the flow, indicating that the crystals had same density as the lava and therefore did not segregate by flow differentiation. Sometimes zones of crystal alignment and imbrication are interpreted to form when a more plastic flow moves between two non-deforming walls (Ventura et al., 1995). Brittle deformation of phenocrysts is also common as the flow advances. This deformation is the result of abrasion with crystals during flow due to very high strength of the groundmass or high crystal concentration (Smith, 2002).

Crystallinity is often indicative of cooling rates whereas melts of more developed crystal structure and aggregations will develop in areas of slower cooling (Goto and McPhie, 1998). Crystallinity is expressed as hyaline (0-10% crystals), hypohyaline (10-40% crystals), hypocrystalline (50-90% crystals) and holocrystalline (90-100% crystals).

Cooling joints reveal dynamics related to the thermal history of the flow and

are means of showing rapid cooling by steam or water. Cooling structures and their environmental origin will be described in a special subchapter.

Based on these descriptions, a few examples of internal structures for silicic lavas can be given. A submarine dacite cryptodome 200-300 m in diameter and 190 m high in Rebun Island, Hokkaido, Japan presented a concentric three-part structure formed by a massive core, a banded rim and brecciated border (Goto and McPhie, 1998). The massive core (forming 75% of the dome) is characterized by columnar joints radiating from the core to the margins ranging in size from 150-200 cm in the center to 60-80 cm at the margins of the core. The core is porphyric (5%) with a pilotaxitic texture. Plagioclase microlites are stongly aligned and deflect around phenocrysts. No vesicles occur in the core and the change from the core to the next zone is gradual with banding increasing from microscopic to macroscopic. The banded rim represent 25% of the dome and is composed of alternating bands (80-150 cm thick) of pale and dark grey bands like a series of shells equally sized through the rim. Cooling joints of the margins connect to the joints in the core but decrease in size to become 40-60 cm. The dacite in the rims becomes more vesicular (5% amoeboid and elongated vesicles) and more glassy with hyalopilitic texture (crystallinity 50%) in the pale gray band but a more glassy texture forms the dark grey band. The brecciated border is comprised of in situ breccia and peperite derived from the highly fractured pale gray band that is more vesicular (20% spheroidal) at the outermost border.

As described by Goto and McPhie (1998), the cryptodome is interpreted to have intruded into relatively thin layer of wet ocean sediments (to explain vesicularity of 20% in the border necessitates low confining pressures) by continuous injection of magma into the dome. As the lava encountered the wet sediment the margins cooled more rapidly forming a chilled brecciated crust insulating the interior where magmas injected into with consequent inflation. The fragmented border reflects dynamic stress at the brittle chilled crust induced by inflation as the dome was fed by magmas into the interior. The three-part internal structure is thought to represent continuous injection of magma into the core of the cryptodome. This is supported by the gradual contact change between the zones, identical phenocrystal distribution within the dome, and continuous radial cooling joints extending throughout the core and banded rim. Larger columns and higher crystallinity in the core suggest lower cooling rates as expected for bodies insulated by a coherent crust. Interlayered bands of pale gray and more glassy dark grey bands are interpreted as flow bands of large scale in comparison to regular banding. However, their formation mechanism is the same attributed to

laminar shear in response to higher viscosities in the lava.

Lava lobes from Bláhnúkur in Iceland, considered to have intruded into subglacial cavities (see subchapter above and Figure 2.3C) have shown to hold a similar internal structure although being smaller in size ($<$ 10 m in diameter) representing continuous inflation as magma is injected into the interior (Goto and McPhie, 1998). These form concentric zonal structures and radial columns extending through all three zones; a massive, microcrystalline, poorly vesicular core; a flow banded rim of alternating layers of highly vesicular devitrified glass, obsidian and partly crystalline, poorly vesicular rhyolite; and a border of intensely fractured obsidian that grades outwards into hyaloclastite breccias (De Rosen-Spence et al., 1980; Tuffen et al., 2001).

2.4 Rheology of silicic lava flows

Flow of lava is controlled by topography, effusion rates and its rheological properties. These properties are influenced by composition, temperature, pressure and volatile content (Manley, 1992; Spera, 2000; Yokoyama, 2005; Cordonnier et al., 2009).

Silicic melts are more viscous than basaltic melts due to their high content of silicate tetrahedra resulting in them being highly polymerized (Francis and Oppenheimer, 2004). Factors related to the composition of the melt that may alter the viscosity by breaking the silicon-bonds and causing depolymerization are e.g. addition of water, carbon dioxide and alkalinity (Dingwell and Virgo, 1988; Francis and Oppenheimer, 2004). Other components, such as high fluorine contents may also induce lower viscosities in silica-rich melts (Sigvaldason and Óskarsson, 1986).

The physical parameter that is most influencial in affecting the viscosity of magma is temperature, since variations in temperature can change viscosity by several orders of magnitudes (Pinkerton and Norton, 1995). Composition plays an important role and it is well quantified that at 1300°C basaltic lavas have viscosity close to 10 Pa s while rhyolite lavas have viscosity close to 10^5 Pa s (Murase and McBimey, 1973).

Temperature increase in a magma body is usually associated with an increase in volume, where the body becomes highly energized and less highly organized. At the vent system, unless an insulated plumbing system is provided for the lavas, high extrusion rates are important for maintaining a thermally stable body. Thus high eruption rates enable the lavas to overcome the strength of the rigid

cooled crust and advance longer distances while low eruption rates will be rapidly controlled by the thermal gradient and form shorter and steeper flows (Bridges et al., 1991).

Addition of rigid particles as phenocrysts is observed to increase the viscosity of the lavas (Cordonnier et al., 2009). High crystal fractions hamper the dissipation of energy through the magma body adding elastic particles which induces premature generation of cracks, speeding the magmas shifting from a visco-elastic behavior to a brittle behavior (Cordonnier et al., 2009). Topographical changes in the flow geometry may also change the rheological properties by inducing clogging and spilling, collapse, fracturing of the lava, eventually leading to thermal loss and increase viscosity (Harris and Rowland, 2001).

A combination of the above-mentioned factors will determine the final structure and morphology of the flow. In light of lava-ice interaction, water plays an important role adding high thermal gradients to the lava which do alter the rheological properties of the flow.

2.5 Cooling fractures and jointing in lava-ice interaction

Joint structures and fractures are important features revealing the thermal history of the lava (DeGraff and Aydin, 1993; Thordarson and Self, 1998; Lescinsky and Fink, 2000). These form by thermal contraction as the lavas are exposed to lower temperatures breaking into well developed polygonal to hexagonal columns. Jointing occurs under atmospheric conditions but extensive jointing and hackly appearance has been diagnostic for water interaction and rapid quenching and cooling (e.g. Peacock and Fuller, 1928; Fuller, 1931, 1934; Long and Wood, 1986; Lescinsky and Fink, 2000). Nevertheless, it is important to differentiate between the patterns of subaerial conductive cooling and convective cooling by water or steam.

Basaltic pahoehoe lava flows emplaced subaerially reveal a cooling history with a three-part jointing structure attributed to conductive cooling during the time of emplacement and post-emplacement, the crustal zone, the columnar zone and the platy zone (Thordarson and Self, 1998). The joints form uneven tapering polygonal columns arranged vertically or subvertically with or without localized sections of horizontal closely spaced plates. The crustal zone forms small hyaline to hypohyaline (crystallinity 10-50%) columns that grow inwards toward the core (h/l of the lava lobe= height/lenght $\approx$ 0.6). The columnar zone forms large

holocrystalline (crystallinity 90-100%) joints (2-3 times larger than the columns of the crustal zone) and the platy zone comprises of decimeter to meter horizons of closely spaced horizontal joints (Figure 2.5A).

It is well documented that during and after emplacement, as the lava looses heat to the atmosphere it forms a coherent, self-supporting crust with closely-spaced columns reflecting rapid cooling rates. This crust will enable the lava to maintain flow internally as thickening occurs with incremental addition of molten lava to the ceiling as magma is transported from the vent to the flow front through an elaborated system of conduits and tubes with minimal thermal loss (Thordarson and Self, 1998). After the lavas come to halt, the molten core forms a pattern of joints reflecting slower rates of cooling under insulated condition. Its is common that one out of three joints in the crust merge with a joint in the core. Platy jointing may form at this stage, usually at the crustal-core boundary, with creeping of the brittle-plastic zone in the flow interior. Smaller columns develop at the basal crust limited to high thermal erosion promoted by the moving flow interior (Thordarson and Self, 1998). On the other hand, a'a lava flows, due to the highly brecciated surface and basal crust (Rowland and Walker, 1990) have higher rates of thermal loss that is clearly revealed in their joint structure. The cooling pattern (relatively smaller columns than those developed in pahoehoe) form vertical to subvertical columnar and crustal joints that are radiative and concentric (from surface and crust) meeting at the center of the lobe ($h/l \approx 0.5$) (Figure 2.5A) (Oskarsson, 2005).

Convective cooling by water and steam penetrating the flow is faster than cooling from radiation and atmospheric convection (Sæmundsson, 1970; DeGraff and Aydin, 1993; Lescinsky and Fink, 2000). Larger thermal gradients will induce narrow striations and more closely spaced fractures and if this process is sustained will result in constant cooling rates and the formation of long elongated columns (Lescinsky and Fink, 2000). Thus a decrease in cooling rates will alter the thermal gradient and increase the fracture spacing.

Cooling structures in lava flows that have been diagnostic for lava-water interaction, have been described as ranging from closely spaced shard-forming, hackly fractures (entablature) to columnar joints extending perpendicular to the flow margin, and if confined by some environment (e.g. ice-walls) may be arranged in steep vertical to subvertical walls (Sæmundsson, 1970; Long and Wood, 1986; DeGraff and Aydin, 1993; Lescinsky and Sisson, 1998; Lescinsky and Fink, 2000). A common morphology for a chilled lava is represented by a thick crust of entablature with a sharp boundary between the underlying colomnade (Figure

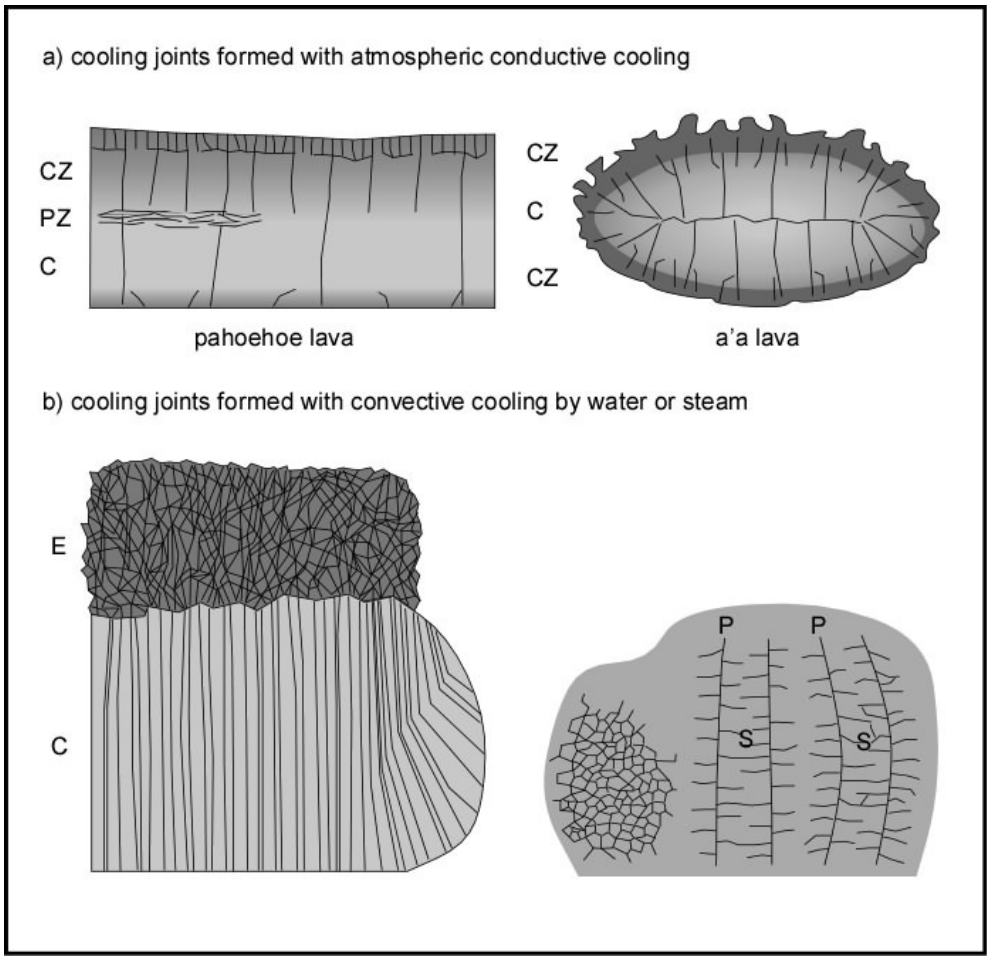

Figure 2.5: Cooling patterns in lavas formed by conductive cooling under the atmosphere and convective cooling by water and steam (based on Oskarsson (2005); Spörli and Rowland (2006); Sæmundsson (1970). A) Examples of conductive cooling in pahoehoe and a'a lavas. The cooling pattern forms a three part division structure reflecting the thermal history of the lava, the crustal zone (CZ), the platy zone (PZ) and the columnar zone (C). B) Examples of convective cooling induced by water into the fractures or steam. Due to faster rates of cooling the structure pattern is formed by irregularly spaced joints with hackly appearance (entablature E) and/or columnar joints (C). Late stage convection can induce further formation of secondary joints (S) that extend perpendicular to the primary joints (P) as illustrated above.

2.5B)(Long and Wood, 1986; Sæmundsson, 1970). Columnar joints of this type are often in the form of thin oblong regular spaced columns extending entirely through the lava body normal to the flow margins even bending and twisting when extending from radial margins in spherical bodies (Figure 2.5B) (e.g. Hull and Caddock, 1999; Tuffen et al., 2001). Another pattern as described by Lescinsky and Fink (2000) shows columns forming a closely-spaced columnar crust perpendicular to the margins that shift inwardly into larger vertical regular-spaced polygonal columns (Figure 2.3B). The interior reflects decreasing cooling rates in the crystalline flow interior similar to the structure of lava tubes (e.g. Lescinsky

and Fink, 2000). Often a glassy selvage several meters thick characterizes the margin of the flow (Lescinsky and Fink, 2000).

Extended convection of water and steam at the surface of an already fractured lava can induce further intrusion into the network of cracks and form secondary joints perpendicular to the primary fractures (Figure 2.5B) (Spörli and Rowland, 2006; Lescinsky and Fink, 2000). Spörli and Rowland (2006) describes a lava flow interpreted to have rested against ice walls during its advancement later to be washed by flooding meltwaters forming such pattern.

The most intense form of heat transfer, as sometimes generated when lavas are erupted into shallow subaquatic environments, causes intensive steam generation and rapid expansion leading to complete granulation and the formation of glass shards (hyaloclastites) (e.g. Zimanowski, 1998; Gudmundsson, 2003). Hyaloclastites are thus diagnostic for explosive phreatomagmatic interaction and extremely high heat flux.

Composition affects the pattern observed when magma is cooled. Silicic magmas have higher thermal diffusivities in comparison to mafic magmas enabling more rapid cooling rates (Gregg and Fink, 1996; Lescinsky and Fink, 2000). Other compositional properties that produces e.g. more closely-spaced fractures in rhyolites than in basalts are different Young's modulus, Poisson's ratio, and thermal expansivity (Nemat-Nasser and Oranratnachai, 1979).

Polygonal columns attributed to quenching by water and ice are sometimes similar to columns formed under atmospheric conditions. Quantitatively this difference in cooling rates and fracturing is poorly constrained and the relation between effusion rates, viscosity and the volume of water available at the eruption site has not been clearly established.

2.6 Meltwater production and flooding hazards

Meltwater is an inevitable by-product of lava-ice interaction. Heat is dissipated at high rate from the magma to the ice forming water-filled cavities in which effective convective and conductive heat transfer takes place (Hoskuldsson and Sparks, 1997; Gudmundsson, 2003). In both basaltic and rhyolitic eruptions, the thermal energy released in the erupted lava can melt a volume of ice many times greater than the volume of the lava itself (Hoskuldsson and Sparks, 1997). Rhyolitic magmas have lower temperature, viscosity and heat capacity, with a heat content only 60-70% of basaltic magmas and thus with less ice-melting potential (Hoskuldsson and Sparks, 1997; Spera, 2000; Gudmundsson, 2003). Nevertheless

given same eruption rates the melting and heat transfer should be in the same order of magnitude as in basaltic eruptions (Gudmundsson, 2003).

Meltwater will either be drained directly from the eruption site or if conditions permit accumulate in a temporary englacial lake (Gudmundsson, 2005). Two ways are possible for this discharge 1) supraglacial discharge where water spills over the surface rims of the vault or cauldron in the ice and flows to lower regions or 2) subglacial discharge where the meltwaters are directed by hydrostatic pressure along the bottom of the ice and delivered at the flanks (Hoskuldsson and Sparks, 1997). Supraglacial flows of warm meltwaters can also easily carve large canyons which merge and form preferred pathways for meltwaters and even lava flows (Lescinsky and Fink, 2000; Gudmundsson, 2005; Smellie, 2006). Eruptions underneath thin ice covers are less likely to produce great volumes of meltwater and retain water (Gudmundsson, 2005). The brittle nature of the ice, fragmenting and collapsing, provides little resistance to warm meltwaters responding to the force of gravity or hydrostatic pressures (Hoskuldsson and Sparks, 1997; Gudmundsson, 2003).

No modern subglacial eruption has been observed to pond meltwater with a semi-stable water level for considerable periods of time as interpreted to be the formation mode for several tuyas in the Pleistocene (Gudmundsson, 2005). The eruptions in Grímsvötn in 1934, 1983 and 1998, occurred at relatively stable meltwater levels, but it has to be taken into account that these eruptions occurred within an ice-covered, pre-existing lake (Thorarinsson, 1974; Björnsson, 1988).

Chapter 3

Geological setting

3.1 The East Volcanic Zone

The main axial rift in Iceland is divided into two types of zones, the volcanic flank zones with little spreading and the volcanic rift zones with extensive crustal spreading. These zones vary also in composition of eruptive products where the volcanic rift zones form tholeiites and the flank zones form products of more alkalic and mildly alkalic composition (Jakobsson, 1979a; Sæmundsson, 1979; Gudmundsson, 1995; Sigmundsson, 2006). The volcanic rift zones are the West Volcanic Zone (WVZ), North Volcanic Zone (NVZ) and the northern part of the East volcanic zone (EVZ). The EVZ is divided into two zones, the northern East Volcanic Rift Zone (EVRZ) and the South Iceland Flank Zone (SIFZ). Thus the Flank zones in Iceland comprise three zones which are the Snæfellsnes Volcanic Zone, the SIFZ and the Öræfajökull-Snæfell Flank Zone. Actual spreading rate in Icelandic is estimated to be about 18.9 to 20 mm/y from the Kolbeinsey ridge to the Reykjanes ridge (Sella et al., 2001) and models indicate that the EVZ is in the process of taking over from the WVZ as the ridge spreads apart (Thordarson and Larsen, 2007). The ridge is interpreted to be propagating southwards with the southern part of the EVZ being a flank zone while the northeast part has the characteristics of the axial rift zone. The EVZ connects with the WVZ through the Mid-Iceland Belt (MIB) and a transform zone named South Iceland Seismic Zone (SISZ). The SISZ extends from the the Hengill triple junction through north-south faulting in a "bookshelf" style to the Torfajökull area where the EVZ changes character from rift zone to flank zone (Sigmundsson, 2006).

The volcanic zones in Iceland are composed of several volcanic systems in which the volcanic activity takes place. A volcanic system has the tendency to trend perpendicular to the direction of spreading and is usually composed of a

fissure swarm, a central volcano or both (Figure 3.1). Fissure swarms are narrow and elongated stripes, 5-20 km wide and 50-200 km long, with normal faults, tensional cracks and volcanic fissures. Dikes are intruded along the fissure system feeding eruptions and enlarging the fissure (Thordarson and Larsen, 2007) e.g. Krafla fires in 1975-84 (Einarsson et al., 1991). In contrast, a central volcano is the surface expression of a magma chamber or an intrusive domain, that erupts in episodes of tectonic deformation or chamber depressurization (Gudmundsson, 1995; Jónasson, 2007). These volcanoes tend to form edifices of complex architecture characterized by different eruption styles, often with a large caldera as known for several central volcanoes in Iceland e.g. Askja caldera, the stratovolcano Hekla and Eyjafjallajökull.

Of the 30 volcanic systems that form on the Icelandic axial rift (Jóhannesson and Sæmundsson, 1998), eight are a part of the east volcanic zone. These systems are Vestmannaeyjar, Eyjafjallajökull, Katla, Tindfjöll, Hekla-Vatnafjöll, Torfajökull, Bárðabunga-Veiðivötn and Grímsvötn (Figure 3.1). Five are characterized by a fissure swarm and a central volcano while three are central volcanoes without associated fissure swarms. Vestmannaeyjar is considered to be in its earliest stage of growth and therefore classified as a domain not a central volcano (Thordarson and Larsen, 2007). The largest of the volcanic systems associated with the EVZ is Bárðabunga- Veiðivötn, covering about 2500 km^2, while the smallest is Tindfjöll with an area of about 230 km^2.

3.2 Eyjafjallajökull

Eyjafjallajökull is a central volcano with a shield-like edifice covering an area of 400 km^2, slightly elongated east-west and rising about 1600 m above its surroundings. It has a 2.5-3 km caldera at its summit and above about 1000 m a.s.l. the slopes are covered by an ice cap named Eyjafjallajökull (see map Figure 3.2). Eyjafjallajökull has been in construction throughout the upper Pleistocene (800 ky); an estimate based on paleomagnetic survey of a sequence of lavas from near the Brunhes-Matuyama boundary near Núpakot supplemented by K-Ar radiometric datings (Kristjánsson et al., 1988; McDougall et al., 1984; Wiese, 1993).

Eyjafjallajökull volcano shows evidence of both subglacial/subaquatic and subaerial eruption phases (e.g. Jónsson, 1998). Large parts of its basement are composed of basaltic hyaloclastites, pillow lavas, glassy (sideromelane) clasts, water-lain sedimentary rocks and entablature lava indicating subglacial/subaquatic setting during early stages in the formation of the volcano (Sæmundsson, 1970;

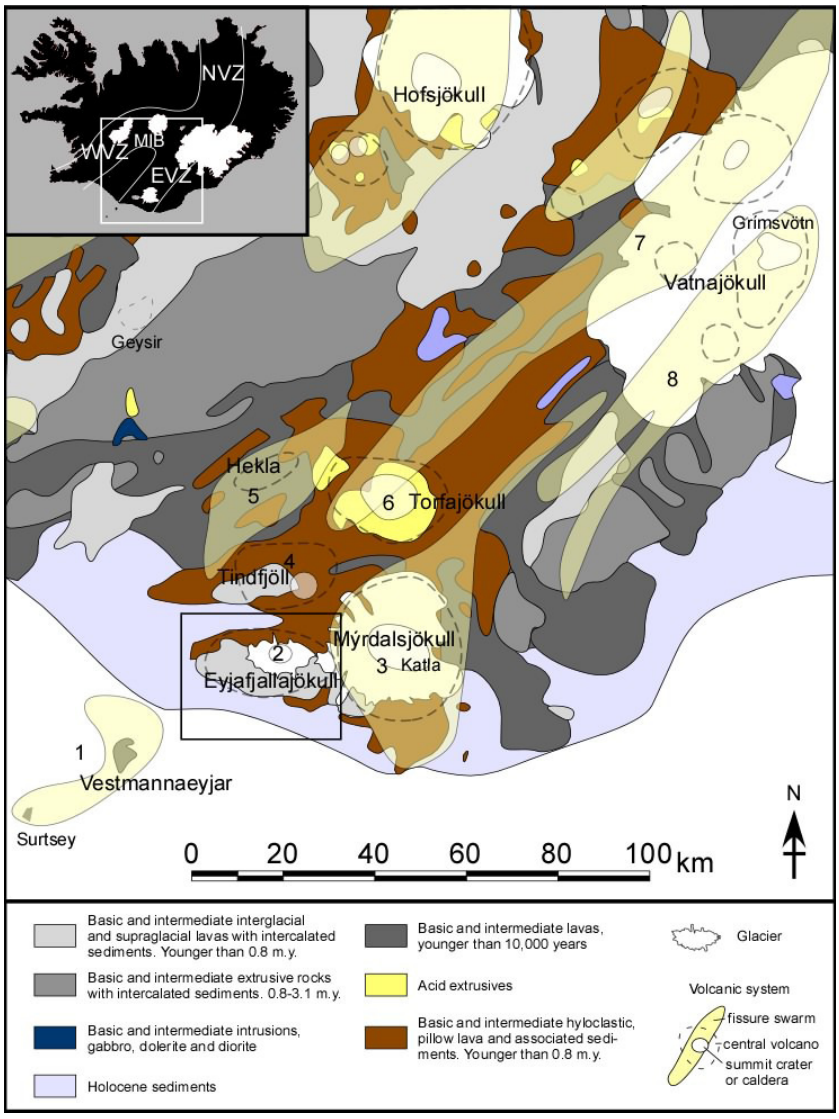

Figure 3.1: Sketch of the East Volcanic Zone (EVZ). The figure shows the WVZ and the NVZ forming the main axial rift and the EVZ being the flank zone connected by the MIB. Each volcanic zone has several volcanic systems, composed of a fissure swarm, a caldera or both. Eight volcanic systems occur on the EVZ: 1) Vestmannaeyjar, 2) Eyjafjallajökull (see map Figure 3.2), 3) Katla, 4) Tindfjöll, 5) Hekla-Vatnafjöll, 6) Torfajökull, 7) Bárðabunga-Veiðivötn and 8) Grímsvötn. Map modified from Landmælingar Íslands (1990) and Thordarson and Larsen (2007).

Loughlin, 2002). Compound lava flows of basaltic to intermediate composition, with radial to semi-radial eruptive fissures and ridges, make up the upper part of the volcano, which has been formed under both interglacial and glacial conditions. Silicic lavas represent a very low percentage of the total mass budget of the volcano but are found e.g. in the Skerin ridge (Jóhannesson and Sæmundsson, 1998, this study).

Over the last 1500 years, four eruptions in Eyjafjallajökull have been registered: The oldest occurred about 500 AD (main crater), followed by an eruption

in the 10th century (Skerin ridge), an eruption in 1612 (main crater) and the latest was most likely a vulcanian explosive eruption at the main crater in 1821-1823 AD (Larsen, 1999; Dugmore and Larsen, 2009, in prep.). In comparison with the more active volcanoes in Iceland, and in particular its neighbour Katla, the frequency of eruptions in Eyjafjallajökull is low. Interestingly, although Katla has erupted far more frequently than Eyjafjallajökull, some eruptions in these volcanoes have been documented to be synchronous in time, since eruptions occurred in both volcanoes in 920 AD, 1612 AD and 1821-1823 AD (Larsen, 2000), indicating that these two volcanoes are sometimes simultaneously affected by the same volcano-tectonic event. Recent geophysical study did not detect a possible magma chamber beneath the Eyjafjallajökull volcano, although seismic activity and surface deformation indicated a sill intrusion at relatively shallow depth under the volcano in 1994 and 1999 (Sturkell et al., 2003; Pedersen and Sigmundsson, 2004).

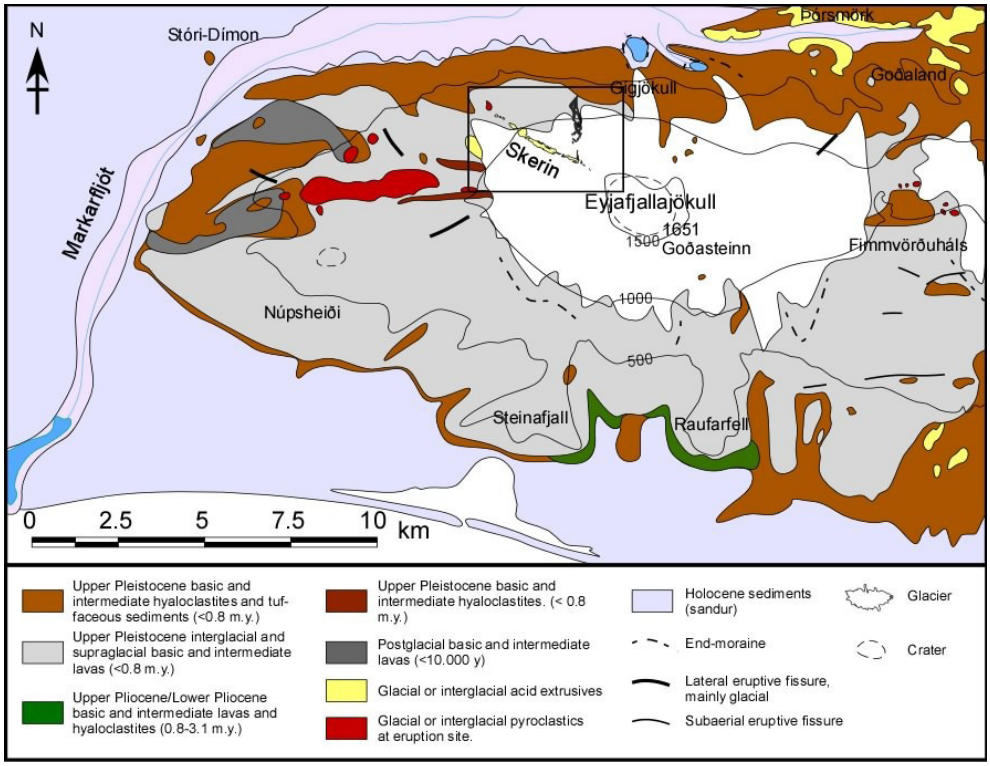

Figure 3.2: Geological map of Eyjafjallajökull. Map based on a geological map from Landmælingar Íslands (1990) sheet 6 south Iceland and Jónsson (1998). Map of Skerin in Figure 5.1.

Glaciers of the Weichselian glaciation (Sæmundsson, 1979) played a significant role in shaping the volcano edifice of Eyjafjallajökull. The Markarfljót valley glacier eroded the northern and western flanks while a combination of sea erosion from sea level rise (Sigmundsson, 1991) and outlet glaciers eroded the south side

forming cliffs over 500 m high. The ice cap on Eyjafjallajökull also shows evidence of having advanced to cover the entire volcano leaving small valleys and striated lava flows.

The size of the ice cap covering the upper part of Eyjafjallajökull was measured to be approximately 80 km^2 (e.g. Pedersen and Sigmundsson, 2006) in 2000. The ice cap is thin reaching maximum thickness of about 260 m on the east side (Strachan, 2001). The glacier reaches down to about 1000 m elevation on the flanks while two outlet glaciers, Gígjökull and Steinsholtsjökull, extend down to the lowlands on the north side. Fluctuations of these outlet glaciers have been used to estimate climate fluctuations over the past 2000 years (Kirkbride and Dugmore, 2008), since they do not have a history of surging and are considered to respond fast to climate fluctuations. According to Kirkbride and Dugmore (2008), the ice cap of Eyjafjallajökull advanced before the 3rd century AD, in the 9th and 12th centuries, and with a series of advances within the Little Ice Age (1700-1930 AD).

3.3 Skerin

Skerin ridge is located on the NW side of Eyjafjallajökull. Skerin extends about 4.5 kilometers from the NW margin of the volcano starting at Rauðhyrna (856 m a.s.l.) to the SE, with its upper end close to the craters rim (about 1400 m a.s.l.; Figure 5.1) lying on slopes of 7-12°. Skerin ridge is covered by the ice cap with only the upper part exposed above the glacier except for few segments on the NW end where the glacier has retreated completely. Bulk of the ridge is of silicic composition and scoria deposits are found on top of the ridge. A lava flow to the north of the ridge is connected to it. The bedrock in the area is mostly lava flows, still partly covered by the ice cap.

Clues about the timing of the eruption that produced the Skerin ridge are found in the form of glacial flood deposits produced by the eruption and present in alluvial fans in the lowlands of Langanes. The stratigraphy at this site shows that the flood deposits are synchronous with the tephra layer from Katla eruption in 920 AD (Dugmore and Larsen, 2009, in prep.). These floods must have been formed by a subglacial eruption on the northwest side of Eyjafjallajokull because floods that would result from an eruption at the summit crater are most likely to flow north through Gígjökull. Deep gullies that come out parallel to Skerin ridge, Miðtunga and Akstaðaá and washed soil on the plains of Litlaheiði may bear witness to floods from subglacial eruptions in recent times in this region. A

brief discussion on the age of Skerin ridge will be given in Chapter 6.

Chapter 4

Methodology

4.1 Study site

Several structures in Iceland and overseas have been interpreted to be the product of lava-ice interaction but very often the glacier present at the eruption has disappeared completely (e.g. Lescinsky and Sisson, 1998; Lescinsky and Fink, 2000) or has retreated significantly since eruption occurred (e.g. Tuffen et al., 2001, 2002b). The predominantly silicic Skerin ridge in Eyjafjalljökull was chosen for this project due to its apparent limited glacial erosion and clear association with the present ice cap of Eyjafjallajökull. Rapid recession of the glacier in the last decades has provided good exposures, especially in the lower parts, enabling systematic mapping of its main structures and architecture including the inner structure found in glacial-eroded outcrops (Figure 4.1).

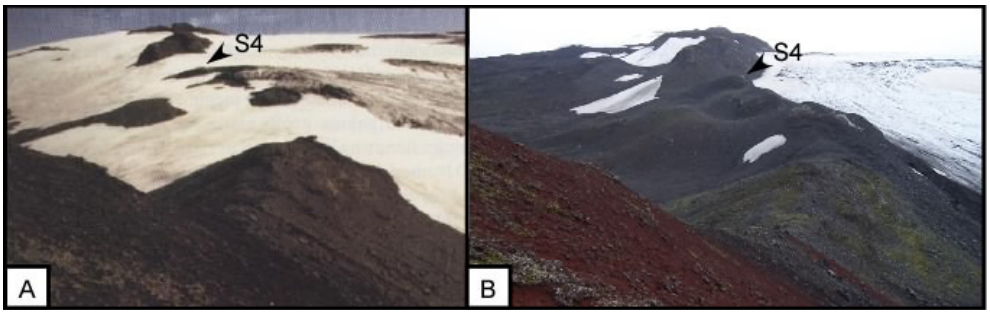

Figure 4.1: Pictures taken from the south side of Rauðhyrna A) by Jón Jónsson around 1990 (Jónsson, 1998) B) by Ronni Grapenthin in 8.8.2008. Glacial retreat has exposed sections of the lower NW part of the ridge. Arrows indicate the location of segment S4 for comparison, see map Figure 5.1.

4.2 Geographical and stratigraphy mapping

The first aim was to survey and map systematically the ridge describing the geological and physical aspects of the structures there encountered. This was done in field trips in the companion of one or two mountaineers in which the ridge was surveyed by foot and key structures measured, photographed, described, sampled and located geographically using a hand held navigation GPS (horizontal accuracy approx. 10 m).

For the purpose of systematic analysis, organization of data and description, the silicic ridge was divided into 12 segments (Figure 5.1). The size, volume and aspect ratio of each segment are defined in Table 5.2. Each segment was then analyzed on the basis of 1) surface structures: lobe aspect ratio, slope and morphology of marginal facies, arrangement of cooling structures (joints) in the outcrop, morphology of surface structures, environmental constrains for these products (subaerial or subglacial) 2) internal structures: Cooling joint pattern and distribution, vesicularity, crystallinity and flow-related features. Rauðhyrna, the tephra mound N of segment S7 and the north lava flow are sectors connected to the ridge and reflect products created by the eruption at synchronous time or before/after the formation of the main silicic ridge. Following I observed possible evidences for the flow of meltwaters as flood plains and gorges. The data was added to maps and the structures compared to known examples of ice-volcano interaction as Lescinsky and Sisson (e.g. 1998); Lescinsky and Fink (e.g. 2000); Tuffen et al. (e.g. 2001) and the flow emplacement dynamics revealed in the surface and internal structure of the silicic flow compared to known studies of this genre (e.g. Goto and McPhie, 1998; Thordarson and Self, 1998; Harris et al., 2004; Maeno and Taniguchi, 2006; Tuffen et al., 2001). This work was conducted with the aid of aerial photographs, older maps and scientific articles.

4.3 Radio-echo sounding

A mobile radio-echo sounding (RES) equipment (Mark II) was directed by foot on selected locations parallel to the ridge to estimate the ice thickness and to determine the actual thickness of the ridge still embedded in the glacier. Instrument handling was conducted as described in Sverrisson et al. (1980) and calculations associated to the RES were done by Eyjólfur Magnússson at the University of Iceland (see appendix B).

The RES technique operates through the emission of a radio wave which

propagates through air and into the ice sheet, and is reflected off any boundaries separating media with differing dielectric properties (Sverrisson et al., 1980). The velocities of radio waves in ice (168 m μs-1) and air (300 m μs-1) are known and, where a glacier bed echo is recorded, time delay is thus converted to ice thickness. Mark II operates at frequencies between 2 and 10 MHz, the range is from 30 to 400 m and the range resolution is 8 m.

4.4 Petrographic analysis and petrology

Samples collected at Skerin ridge and surroundings (see map Figure 5.1), were labeled and analyzed. Firsly in hand-specimen, secondly in thin sections and thirdly through geochemical analysis. Hand specimens were firstly described with the aid of hand-lens in terms of texture, phenocrysts, vesicularity and general structure of the specimen (Table 5.3). A total of 25 samples were analyzed with XRF and 17 of these were selected for thin-section analysis. Thin sections were prepared at the University of Edinburgh and examined by the aid of petrographic microscope (Ortholux 2 Pol BK, Leitz Wetzlar-Germany) at the University of Iceland. Modal percentage of the groundmass and phenocrysts was determined using model sheets. The geochemical analysis was made with XRF, X-ray Fluorescence at the University of Edinburgh for both major and trace elements (see Tables 5.4, 5.5, 5.6 and 5.7). Trace elements are included for completeness, not utilized in this thesis. The procedure and precision is described in appendix A.

4.5 Methods for calculating meltwater produced in a subglacial eruption

Order of magnitude estimates of ice melting rates and volume of meltwater created by the eruption can be made if the mode of eruption is established (effusive/explosive). Such estimates require knowledge of physical properties of the lava (eruption temperature, density, thermal diffusivity, viscosity)(see Table 4.1).

Volume constrains of the Skerin ridge where acquired with direct calculations (height, width and length), were the area was measured from aerial photographs and the thickness with the aid of pictures, GPS and ice-radar (RES). Useful properties (e.g. ice density ρ_i, density of meltwater ρ_w, density of magma ρ_m and viscosity μ are from known examples and are listed in Table 4.1.

Products of subglacial eruptions provide useful clues about the energy dissipated in the eruption that can be used to estimate the volume of ice melted

Symbol		Units		
Δt	eruption time	s	Properties of ice	
Δb	canyon width	m	Ti	0°C
h	ice thickness	m	ρi	917 kg m^{-3}
l	length of canyon	m	Properties of trachyte magma	
Q	melting rates	m^3/s	T_l	900-950°C
F	effusion rates	m^3/s	p_m	2500 kg m^{-3}
Vi	volume of ice	m^3	μ_m	10^4 - 10^7 kg m^{-1} s^{-1}
Vw	volume of meltwater	m^3		
h_d	half dike thickness	m		
x_d	length of the dike	m		
g	gravitational acceleration	9.8 m s^{-2}		
μ	dynamic viscosity	kg m^{-1} s^{-1}		
ρ	density	kg m^{-3}		
ρ_c	density of the crust (Iceland)	2700 kg m^{-3}		
ρ_w	density of water	998.23 kg m^{-3}		

Table 4.1: Physical properties of lava and ice (Hoskuldsson and Sparks, 1997).

(V_i) and the volume of meltwater (V_w) (Gudmundsson, 2003). A very simplified model for an eruption under thin ice (<100-150 m) in Gudmundsson and Högnadóttir (2005) was used and is based on the gradual growth and melting of an ice canyon with width Δb in time Δt. Melting rates Q (m^3/s) are expressed as

$$Q = \frac{\rho_i}{\rho_w} hl \frac{\Delta b}{\Delta t} \tag{4.1}$$

were ρ_i is the density of ice, ρ_w is the density of water, h the height of the ice canyon and l the length of the fissure.

The effusion rate of the eruption that created Skerin ridge is an unknown parameter. Constrains on the order of magnitude can be made by combining observations of the relationship between dike thickness and dike length (Gudmundsson, 1983), and model of buoyancy rise of silicic magma in a dike proposed by Hoskuldsson and Sparks (1997). The effusion rates F (m^3/s) are then determined as (from Hoskuldsson and Sparks (1997) modified by Tuffen and Castro (2008))

$$F = \frac{2(\rho_c - \rho_m) g h_d^3 x_d}{3\mu} \tag{4.2}$$

where ρ_c is the density of the crust ($\approx$2700 kg/m^3 in Iceland), ρ_m the magma density, g acceleration of gravity, x_d the length of the dike, h_d half dike thickness (h=2.5 m expected for a dike with length 2.5 km), μ viscosity and η is the average aspect ratio (x_d/2h) of the conduit (estimated to be around 500 for rhyolitic dikes in Iceland (Gudmundsson, 1983)).

Chapter 5

Field observations and data analysis

In this chapter the field observations conducted on the Skerin ridge are presented beginning with a description of the ridge as a whole then moving towards a more detailed account on the volcanic architecture of individual ridge segments and related structures. Petrographic descriptions of representative samples along with whole-rock major and trace element chemical analysis are also presented.

5.1 Overall description of the ridge

5.1.1 Bedrock and close vicinity

Skerin ridge lies on a greatly north trending slope that is truncated at 400-500 m elevation by steep lower slope that reaches down to the lowlands of Markarfljót. Gullies reveal a bedrock composed of hyaloclastites and lava flows that exhibit evidence of being subjected to a range of cooling rates. On top of this bedrock are thin lava flows that advanced into the valleys on the north margins of Eyjafjallajökull. Certain sectors of these flows are intermingled with tuffs and in these areas the lavas exhibit evidence of strong quenching, while in other locations the lava flows bear characteristics of subaerial flows. Glacial activity is clearly visible on the slopes with moraines and marginal dead-ice zones whereas areas recently uncovered by the glacier are covered by till and boulders highly striated. Soil erosion and washed bedrock most likely attributed to flooding is prominent at the Litlaheiði plains (see map Figure 5.1).

The ridge forms a glacial divide. On the south, the glacier is over 80 m thick and flows down a 7-12° slope towards west-northwest. On the north side the glacier is much thinner (<40 m) with a slope of 13-15° towards north. Deep gullies cut into the steep lower slopes on both sides of the ridge: Akstaðaá gorge

on the west side and Miðtunga gully on the east (see RES measurements attached to the Appendix B).

Two lava flows are found downslope the scoria deposit Rauðhyrna and were analyzed in this study (samples ESK10 and ELAVA08 see map Figure 5.1). On the southwest side is a lava flow of basaltic composition (sample ESK10) with well-developed columnar joints (15-30 cm wide) and a scorious surface and a basal crust. The columns are mostly orientated vertically in the outcrop but features sections with chaotic and prismatic patterns. Macrophenocryst content is between 15-20% modal. Two lobes were identified lying on top of each other. The lava flow appears to be trending between 240-290° W. Large bodies of lava 20-40 m high, with well-developed columnar joints are exposed on the lower part of the southwest gully. These columns are dipping to the NE. On the north side of Rauðhyrna a large body of intermediate lava (basaltic trachyandesite) with vertical walls as high as 20 m high with small glassy columns ranging from 5-10 cm with subvertical orientation. Inwards these columns become microcrystalline of a bluish color (>30 cm wide, sample ELAVA08). These columns have a general southwest dip of 40° (Figure 5.2). The lava contains 15-20 modal % of plagioclase macrophenocrysts. The section further northwest of these lava flows build the older hyaloclastite plateau of Eyjafjallajökull.

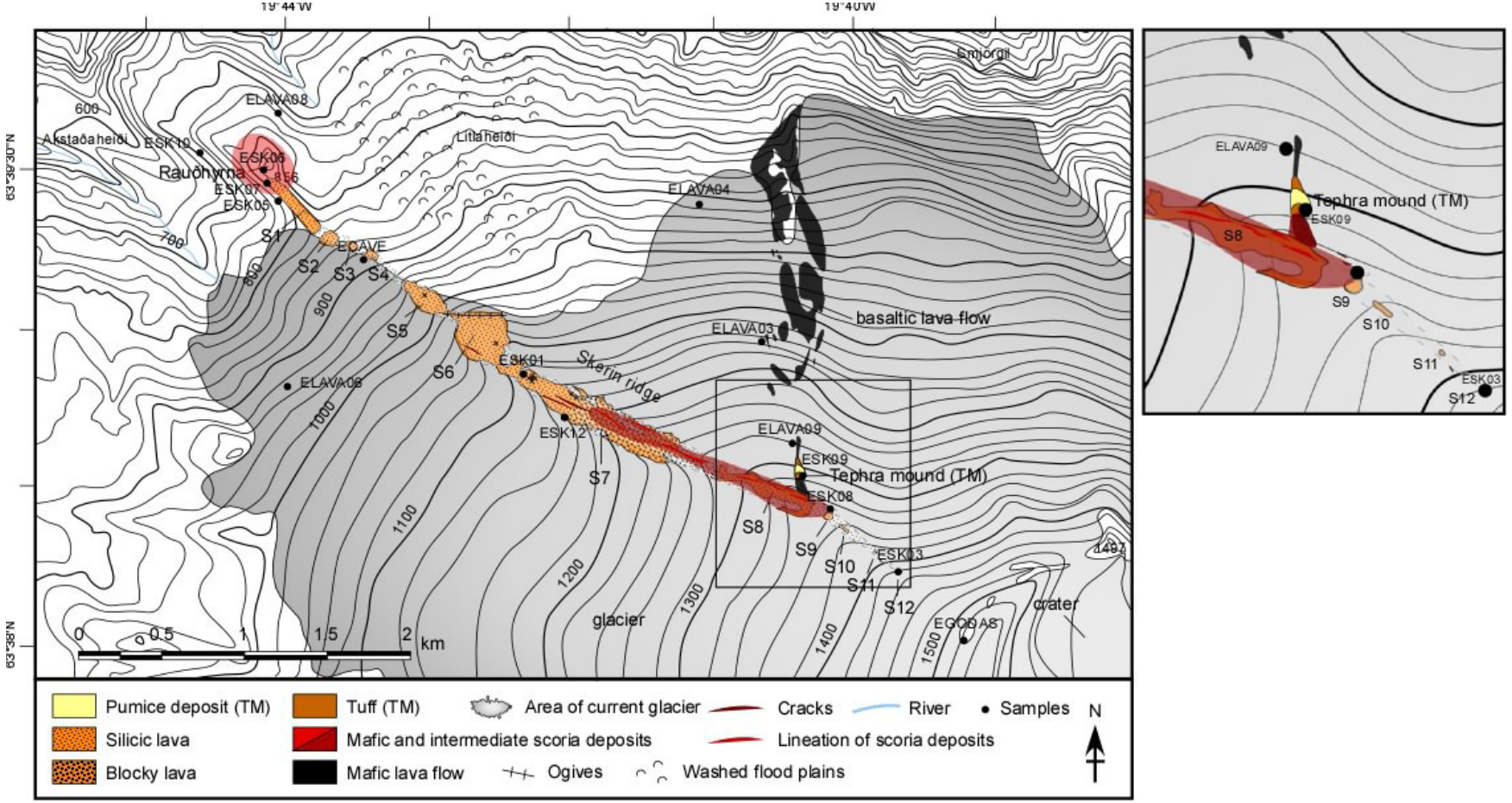

Figure 5.1: A map of the northwest sector of the Eyjafjallajökull ice cap, showing the location of the Skerin ridge as well as the structure and lithology of key segments found on the ridge. The ridge was divided into segments (S) to enable a more systematic analysis. A lava flow extends to the north and is described in this study. Map based on a SPOT 5 Image provided by Landmælingar Íslands.

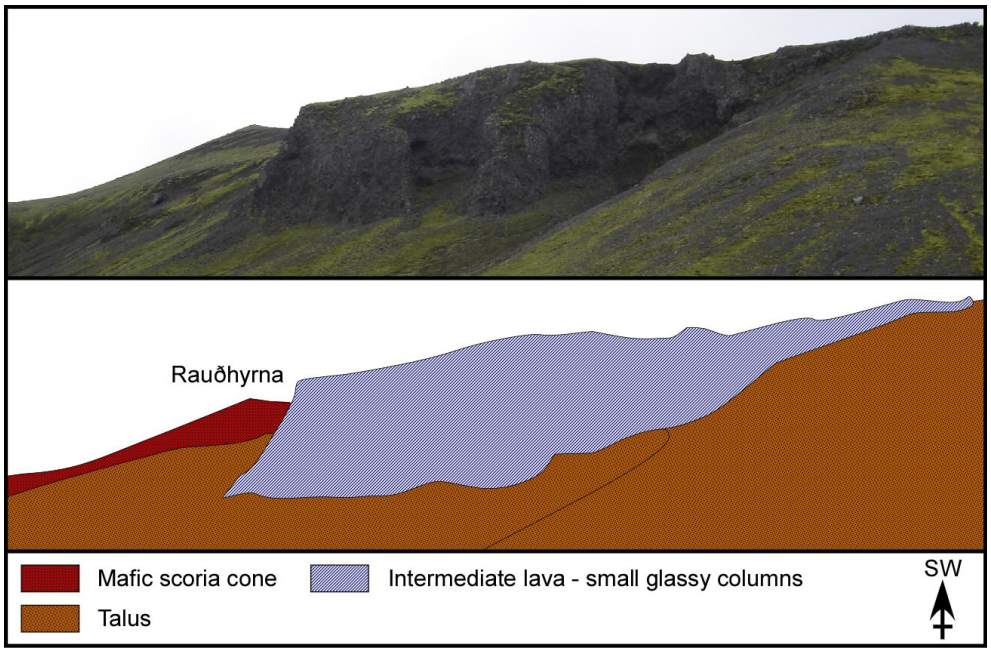

Figure 5.2: Picture and sketch of the north side of Rauðhyrna. A large body of lava over 15 m high with vertical walls of glassy columnar joints forms slightly beneath Rauðhyrna. This rock is of intermediate composition. Rauðhyrna appears in the background.

Two nunataks were also sampled, namely ELAVA06 on the south side and ELAVA 04 (Figure 5.1) on the north side for comparison with Skerin lithologies. Both lavas are highly striated.

5.1.2 Skerin ridge

The Skerin ridge and its immediately associated volcanic features can be divided into:

i) The 4.5 km long, on average 0.1 km wide and 80 m thick Skerin ridge, composed of silicic lava. The SE top of the ridge is partly covered by red scoria deposits. The silicic lavas have an aspect ratio of ≈1.0, widest in the center of the ridge (300-meters) but tapers out toward northwest and southeast (Figure 5.1). The ridge features a slight northward curvature at the northwestern end and its outlines are irregular and undulous at amplitudes of 10-20 meters (Figure 5.3).

Detailed inspection of the silicic ridge shows that the central and upper parts consist of massive light colored lava with remnants of glassy margins along its subvertical sides; the flow top is characterized by crystalline breccia and ogives. The silicic lava has a volume of about 0.043 km^3 and is most prominent at the northwest section of the ridge where the glacier margins has retreated the most. The silicic lava consists of interconnected lobes in the central part of Skerin and continues as a series of 3-4 small mounds at both ends. In the upper reaches the

silicic lava is partly covered by red scoria deposits with volume of ≈0.002 km^3 (volume calculated for a triangular prism) of trachyandesite composition (Figure 5.1).

ii) The Rauðhyrna scoria cone of basaltic composition at the northwestern end of the ridge, now completely free of the glacier.

iii) The north lava flow: A narrow, 2 km long northwards trending lava field, extending from a point at about 1350 m elevation near the southeast end of the ridge.

iv) At elevation of 1350 m a.s.l, a small north-trending mound consisting of tephra layers (tephra mound). Estimates of overall volume of each unit is given in Table 5.1.

Name	Length (km)	Volume (10^6 m^3)	Composition
Skerin ridge	4,5	~43	trachyte
Scoria cover	~2	~2	trachyandesite
Rauðhyrna	~0,4	~10	basaltic
North lava flow	~2	~13	basaltic
Tephra deposits	~0,15	<0,05	trachyandesite/trachyte/basaltic

Table 5.1: Skerin and associated volcanic features: Volume and composition.

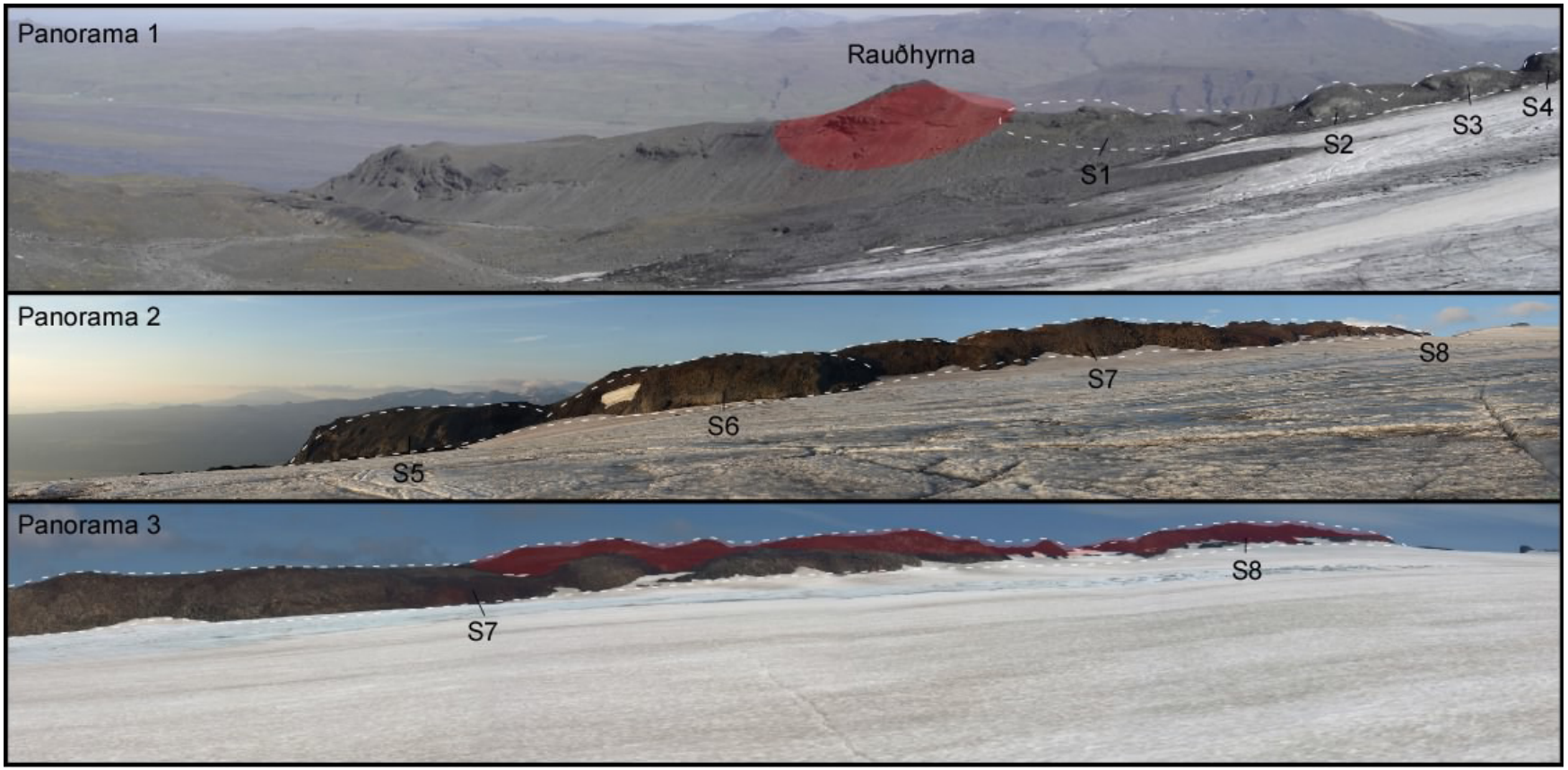
Panorama 1
Rauðhyrna
S1
S2
S3
S4
Panorama 2
S5
S6
S7
S8
Panorama 3
S7
S8

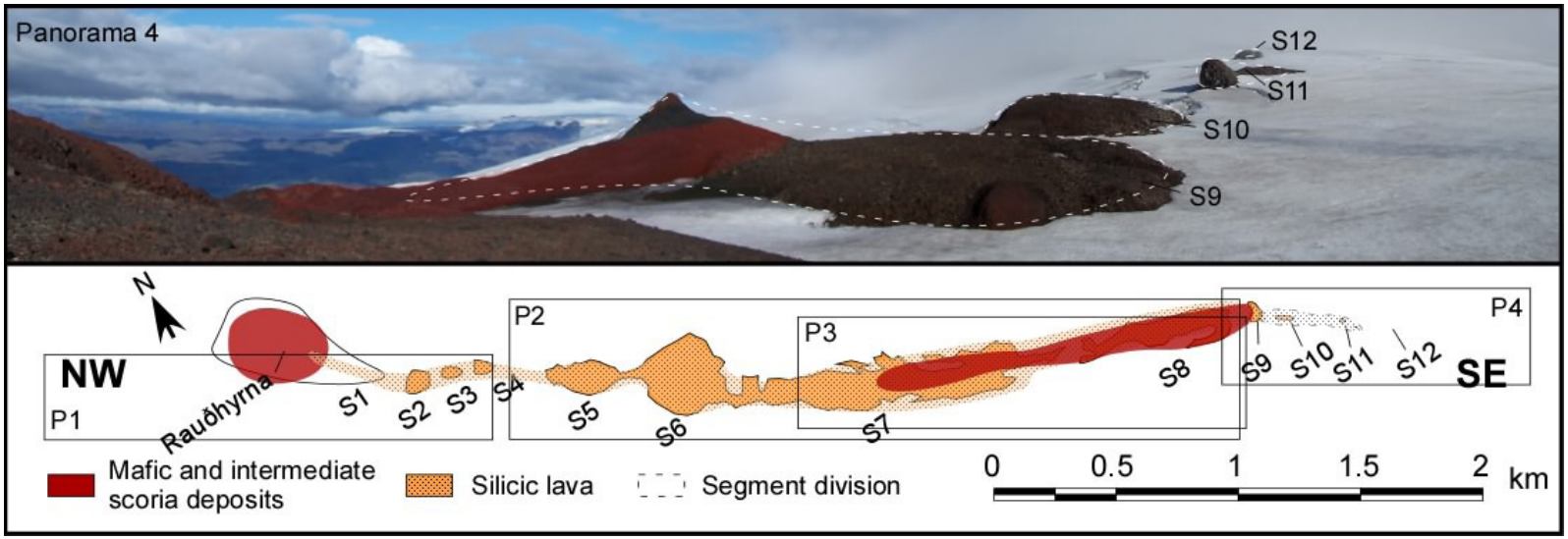

Figure 5.3: Skerin ridge depicted in four panorama pictures and a map. Dots mark the silicic lava, the red area marks the scoria deposits and each segment is delineated by dashed lines in the panorama pictures. Panorama 1 shows the NW end of the ridge beginning at the scoria cone Rauðhyrna and showing segments S1 to S4. Panorama 2 extends from segments S5 to S8. Panorama 3 shows segments S7 to S8 with better view of the scoria deposits. Panorama 4 shows segments S9 to S12 at the SE end of the ridge.

5.2 The silicic ridge-segment: description and internal structure

As described in chapter 4, observations on Skerin ridge led to a division of the ridge into segments in order to simplify descriptions of lithologies and structures. The word segment is here used for a portion or section that forms a distinct geographical feature. Additional units are the Rauðhyrna, the tephra mound and the North lava flow. Picture 5.3 illustrates this division. The size and width of each segment is presented in Table 5.2.

5.2.1 Segment S1

Segment S1 is long but narrow (approx. 400 x 45 m and max. 20 m thick) that extends from S2 with an undulous profile structure and is partly embedded in the scoria cone Rauðhyrna ($\approx$ 25% of the lobe) (Figures 5.3 and 5.4). The south side is highly eroded with accessible outcrops while the north side and top is covered by glacial till. The segment is composed of light colored trachyte (samples ESK05 and ESK07).

The interior of the segment exposed above the talus on the south side is formed mainly of parallel, wedge shaped plates 30-60 cm (or larger) in diameter and 0.5 to 2 cm thick. At the SE margins of Rauðhyrna, an outcrop in the silicic lava shows an internal structure that grades from small glassy regular or well-defined joints, about 15-20 cm, on the surface followed by wedged platy joints with joints about 60 cm wide and a massive interior with unclear jointing. The glassy crust is non vesicular while the inner core shows folded flow bands and vesicular zones featuring megavesicles and vesicle clusters (regularly about 15 cm but two sizing over 60 cm) aligned parallel to the folding. Two cross sections, S1a and S1b, were measured within this segment (Figure 5.5). The lava that extends into the scoria cone becomes almost entirely platy at that locality (sample ESK07). The basal zone is thin (10-20 cm) highly vesicular with no breccia covering the underlaying scoria. Scoria lies on the top of the lava as well covering the entire lobe (Figure 5.4). Porphyric dark gray xenoliths about 5 cm in diameter are found embedded in the lava at several localities.

5.2.2 Segment S4

This segment is in overal a structure very similar to S2 and S3. It is a hemispherical mound rising approx. 30 meters above a talus of glacial till and has the

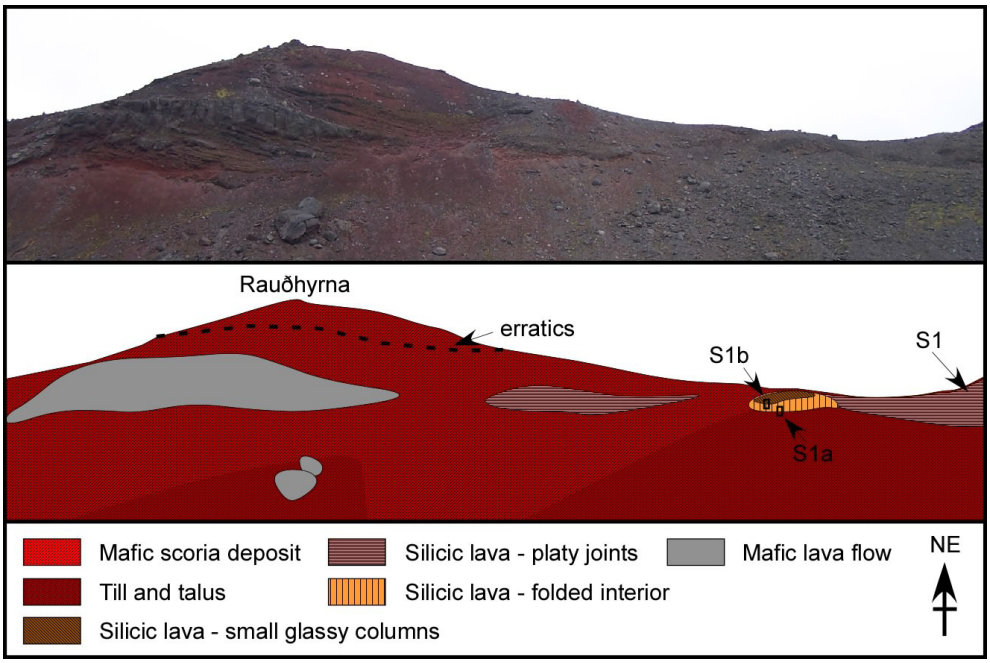

Figure 5.4: Picture and sketch of Rauðhyrna. Rauðhyrna is a scoria deposit located on the NW end of the ridge with lava flows embedded in it. A large part of the cone has been eroded away by the glacier. Signatures of the outlet glacier which flowed by the S side of Rauðhyrna are erratics on the upper part of the deposit, highly eroded margins and striations on the basaltic lava lobes attached to the upper south part of Rauðhyrna. A dashed line shows the upper extent of the erratics. A silicic lava lobe extends from SE into the scoria with smaller lava layers on top. Cross sections S1a and S1b were measured within the silicic lava and their location is marked with frames.

characteristic of being completely covered by a glassy crust with columnar joints radiating toward the interior (Figure 5.6). Glacial till covers part of the top.

The glassy crust has closely spaced joints (typical column width is 10-20 cm) extending 0.25 - 1 m inwards perpendicular to the margin. The glass is of trachyte composition with feldspar macrophenocrysts amounting 10-15% modal. Inwards the rock changes from glassy (hypohyaline-crystallinity 10-50%) to light colored microcrystalline rock (hypocrystalline - crystallinity 50-98%). One out of three and sometimes four joints extend further into the core forming columns, 30-80 cm in diameter extending inwardly several meters ($\approx$ 5 m). We describe these as medium columns where their sizes vary between the small glassy columns of the crust and the large columns of the flow interior described further in this chapter. The columns tend to exhibit prismatic orientation although with a strong downward curvature and strong tendency towards vertical orientation. On the northwest side of S4, parallel wedge shaped plates 30-60 cm in diameter 0.5 to 2.0 cm thick form close to the base of the segment. This platy zone is about 1.8 m thick and 20 m long in the mound. This architecture is representative for

Segment	Approx. length (m)	Approx. width (m)	Approx. thickness (m)	Volume (10^6 m^3)	Aspect ratio[a]	Composition
Rauðhyrna	430	320	80	11,01		basaltic
S1	410	50	20	0,41	0,4	trachyte
S2	90	110	50	0,50	0,5	trachyte
S3	90	50	30	0,14	0,6	trachyte
S4	80	50	30	0,12	0,6	trachyte
S5	350	140	90	4,41	0,6	trachyte
S6	410	340	90	12,55	0,3	trachyte
S7a	70	50	90	0,32	1,8	trachyte
S7b	80	100	80	0,64	0,8	trachyte
S7c	500	170	70	5,95	0,4	trachyte
S7d	790	200	70	11,06	0,4	trachyte
S8	710	140	60	5,96	0,4	trachyte
S9	90	90	60	0,49	0,7	trachyte
S10	90	30	60	0,16	2,0	trachyte
S11	20	20	60	0,02	3,0	trachyte
S12	10	20	60	0,01	3,0	trachyte
Tephra mound	150	30	10	0,05		Interm. /trachyte/basal
N-lava flow	1780	370	20	13,17		basaltic
Scoria dep.[b]	1400	150	20	2,10		intermediate
Maximum:	1450 (S7)	335	100	12,5	3,0	
Minimum:	10	17	20	0,01	0,3	
Average:	253	104	61,33	2,8	1,0	
Total length ridge (m):		4220	Total (ridge)[c]	56		
			Silicic ridge	43		
			Basaltic	11		
			Intermediate	2,1		

a) Aspect ratio is the lobe thickness divided by the lobe width.
b) Volume calculated for a triangular prism.
c) Total volume of the ridge does not include the north lava flow and the tephra mound.

Table 5.2: Volumes of the segments and sectors at Skerin ridge

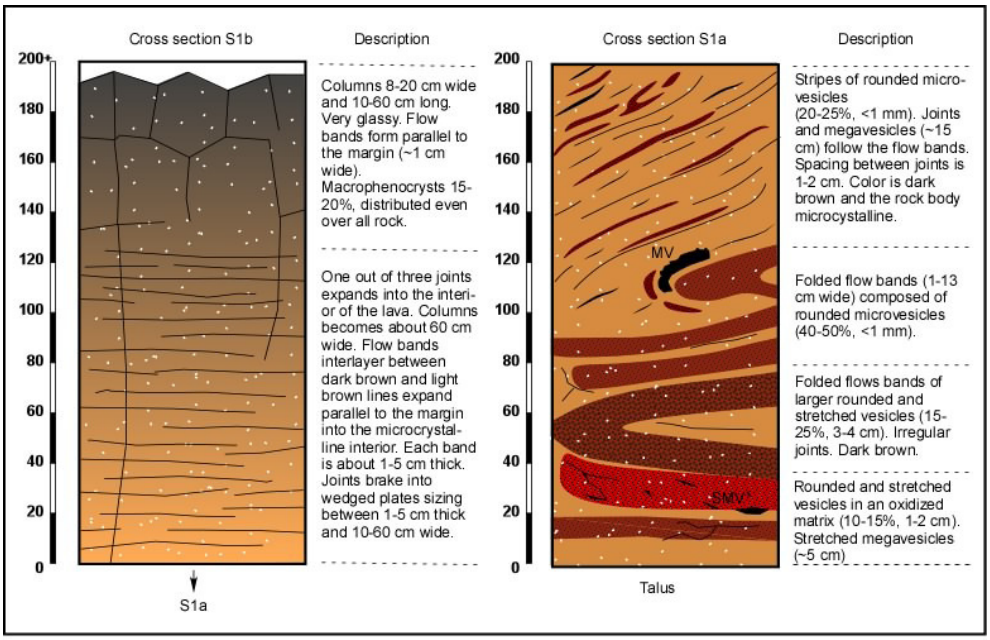

Figure 5.5: Illustrated graphic logs of the internal structure seen in cross sections S1a and S1b located in the silicic lava SE of Rauðhyrna (Figure 5.4). The lava is characterized by a glassy surface crust of close-spaced columns changing inwardly towards larger columns, platy jointing (S1b) and folded flow bands (S1a). Segregation structures related to flow emplacement are in the form of megavesicles (MV) or stretched megavesicles (SMV) found parallel to the folded flow bands. Megavesicles range from 5 to 15 cm with the exception of one location which had two vesicles sizing about 60 cm. Macrophenocryst corresponds to 10-15% modal in the cross sections.

segments S3 to S4 although mounds S2 to S4 and part of S1 have a platy zone that extends almost throughout the entire outcrop.

S4 contains a 15 m long and 33 m wide cave at its NW end (Figures 5.7A). The floor to the ceiling height is up to 10 m. Part of the northwest side of the cave has been eroded leaving an opening of about 1x1 m. A mound of lava characterizes the floor formed entirely by lava, not from rock that had fallen from the ceiling (Figure 5.7D). A concave flow ledge (about 10 cm thick and 2 m wide) sticks about 0.5 m outwards on the south west end of the mound. Several surfaces in the cave are oxidized. Flow lines on the ceiling have a strong northwest trend with a downward push (Figure 5.7A). Flow bands of interlayers of light colored microcrystalline and glassy texture form parallel to the wall (Figure 5.7B). Small stalactites made of coarse, low-density crunchy lava form on the ceiling and little stalagmites form on the floor and mound as well (<10 cm) (Figure 5.7C).

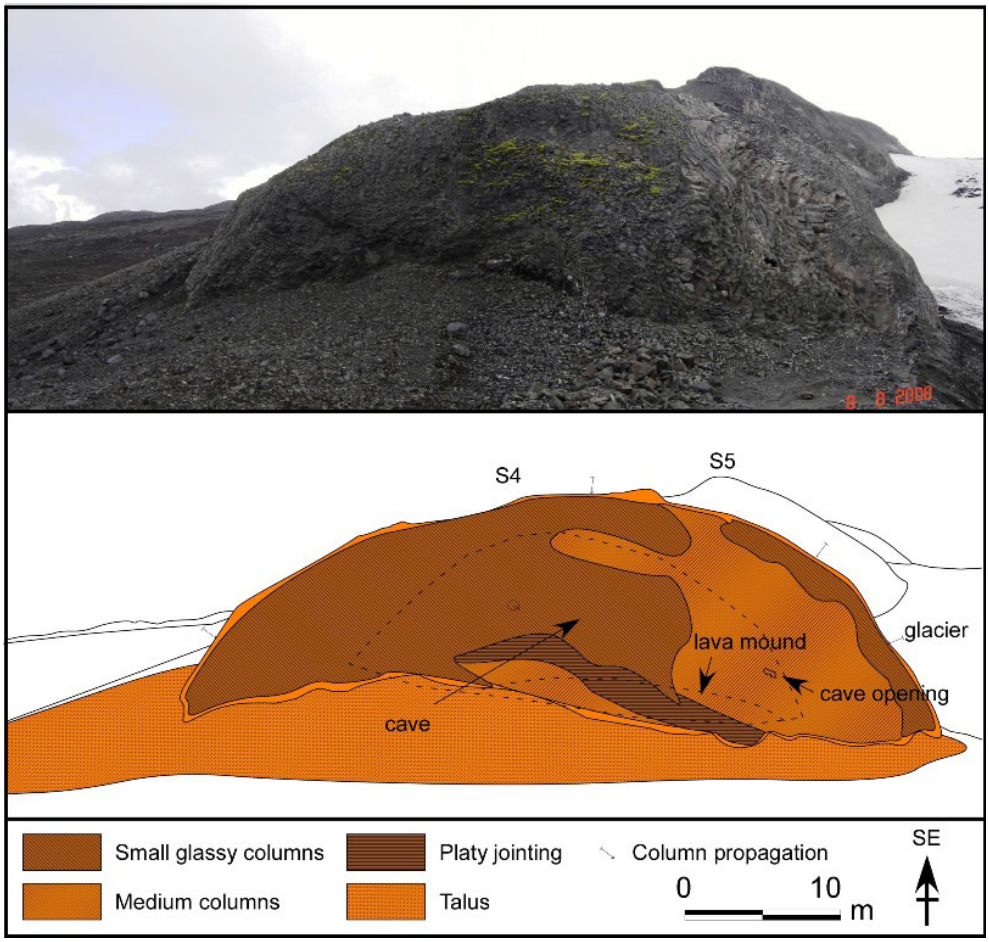

Figure 5.6: Sketch and picture of segment S4, view toward SE. The segment is covered with a well preserved glassy carapace with small columnar joints. Part of the carapace is eroded away at the NW face exposing elongated medium sized joints. Platy jointing mingles between the medium columns and the glassy crust. A cave about 33 m wide (with a SW-NE trend), 15 m long and about 10 m high forms the interior of S4 (marked by dashed lines). The opening of the cave is found at the eroded surface where the medium columns are exposed. The cave and the lava mound in the cave are shown with dashed lines.

5.2.3 Segment S5

Segment S5 is much larger than the mound S4. It is elongated (approx. 350 x 140 m) and reaches elevations of 80 m above the glacier with steep vertical walls on the south, north and west margins. The segment connects through a narrow neck with the adjacent segment S6. A brecciated flow top partly covered by green moss forms the upper surface of the segment (Figure 5.8). The breccia is composed of wedge shaped blocks of bluish/gray lava up to 1 m in diameter (av. 0.3-0.5 m). The lava is vesicular (microvesicles <0.5 mm rounded and elongated) aligned with weak alternating bluish/reddish and light colored bands. Glassy and crystalline light colored to brownish lava make up the breccia as well. No evidence of glacial erosion are found on top of the segment. A structure that

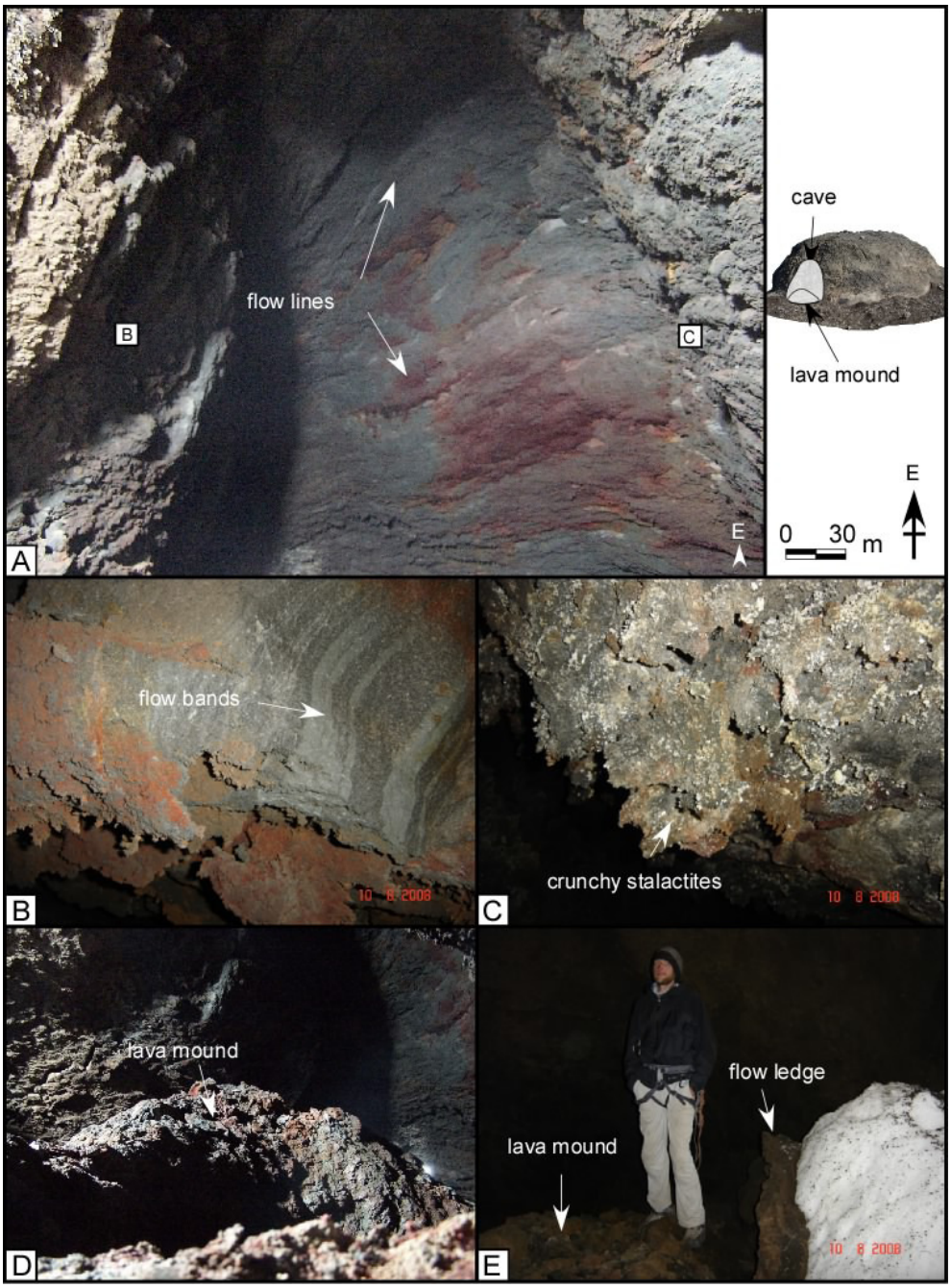

Figure 5.7: Pictures showing the interior of the cave at S4. The cave is located at the NW end of the segment as illustrated on the sketch. The ceiling is about 10 m high and holds flow lines with a NW/SE trend (A) as well as flow bands (B) and crunchy stalactites (C). A lava mound forms on the floor of the cave (D) with a surface of small crunchy stalagmites. A flow ledge is found on the W end of the cave beside the lava mound (E).

we identify as ogive is found within the breccia; a block of massive lava ripped from the ground, dipping into the breccia with a steep face lining upwards and SE (an example from segment S7 is shown on Figure 5.13). The ogives are bluish/gray in color, vesicular (microvesicles <0.5 mm spherical and elongated) arranged horizontally parallel to flow bands and microcrystalline with feldspar

macrophenocrysts content of about 15% modal. Individual blocks in the vicinity of the ogives reach size of 1 m^3.

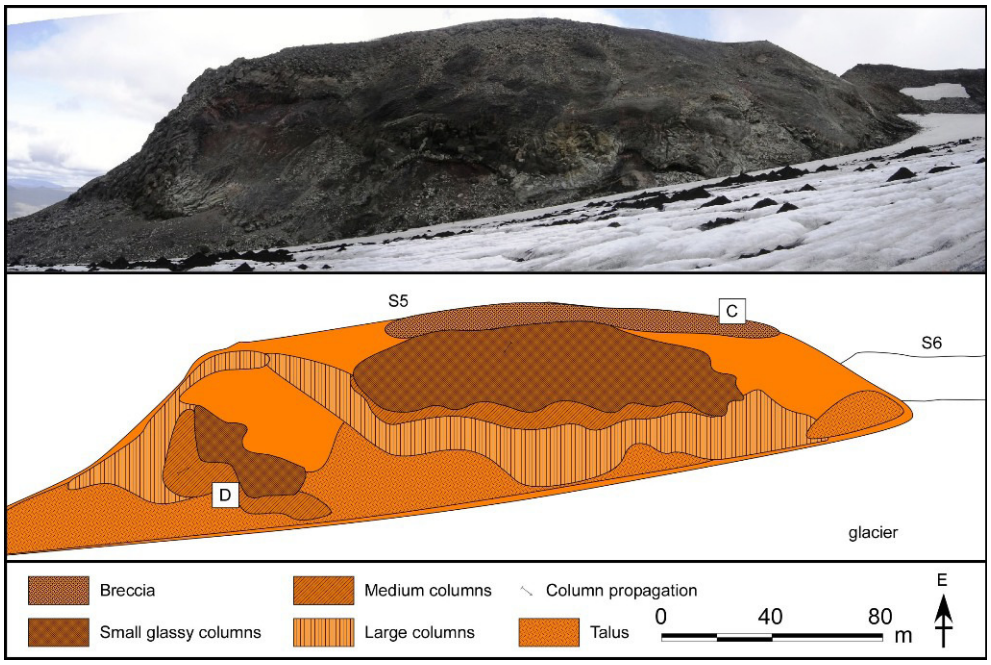

Figure 5.8: Segment S5 as seen from the SW side. Small glassy columns form the lateral carapace. As illustrated on the sketch the lower part of the segment eroded by the glacier is characterized by medium and larger columns. On top of the segment lies a well preserved and uneroded breccia covered partially with moss. Figure 5.10 shows a closeup of areas C) and D).

Vertical to subvertical margins are characterized by a glassy surface crust with columnar joints perpendicular to the margin as on segment S4. The south side has a large area with a preserved glassy carapace. Lower in the segment, parallel to the glacier margins, are exposures of a more massive microcrystalline interior with columns 30-80 cm in diameter (medium columns, Figure 5.10D). In the massive interior, one out of three or four joints extends into the interior forming columns that are 2 to 3 m wide (Figure 5.10A). The north side is almost entirely exposed where the glacier has retreated the most (Figure 5.9). The northwest end of the segment has well preserved vertical walls of small glassy columnar joints dipping subvertically into the rock (Figure 5.10A). Only in one outcrop the interior characterized by larger columnar joints is exposed (Figure 5.10A). No exposed basal crust was observed.

5.2.4 Segment S6

S6 is the widest formation within the ridge, reaching width of 335 m, length of 410 m and with over 80 m high steep cliffs exposed on its south side (Figure 5.11). The north side is still largely covered by the glacier and thus poorly

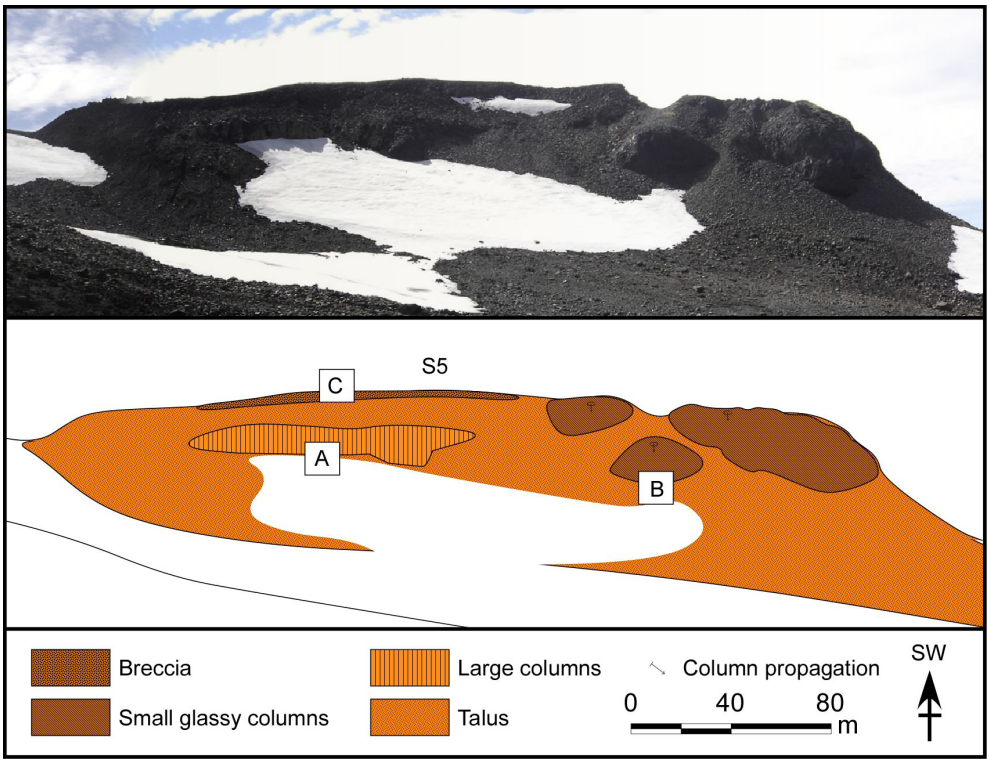

Figure 5.9: Picture and illustrated sketch of the N side of segment S5. Three structures are characteristic for this side; the breccia on top of the segment, small glassy columns and the large columns. A closer look at areas A), B) and C) is shown in figure 5.10.

accessible. A brecciated flow top identical to the breccia described in S5 with a partial green moss cover forms the surface of S6. A row of ogives is found on the north side. Breccia surrounds the ogives often in piles and forming ridges. No indications of glacial erosion are evident on top of S6. The south side of the segment is highly eroded exposing a massive microcrystalline flow interior with columns spacing reaching 2 to 3 m wide in places (Figure 5.12). Feldspar macrophenocrysts (15% modal) are distributed evenly throughout the segment. Flow bands, 1-2.5 cm wide, propagate into the interior parallel to the margin. The bands have homogeneous color, are wavy and brake into plates or larger blocks if the bands are well cemented together (Figure 5.12). Vertical joints with a spacing of 1.5-2 m extend downwards from the flow top breccia into the interior. Smaller joints lie perpendicular to the vertical joints and follow the flow banding. No exposed basal crust was observed.

5.2.5 Segments S7 to S12

Segments S7 and S8 are both long (approx. 1450 and 700 m) with an average width of 130 m and thickness between 60 to 100 m. Half of segment S7 and the entire segment S8 is covered by scoria deposits. Two elongated about 200

Figure 5.10: Pictures of segment S5 (see figures 5.8 and 5.9 for location). (A) A small outcrop exposing rocks with large columns on the N side of S5. (B) Glassy carapace of columnar joints subvertically aligned forming the outermost crust of the ridge. (C) Breccia with a partial moss cover forms the surface top of the segment. The breccia shows no marks of glacial erosion. (D) A large area on segment S5 with medium sized columns arranged chaotically but with a strong trend downwards.

m long cracks form parallel to the ridge on S7. A small pile of breccia trends parallel to the north margin while localized ogives form at the NW end of the segment. Large spherical to subspherical breccia (with average block diameter of 0.5-1.5 meters) formed by interbedded layers of massive light gray lava and reddish vesicular breccia type layers form on the south slopes of S8. Feldspar macrophenocrysts make 15-20% modal of the lava. Only a fraction of the upper part of the ridge is fully exposed, parts of it are covered by the glacier. Ice-radar measurements indicate that about 40-50 meters of the total 70 m height of the ridge in segments S7 and S8 are still embedded in the glacier.

Segments S9 to S12 form the tapering SE end of the ridge. These segments are presently nunataks in the glacier. Only a fraction of their top is exposed above the glacier. S11 reaches elevations of 4 m above the glacier with steep north and south sides exposing an interior of crystalline rock with large joints and platy structures. Till and fragments from glacial erosion largely cover these segments.

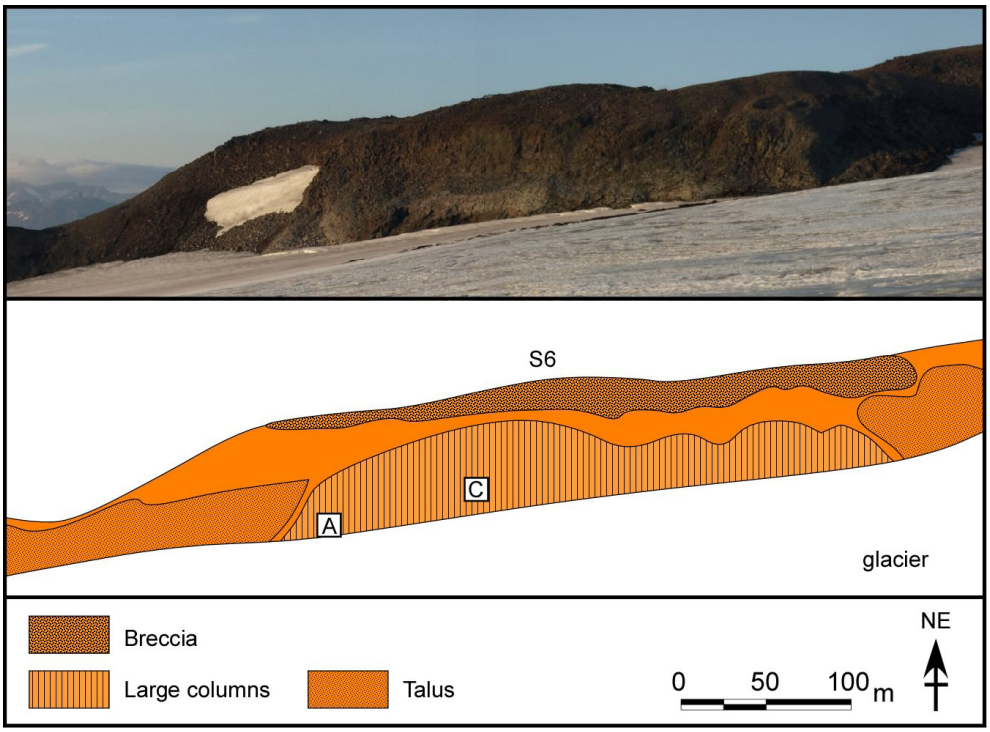

Figure 5.11: Segment S6 as seen from the glacier on the south side. Breccia and a row of ogives forms on top of the ridge and a massive structure of larger columns forms the interior. Figure 5.12 shows in more detail areas A) and C).

No glassy margins were found.

5.3 Scoria deposits

Scoria deposits are found in two locations at the Skerin ridge and their volume sums up to ≈0.02 km^3 (See map Figure 5.1 and Table 5.2): Rauðhyrna and layer partly covering the upper part of the ridge (segments S7, S8 and S9).

Rauðhyrna (856 m a.s.l., Figure 5.4) is of basaltic composition. The original shape of the deposit is no longer present since glaciers have removed large part of its crater. The glacier left erratics up to 840 m a.s.l. on the southwest margins of the scoria deposit and a semi-cirque on the north side. Rauðhyrna is formed by layers of compacted, welded vesicular scoria, interbedded with layers of wet, loose bombs of scoria, poorly vesicular (sample ESK06). These layers have an inclination of about 32°. The scoria has 10-15% modal of feldspar macropenocrysts. Within about 80 m radius from the cones center is characterized by red scoria (deuteric oxidation) while the scoria outside that zone is black. Gray/bluish lava lobes with thickness over 8 m are embedded on the southwest side of the cone. Glacial striations cut the sides of these lavas and fragments are left as erratics down in the valley. Glacial erratics and a small moraine are found on the top

Figure 5.12: Pictures of segment S6. Large columnar joints form the flow interior as seen on figures A) and C). These extend perpendicular to the flow surface into the interior. (B) Flow bands in the flow interior extending parallel to the surface creating lines of weakness less vulnerable to weathering which break into plates or blocks (B).

margins of the SW side of Rauðhyrna (Figure 5.4). The slope of the cone extends gently far north to the slopes break showing little evidence of glacial erosion except on the margins of the south side as described above.

A scoria deposit is also found at 1200 m a.s.l. with a triangular prismatic shape on top of the ridge and extends to approx. 1350 m (Figure 5.14). Scoria, accretionary lapilli and spatter lava are the building blocks of these deposits and a harder core of spatter and more coherent lava extends through the center following elongated lines parallel to the ridge (Figure 5.15A). Three channel shaped structures in the scoria lay open down toward the glacier, two facing north while one faces southwest (Figure 5.15B). Larger blocks of breccia (≈20 cm) make the

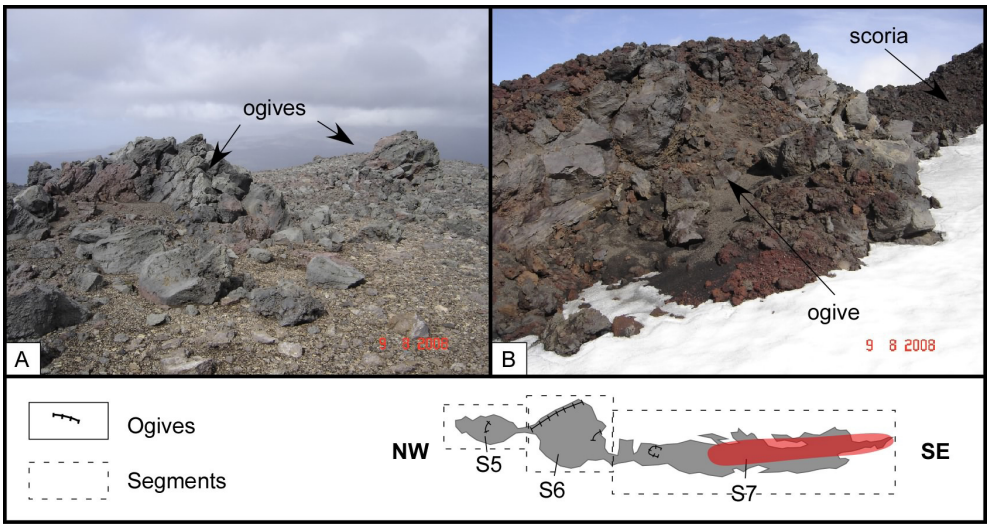

Figure 5.13: Ogives dipping into the surface on top of segment 7. These structures are found in various places on the top of segments S5 to S7. In some areas rows of ogives form surrounded by breccia lava as observed in the north section of S6 while in other places they are located as separate identities (see the map attached to the picture). These formations are characterized by large blocks of ripped lava reaching up to 2 m in height, dipping into the breccia (A). Picture B) shows a similar structure as observed on figure A) partially buried in scoria.

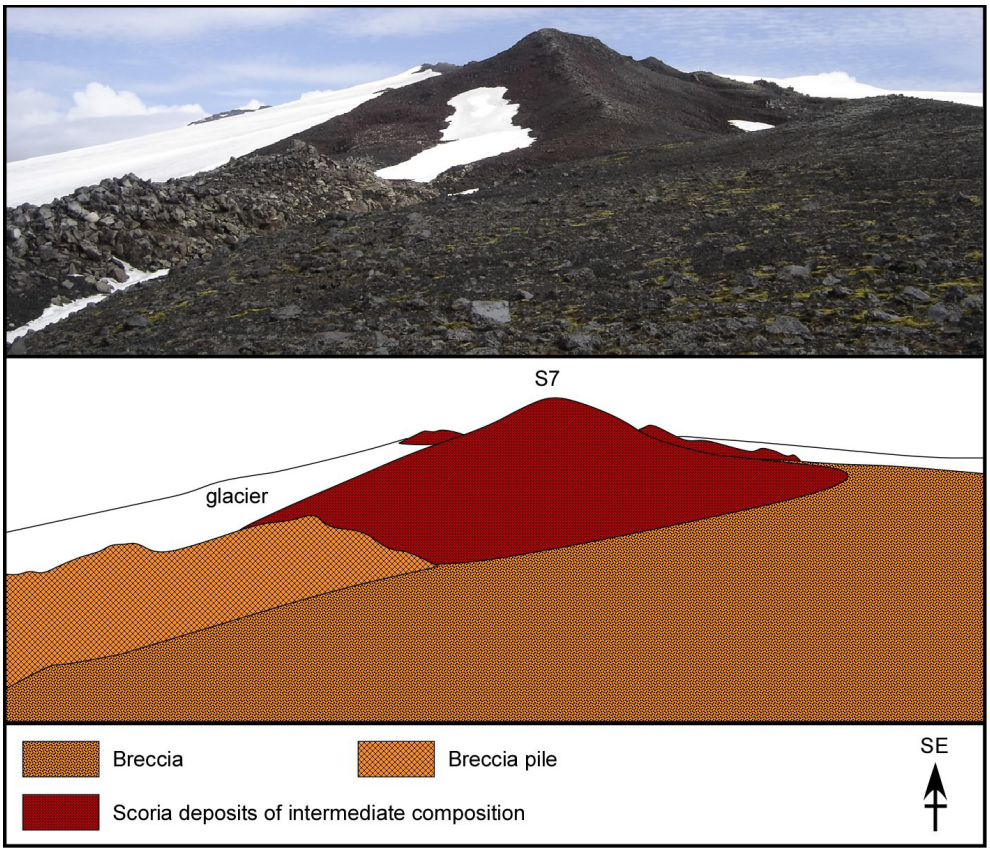

Figure 5.14: Picture and sketch shows a scoria deposit that lies on top of the main silicic ridge at segment S7. Breccia and piles of breccia form on the surface of S7.

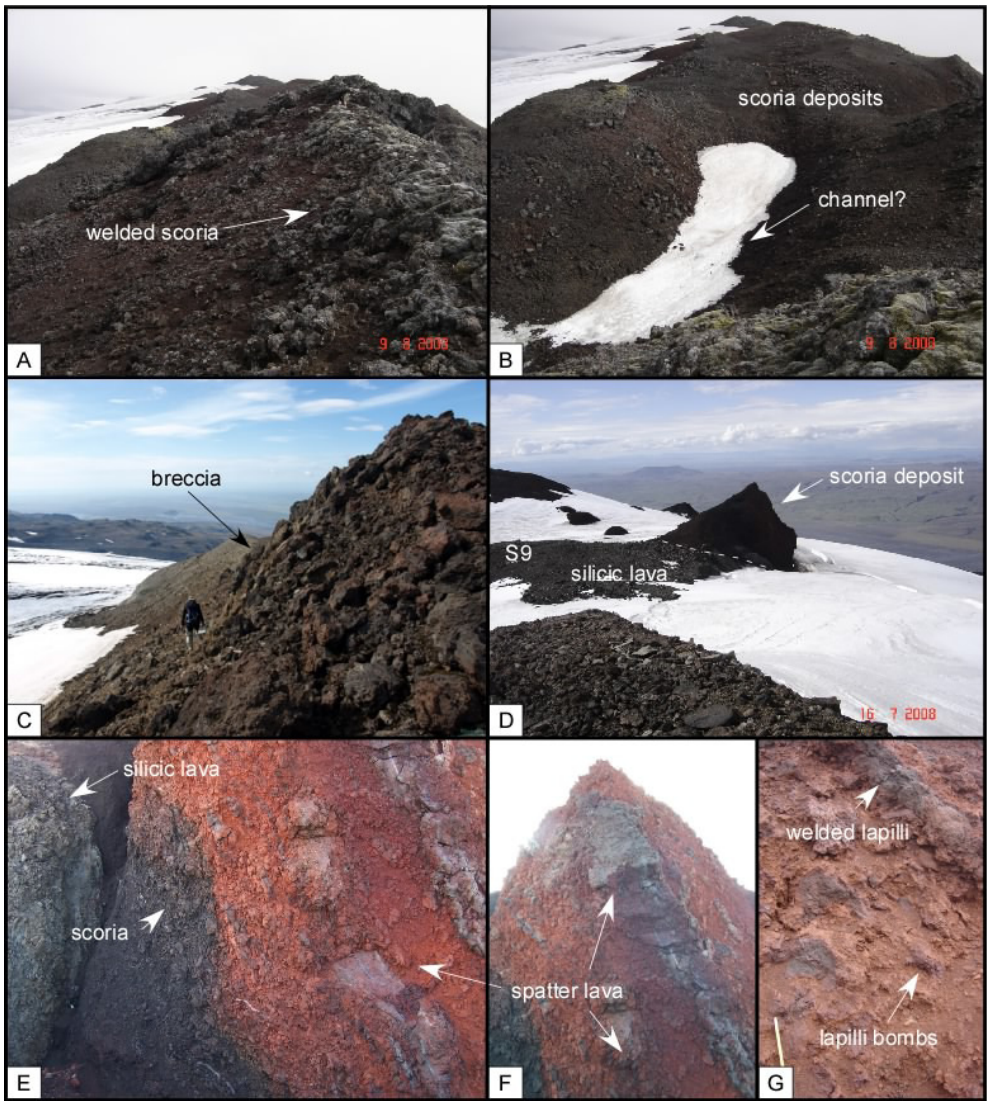

Figure 5.15: Pictures of the scoria deposits on top of the main silicic lava at the upper segments S7 to S9. (A) These deposits are characterized by scoria lapilli and a harder coherent core of spatter lava. (B) A few sections hold channel-like structures. (C) Large rhyolitic blocks of breccia are found in areas around and on sides of the main ridge. (D) Small scoria cone-like structure on top of the silicic lava S9. Its north face is largely eroded away leaving a well exposed cross section of its interior as shown on pictures E to G. (E) The section shows the contact of the scoria cone with the silicic ridge. Sharp boundaries mark the division between the hydrothermally altered red scoria and the unaltered black scoria. (F) Two well defined spatter flows form almost vertically in the center of the cone mixed in a matrix of welded lapilli and lapilli bombs. (G) A closer look at the scorias architecture shows accretion of welded lapilli and lapilli bombs.

ground in few sections between the scoria deposits, while small lava outflows form in several locations as well. On segment S9 we find an isolated cone on the north corner of the silicic lava, with the north face highly eroded (Figure 5.15D). The cone is of intermediate composition (ESK08a). The cone is layered showing a pattern similar to Rauðhyrna, with welded lapilli of finely vesicular scoria (≈10

cm thick and up to 1 m long) interlayered with loose lapilli grains(≈2 cm) (Figure 5.15E). The layering pattern is not regular. From the cone center the layers have an inclination of about 40°. Two parallel very coherent spatter flows, about 0.8 m thick and 8-10 m long, stand almost vertically at the center of the cone seen at the northern outcrop. The scoria surrounding the spatter lava is very oxidized with a defined red color, while extending outwards of the center on both directions, a clear line parallel to the spatter lava (about 1.5 m) changes to black scoria. A sharp contact is between the scoria cone and the ridge beneath which is composed of a light gray trachyte (ESK08b) with hackly jointing of about 10 cm. The lava is microcrystalline with <5% vesicles. Feldspar macrophenocrysts are between 10-15% modal distributed evenly through the scoria cone and lava.

5.4 Tephra mound

A layered mound extends north from the upper part of S8. This mound consists of three different layers; at the botton is a lapilli tuff layer, overlain by a pumice layer which in turn is covered by a lapilli tuff layer (Figure 5.16). Scoria from the ridge extends to the top of the mound and a scoria tongue with coherent lava embedded within extends from below although no clear contact is visible between the lava and the tuff (Figure 5.16). The contact of the tuff and pumice deposits is abrupt and has an inclination and dip of 40°/164 SE. No other location around the ridge was identified to hold a similar tuff/pumice layering as at this location. A tuff layer is located under a lava flow about 1.5 km north of the ridge but was not studied in detail. One sample (ELAVA04) was taken from these lavas for analysis and comparison.

The upper tuff layer is <2 m thick and of angular clasts. The chemical composition is unknown. Following downwards is a pumice layer of trachyte composition about 4 m thick (ESK09A and C, Figure 5.16A). Large angular clasts of pumice (10-50 cm), some with a glassy crust are found within the pumice layer. The clasts are highly vesicular (microvesicles (<0.5 mm) form 70-80% of the matrix while 1 cm vesicles form about 10-20%. Flow bands are about 5mm and the groundmass is of devitrified glass. Rectangular feldspatic macrophenocrysts (1-4 mm) make 20-25% modal of the pumice matrix while the glassy crust has up to 30% modal macrophenocrysts. The lower layer is a basaltic lapilli tuff (ESK09b, Figure 5.16B) cross bedded with layers of coarse grained clast embedded with fragmented angular vesicular lava (≈ 2-5 cm). Following below the mound with an unclear contact is a lava flow of basaltic composistion (ELAVA09) partly cov-

ered by the glacier.

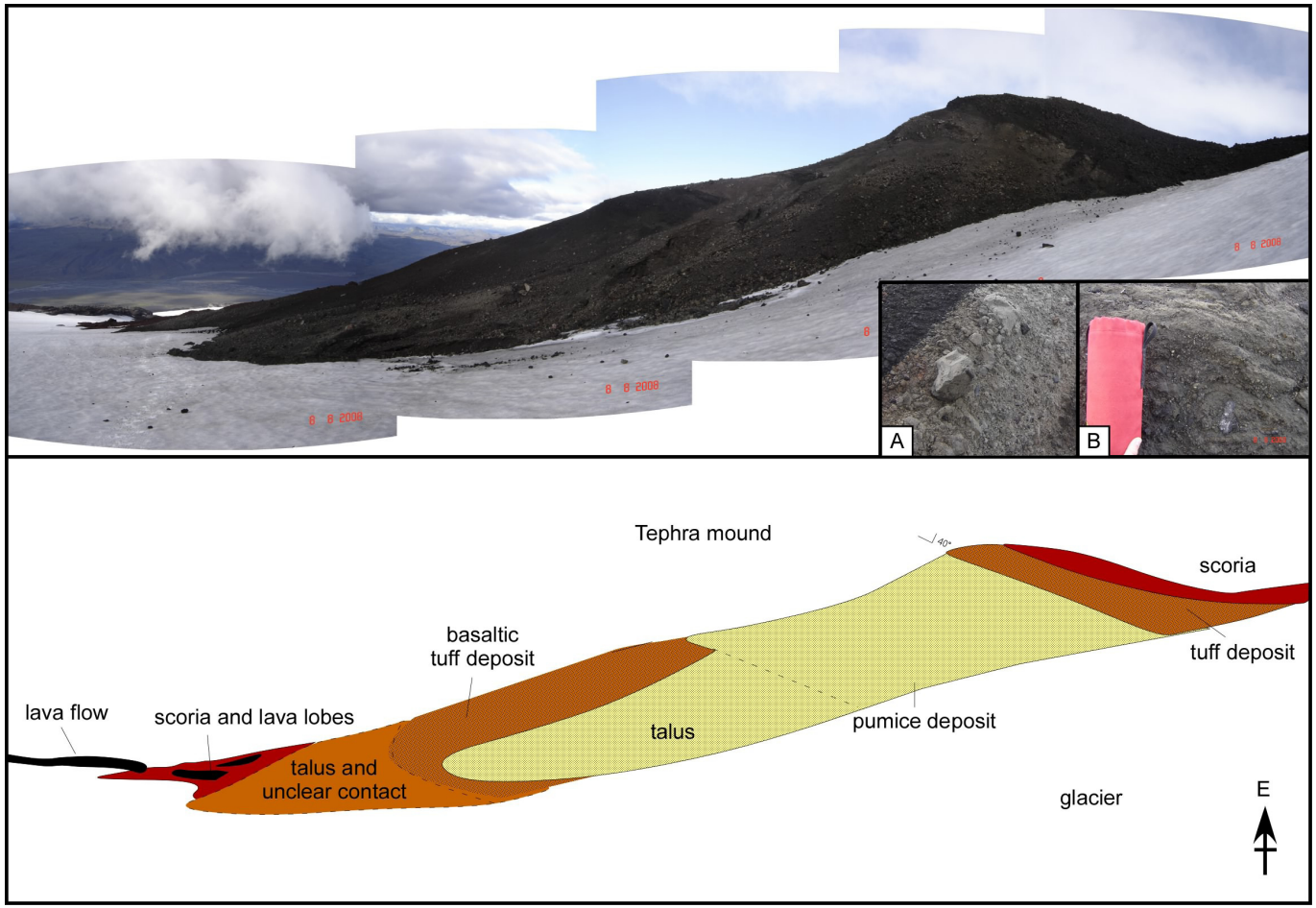

Figure 5.16: The layered tephra mound. The top of the mound is scoria from the deposit at segment S8. Below is a lapilli tuff layer (composition not known), a silicic pumice layer (a) and a basaltic lapilli tuff layer again (b). The tail of the mound is formed by scoria and small lava lobes.

5.5 The north lava flow

A lava flow of basaltic composition has been largely uncovered by recent glacier retreat and extends at least 2.5 km from the tephra mound at the north side of the ridge to the margins of Eyjafjallajökull (Figures 5.1 and 5.17A). The uppermost part of the flow is exposed beneath the tephra mound where a tongue of scoria and lava is found. The lava field is characterized by elongated lava lobes which are clearly exposed on the surface with a wide distribution in sizes and thicknesses (figure 5.17C). On the west side of the flow a pattern of thin lava layers interbedded with compacted red scoria layers where observed (Figure 5.17B). This lava is porphyritic with feldspar macrophenocrysts ($<$ 1 cm) ranging between 15 to 20% modal. The scoria layers are composed of a very coarse glassy matrix but a similar phenocryst content. Darker infiltrations occur between the scoria of a more massive and coarse chunks of glass. Each layer is about 50 cm thick. On the east margin, a massive elongated lava lobe ends with a vertical wall over 10 m high, implying severe glacial erosion. One section of the lobe wall has columnar joints with almost vertical primary joints and horizontal secondary joints (figure 5.17D). Cooling joints (5 to 15 cm) extending perpendicular to the flows margin where also observed on another place at the east margin. All lava lobes are striated with a north strike and partially covered by glacial till. A small section of the east margin partly collapsed separating from the flow by a wide fissure. The flow front disappears gradually and its northern margins are not clearly distinguished. A lateral moraine north of the flow margin marks a recent maximum extent of the glacier.

5.6 Petrography and chemical composition

Samples collected at Skerin ridge plot into the transitional alkali series (MacDonald and Katsura, 1964; Le Maitre, 2002) and have representatives of all three compositional groups; mafic, intermediate and silicic (see map Figure 5.1 and Table 5.3 for location).

5.6.1 Lavas underlying the ridge and in nearby vicinity

On the flanks of the NW end, two samples were analyzed from lava flows lying beneath Rauðhyrna scoria deposit; sample ELAVA08 giving whole-rock SiO_2 content 55,86 wt% being trachyandesite and sample ESK10 giving SiO_2 content 48,75 wt% being alkali basalt. Two other lava flows with no direct connection to

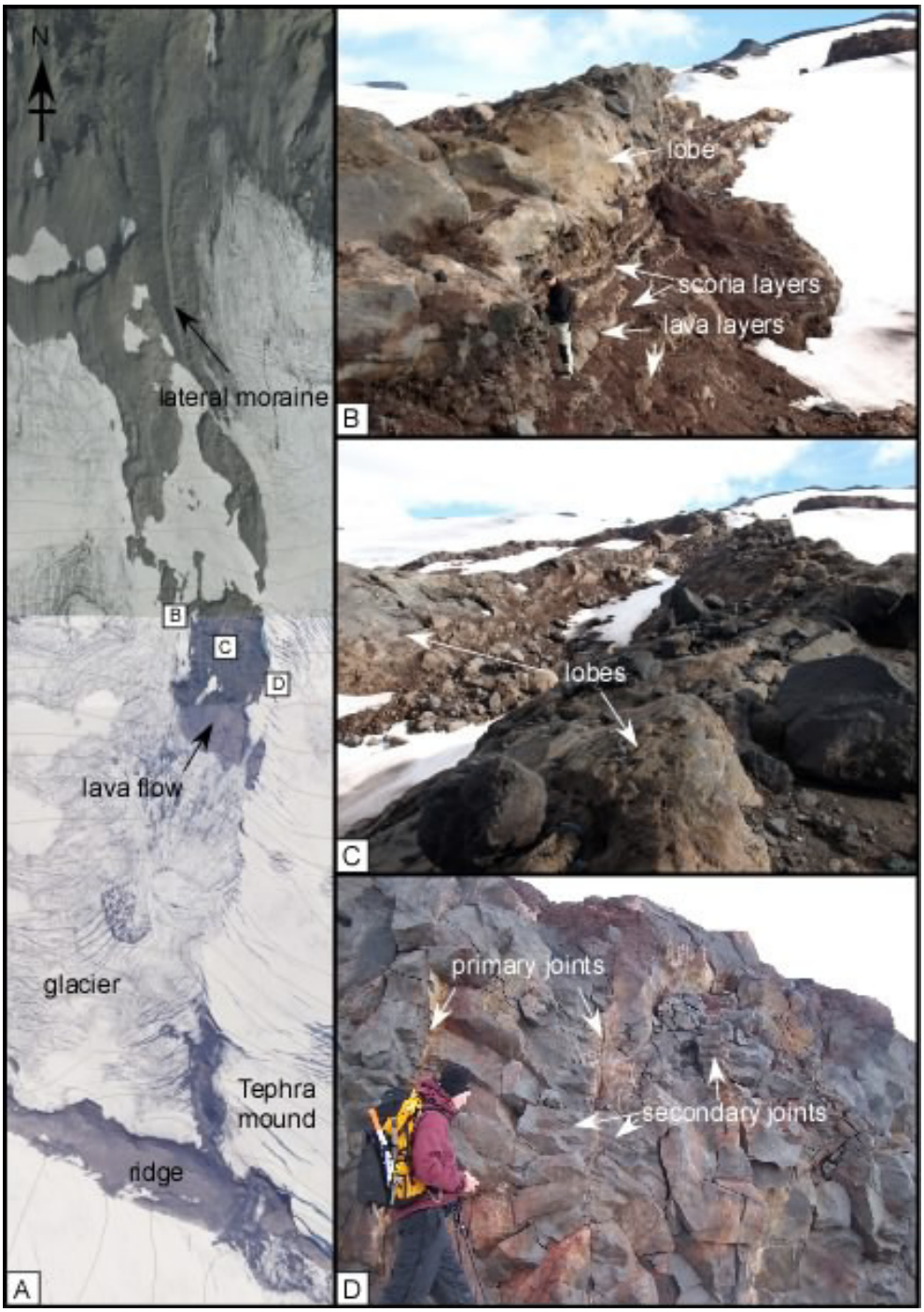

Figure 5.17: The north lava flow. A) The lava flow extends from the tephra mound N of S7 to the north margin of Eyjafjallajökull. Large part of the flow appears to be beneath the glacier cap although several new areas are being exposed with the melting of the glacier. B) One location exposed a section of interbedded layers of scoria and lava. A larger lobe forms on the top. C) The surface of the lava flow is characterized by elongated inflated lobes that are highly striated and partly covered with till. C) The east margin had a location with preserved cooling joints with primary and secondary joints. These structures are rare due to the margins being largely eroded by the glacier.

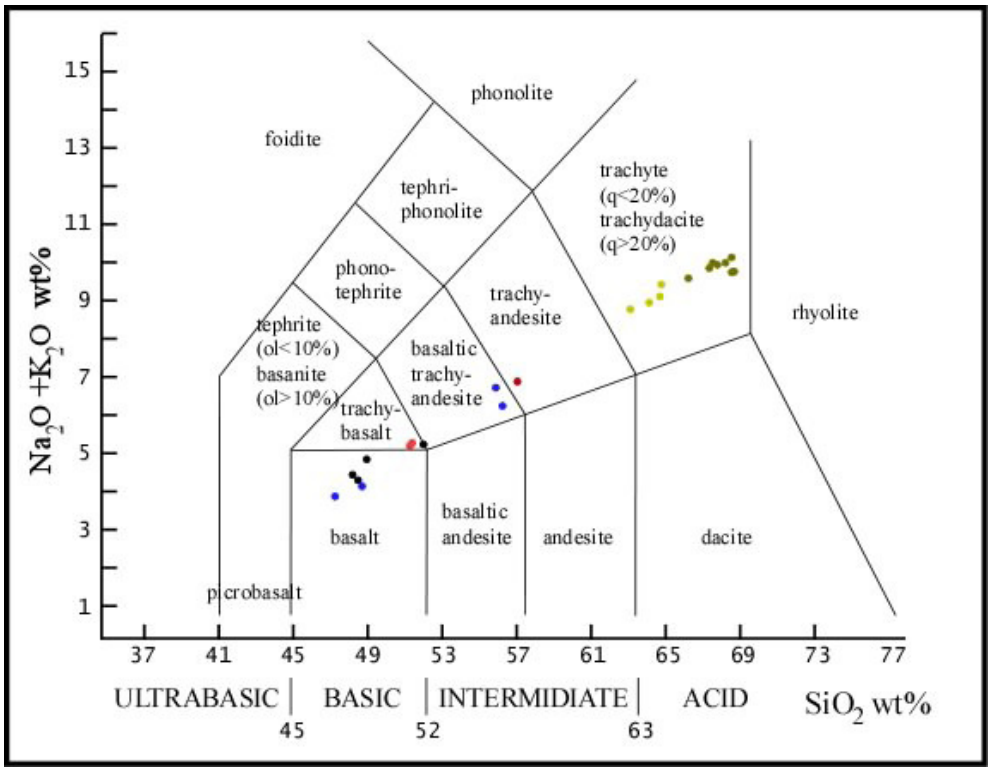

Figure 5.18: Transitional alkali versus silica diagram (TAS). Samples follow the Hawaiian line of the transitional alkalis. Diagram based on (Le Maitre, 2002). Green dots-main silicic ridge, yellow dots-silicic ridge (S1), blue dots-basement lava flows, red dots-Rauðhyrna scoria deposit and lavas, dark red-intermediate scoria deposits and black dots-north lava flow.

the ridge - sample ELAVA04 north of the ridge with SiO_2 content 47,24 wt% and ELAVA06 south of the ridge with SiO_2 content 56,23 wt%. A sample was taken from a tuff layer on top of the main crater of Eyjafjallajökull for comparison, not related to Skerin ridge (EGODAS SiO_2 content 53,96 wt%).

The basaltic lava flow NW and beneath Rauðhyrna (ESK06) has phenocrysts plagioclase, augite, olivine and magnetite. Crystals are subhedral with few being rimmed. Texture is hypocrystalline. Intermediate lava flow highly columnar N of Rauðhyrna (ELAVA08) has phenocrysts plagioclase, augite, magnetite, olivine and apatite. Crystals are zoned, rimmed, fragmented and resorbed. Texture is hypocrystalline.

The basaltic lava flow ELAVA04 has phenocrysts plagioclase and augite that are zoned, rimmed with pyroxene inclusions. Texture is hypocrystalline and oxidation is deuteric.

5.6.2 Skerin ridge

The main silicic ridge is divided into two compositional ranges; the NW end (segment S1, samples ESK05a, ESK05b, ESK07a, ESK07b, see Table 5.3, diagram

5.18 and map 5.1) with whole-rock SiO_2 content range from 63,11-64,76 wt%, and the central part and SW end (S4-S12, samples ESK01a, ESK01b, ESK03, ESK08b, ESK12, ECAVE) with whole-rock SiO_2 content range from 67,56-68,67 wt%. The silica group is classified as trachyte (Le Maitre, 2002).

The scoria deposits have two compositions as well, Rauðhyrna (samples ESK06a and ESK06b) with SiO_2 content 51,25-51,98 wt% classified as alkali basalt (icelandite/hawaiite) and the upper scoria deposit (sample from S12 ESK08a) with SiO_2 content 57,07 wt% being trachyandesite.

On the tephra mound, three deposits form a layering of tuff, pumice and tuff. The lower tuff and pumice deposits were analyzed (samples: tuff-ESK09b and pumice clast with a glassy crust-ESK09a and ESK09c). The tuff has whole-rock SiO_2 content 51,63 wt% classified as alkali basalt (icelandite/hawaiite) and the pumice clast whole-rock SiO_2 content 66,21 and 67,28 wt% of trachyte composition.

Three samples were taken from the north lava flow for analysis. Two locations where chosen for sampling, a lava tongue on the N sector of the tephra mound (sample ELAVA09) giving whole-rock SiO_2 content 48,20 wt% and on the main flow (samples ELAVA03a and ELAVA03b), whole-rock SiO_2 content 48,20 and 48,54 wt%.

All samples are very fresh and porphyric. The main silicic ridge has phenocrysts evenly distributed through the lavas ranging from 10-20% modal. The phenocrysts are plagioclase, olivine-fayalite (rare), magnetite, Fe-augite and anorthoclase. The glassy margins of the pumice clast showed higher proportions of feldspatic phenocrysts with around 25-35% modal. Plagioclase phenocrysts are subhedral to anhedral (1-5 mm) and have several degrees of zoning and resorbtion. Olivine inclusions were also common in the plagioclase. Olivin crystals are mainly anhedral, rimmed, sometimes resorbed and with a corona of pyroxenes. The groundmass is mainly hypocrystalline (crystallinity 50-90%) but hypohyaline (crystallinity 10-40%) at the glassy margin. The texture is mostly pilotaxitic to trachytic few being flow banded.

Basaltic samples from the scoria deposit Rauðhyrna have phenocrysts plagioclase, olivine and augite many zoned, rimmed and resorbed. Texture is pilotaxitic and scoria has a modal percent of 30-50% vesicles.

The north lava flow of basaltic composition (ELAVA03 A and B and ELAVA09) have phenocrysts plagioclase, olivine, augite, and magnetite. Crystals are zoned and rimmed. Scoria has a modal percent of 30-40% vesicles ($<$0.5 mm). Texture is hypocrystalline and oxidation of Fe minerals is deuteric.

Table. Petrographic analysis

nr.	Sample	Location (coordinates)	Elevation (m)	Date collected	Sample description	Texture	Phenocrysts * (macro)	Pcrysts size *	Vesicles
1	ESK01	N63°38.877' W019°42.265'	1150	16.7.2008	a) Light colored breccia b) Glass	a) Crystalline b) Glass	a) 10-15% (F), 1% (P) b) 10-15% (F)	2 mm	
2	ESK03	N63°38.263' W019°39.572'	1453	16.7.2008	Light colored lava	Crystalline	10-15% (F), 5-8% (P)	3x1mm (F), 0,5 mm (P)	
3	ESK05	N63°39.429' W019°44.034'	821	30.7.2008	a) Glass b) Light colored lava	a) Glass b) Crystalline	a) 10-15% (F) b) 10-15% (F), 1% (P)	4mm (2-5%), < 1mm (10-13%) (F), 4mm (P)	b) 20%
4	ESK06	N63°39.515' W019°44.112'	861	30.7.2008	a)Red scoria b) Bluish gray lava	a) Glassy b) Microcrystalline	a) 10-15% (F), b) 20-25% (F) 5% (O)	a) 3mm or 3x1mm b) 2mm	a) 40-50% b) 10-15%
5	ESK07	N63°39.480' W019°44.121'	806	30.7.2008	a) Light gray lava b) Light gray lava	Microcrystalline	a) 10-15% (F) b) 10-15% (F)	2mm	
6	ESK08	N63°38.457' W019°40.053'	1360	8.8.2008	a) Red scoria b) Light colored lava	a) Glassy b) Microcrystalline	a) 10-15% (F) b) 10-15% (F), 2% (P)	a) 3-4mm b) <2mm (F), <0,5mm (P)	a) 30-40%
7	ESK09	N63°38.562' W019°40.253'	1330	8.8.2008	a) Glassy lava b) Tuff c) Pumice	a) Glass b) Crystalline c) Glass	a) 30% (F) b) -- c) 20-25% (F)	a) 1-5mm b) -- c) 1-5mm	c) >50%
8	ESK10	N63°39.571' W01944.614'	739	14.8.2008	Lava	Microcrystalline	10-15% (F) 1% (O)	2mm (F), 1mm (O)	
9	ESK12	N63°38.741' W019°41.973'	1170	14.8.2008	Lava with breccia	Microcrystalline	15-20% (F)	2mm	
10	ELAVA03	N63°38.987' W019°40.557'	1150	29.7.2008	a) Red scoria b) Bluish/gray lava	a) Glassy b) Microcrystalline	a) 10-15% (F) b) 25-35% (F)	a) 2-4mm b) 3mm	a) not clear
11	ELAVA04	N63°39.425' W019°41.012'	909	29.7.2008	Glassy lava	Glass	20-30% (F)	1-5mm	
12	ELAVA06	N63°38.825' W019°43.963'	921	30.7.2008	Gray lava	Microcrystalline	3-5% (F), 2-3% (P)	<1mm (F), 1mm (P)	
13	ELAVA08	N63°39.703' W019°44.055'	709	8.8.2008	Glassy lava	Glass	15-20% (F), 1% (P)	1-5mm (F), <1mm (P)	
14	ELAVA09	N63°38.663' W019°40.323'	1290	8.8.2008	Scoria	Glass	15% (F)	1-5mm	>50%
15	ECAVE	N63°39.236' W019°43.421'	877	8.8.2008	Light colored lava	Crystalline	15-20% (F)	2-5mm	
16	EGODAS	N63°38.044' W019°39.082'	1583	16.7.2008	Tuff	Crystalline			

* Macrophenocrysts are (F) feldspatic (P) pyroxene and (O) olivine.

Table 5.3: Location of samples and general features.

Sample	ELAVA04	ELAVA09	ELAVA03a	ELAVA03b	ESK09a	ESK09b	ESK09c	ESK07B	ESK07A	ESK05B	ESK05A	ESK06a
Major elements (XRF, wt%)												
SiO_2	47,24	48,97	48,20	48,54	67,28	51,63	66,21	63,11	64,14	64,71	64,76	51,25
TiO_2	3,74	3,34	2,89	3,05	0,32	2,96	0,36	0,85	0,79	0,69	0,65	2,34
Al_2O_3	14,23	14,82	16,42	16,40	14,05	13,98	13,83	14,96	15,18	15,08	14,98	15,77
Fe_2O_3 [a]	15,51	13,65	12,11	12,72	4,57	12,98	4,76	6,67	6,22	6,09	5,93	11,59
MnO	0,22	0,22	0,18	0,19	0,13	0,24	0,14	0,16	0,16	0,18	0,16	0,20
MgO	5,12	4,01	3,84	4,17	0,16	3,39	0,17	0,91	0,78	0,65	0,65	3,88
CaO	10,09	8,82	9,72	9,98	1,22	6,74	1,24	2,82	2,69	2,20	2,24	8,18
Na_2O	3,02	3,7	3,47	3,37	6,31	2,78	6,15	5,98	6,09	6,12	6,52	3,96
K_2O	0,69	0,989	0,86	0,77	3,46	1,14	3,42	2,70	2,78	2,95	2,86	1,07
P_2O_5	0,44	0,585	0,44	0,45	0,04	0,72	0,05	0,24	0,22	0,17	0,16	0,59
LOI[b]	-0,98	0,23	-0,06	-0,60	-0,47			0,04	-0,02	0,47	-0,04	
Total	99,32	99,33	98,07	99,05	97,07	96,57	96,33	98,44	99,03	99,30	98,86	98,84
Trace elements (XRF, ppm)												
Zn	133,7	133,8	116,1	112	163,5	167,2		132,4	120,8	136,6	138,6	131
Cu	86	39,8	52,6	37,5	8,5	23,7		10,8	10,9	11,3	9,4	50,1
Ni	29,4	16,9	24,2	30,6	n.d.	3,2		n.d.	n.d.	n.d.	n.d.	33,4
Cr	15,8	n.d.	n.d.	11,5	n.d.	n.d.		n.d.	n.d.	n.d.	n.d.	42,5
V	356,4	261	263,5	290,8	n.d.	128,9		10,9	10,7	10,6	2,6	172,4
Ba	176,7	235,9	179,9	190,6	597,4	317,5		536,5	543,8	571,6	572,4	257,4
Sc	32,1	26	25,7	25,7	1	24,3		5,3	4,2	3,5	3,5	23
La	20,9	29,6	23,4	23,7	93,2	46,5		78,4	78,5	88,7	79,7	37,3
Ce	60	81,1	64	63,3	195,6	116,9		161,1	164,7	176,9	170	88,6
Nd	36,3	46,9	39,4	37,8	94,5	67,1		80,7	81,1	87,5	82,3	51,9
U	0,8	1,2	0,9	1	3,6	1,4		2,9	3	2,8	3	1,4
Th	1,9	3,1	2,4	2,1	11,4	5,3		8,8	8,6	9,5	9,8	4,5
Pb	1,9	2,7	2,5	2	7,6	3,3		5,7	7	5,6	6	2,3
Nb	35	44,2	35,7	34,1	119,7	61,5		98,5	98,7	103,1	104,9	50,1
Zr	237,2	324,9	260	251,3	974,6	443,1		799,6	804,7	842,4	863,1	347,6
Y	39,6	51,8	41,9	41,5	107,3	66,1		89	90,1	92,3	91,1	52,1
Sr	433,7	404,3	435,4	449,4	69,1	335		222,9	215,7	189,5	181,7	459,5
Rb	12,6	19,7	16,6	14,2	77,8	25,1		55,4	56,9	62,8	64,5	20,7

Table 5.4: Whole-rock major and trace element composition (XRF)

Sample	ESK06B	ESK01B	ESK01A	ESK12	ESK03	ESK08A	ESK08B	ECAVE	ESK10	ELAVA08	ELAVA06	EGODAS
Major elements (XRF, wt%)												
SiO_2	51,43	68,53	68,55	67,73	68,67	57,07	68,18	67,56	48,75	55,86	56,23	53,96
TiO_2	2,32	0,31	0,31	0,31	0,31	1,57	0,31	0,35	2,67	1,85	1,74	2,35
Al_2O_3	15,68	14,11	14,16	13,93	14,20	14,74	14,05	14,27	15,00	15,63	14,98	14,74
Fe_2O_3 [a]	11,60	4,57	4,59	4,56	4,55	10,83	4,59	4,55	12,96	10,15	11,34	11,47
MnO	0,21	0,14	0,13	0,14	0,14	0,23	0,14	0,13	0,21	0,21	0,22	0,20
MgO	4,04	0,12	0,12	0,12	0,13	2,03	0,12	0,17	5,88	2,59	2,36	2,88
CaO	8,26	1,12	0,90	1,09	1,15	5,30	1,14	1,28	9,70	6,10	5,89	6,16
Na_2O	4,11	6,56	6,12	6,39	6,19	5,03	6,43	6,52	3,23	5,02	4,53	3,48
K_2O	1,07	3,56	3,59	3,52	3,54	1,80	3,54	3,41	0,72	1,65	1,60	1,58
P_2O_5	0,60	0,03	0,03	0,03	0,04	0,58	0,04	0,05	0,48	0,62	0,68	0,51
LOI[b]	-0,16	0,26	-0,01	0,24	0,00	0,12	0,31	0,20	-0,36	-0,26	-0,44	
Total	99,16	99,31	98,50	98,06	98,92	99,31	98,85	98,49	99,22	99,42	99,13	97,32
Trace elements (XRF, ppm)												
Zn	123,2	162,1	126,6	162,6	126,4	160,7	160,4	144,1	127,3	131,8	145	155
Cu	48,4	8	5,5	7,9	7,7	17,3	8,4	7,6	88,9	21	15,4	40,1
Ni	30,8	n.d.	n.d.	n.d.	n.d.	1,8	n.d.	n.d.	71,8	5,7	1,5	16,4
Cr	44,4	n.d.	n.d.	n.d.	n.d.	n.d.	n.d.	n.d.	158,8	n.d.	n.d.	n.d.
V	172,3	n.d.	n.d.	n.d.	n.d.	23,8	n.d.	n.d.	263	81,5	37,1	157,1
Ba	261,9	600,4	600,5	599,6	615,2	377	603,5	611,8	186,3	357,5	331,4	340,8
Sc	21,9	0,1	n.d.	0,5	0,4	14,1	0,3	0,2	29,5	14,5	16,3	20,9
La	35,7	96,4	52,6	93,2	92	57,5	96,7	89,1	26	51	52,2	50,5
Ce	87	196,6	171,9	196,9	188,3	129,7	202,4	191,5	69,9	117,9	116,5	116,4
Nd	50,4	95	60,8	94,6	91	74,1	97,1	91,3	40	64,8	66,8	64,9
U	0,8	3,9	3,4	3,9	3,5	2	3,9	4	0,9	1,5	1,6	1,5
Th	4,1	11,6	11,8	11,9	11,8	5,8	11,4	10,9	2,9	5,5	5,8	5,7
Pb	2,5	7,5	6,3	7,8	7,4	4,8	7,2	6,4	1,6	4,1	3,9	4,1
Nb	49,1	122,1	122,8	122,8	118,8	70,3	122,5	117,6	38,5	69,4	59,7	63,1
Zr	343,3	984,5	1003,7	994	962,5	576,4	986,8	919,8	264,3	513,1	463,7	460,2
Y	51,6	109	56	109	103,3	75,6	110,8	104	41,7	67,2	67,9	63,2
Sr	459	61,8	62,3	60	67,6	390,4	64,6	85,6	417,8	408,6	423	356,2
Rb	20,8	79,2	69,2	79,9	78,7	36,8	80,5	77,1	12,8	34,1	28,5	34,3

a) Total Fe as Fe_2O_3. b) LOI - Loss on ignition

Table 5.5: Whole-rock major and trace element composition (XRF)

Sample	ESK03 - trace elements					ESK06b		error	average	1σ*
Major elements (XRF, wt%)										
SiO_2			68,67			51,98	51,43	0,55	51,71	0,39
TiO_2			0,31			2,35	2,32	0,03	2,34	0,02
Al_2O_3			14,20			15,90	15,68	0,22	15,79	0,16
Fe_2O_3 [a]			4,55			11,74	11,60	0,14	11,67	0,10
MnO			0,14			0,21	0,21	0,00	0,21	0,00
MgO			0,13			4,08	4,04	0,04	4,06	0,03
CaO			1,15			8,39	8,26	0,13	8,33	0,09
Na_2O			6,19			4,07	4,11	0,04	4,09	0,03
K_2O			3,54			1,09	1,07	0,02	1,08	0,01
P_2O_5			0,04			0,61	0,60	0,01	0,60	0,01
LOI[b]			0,00				-0,16			
Total			98,92			100,42	99,16	1,18		
Trace elements (XRF, ppm)						max.	min.	error	average	1σ*
Zn	127	124,7	126,1	125,7	126,4	127	124,7	2,3	125,98	0,86
Cu	7,2	7,1	7,4	7,5	7,7	7,7	7,1	0,6	7,38	0,24
Ni	n.d.	n.d.	n.d.	n.d.	n.d.					
Cr	n.d.	n.d.	n.d.	n.d.	n.d.					
V	n.d.	n.d.	n.d.	n.d.	n.d.					
Ba	618,9	615,2	612,5	612,8	615,2	618,9	612,5	6,4	614,92	2,57
La	92,3	90	89,9	89,7	92	92,3	89,7	2,6	90,78	1,26
Ce	184	186,6	186,1	186,8	188,3	188,3	184	4,3	186,36	1,55
Nd	91,4	91	92,3	90	91	92,3	90	2,3	91,14	0,83
U	3,3	3,3	3,4	3,2	3,5	3,5	3,2	0,3	3,34	0,11
Th	11,4	11,7	11,5	11,6	11,8	11,8	11,4	0,4	11,60	0,16
Pb	7,3	7,2	7	7,2	7,4	7,4	7	0,4	7,22	0,15
Nb	118,4	118,3	118,1	118	118,8	118,8	118	0,8	118,32	0,31
Zr	964,9	967,9	966	967,7	962,5	967,9	962,5	5,4	965,80	2,22
Y	103,1	102,9	102,7	103	103,3	103,3	102,7	0,6	103,00	0,22
Sr	67,3	67,3	67,7	67,4	67,6	67,7	67,3	0,4	67,46	0,18
Rb	78,6	78,6	78,6	78,4	78,7	78,7	78,4	0,3	78,58	0,11

a) Total Fe as Fe_2O_3. b) LOI - Loss on ignition *=standart deviation: in wt% for Si to P, in ppm for Zn to Rb.

Table 5.6: Whole-rock major and trace element composition (XRF)-Precision and accuracy

Sample	SCD	SGD	error	average	1σ*	BHVO-1	BHVO-1	error	average	1σ*	SG	SG	error	average	1σ*
Major elements (XRF, wt%)															
SiO_2	43,38	43,22	0,16	43,30	0,11	50,31	50,45	0,14	50,38	0,10	69,42	68,79	0,63	69,11	0,45
TiO_2	3,67	3,65	0,02	3,66	0,01	2,72	2,72	0,00	2,72	0,00	0,52	0,51	0,01	0,52	0,01
Al_2O_3	15,66	15,62	0,04	15,64	0,03	13,83	13,85	0,02	13,84	0,01	14,19	14,10	0,09	14,15	0,06
Fe_2O_3 [a]	13,35	13,32	0,03	13,34	0,02	12,32	12,32	0,00	12,32	0,00	2,34	2,32	0,02	2,33	0,01
MnO	0,14	0,14	0,00	0,14	0,00	0,17	0,17	0,00	0,17	0,00	0,05	0,04	0,01	0,05	0,00
MgO	6,86	6,86	0,00	6,86	0,00	7,19	7,19	0,00	7,19	0,00	1,20	1,18	0,02	1,19	0,01
CaO	6,39	6,41	0,02	6,40	0,01	11,38	11,39	0,01	11,39	0,01	1,79	1,77	0,02	1,78	0,01
Na_2O	3,06	3,02	0,04	3,04	0,03	2,41	2,37	0,04	2,39	0,03	3,53	3,55	0,02	3,54	0,01
K_2O	1,93	1,94	0,00	1,94	0,00	0,53	0,54	0,01	0,53	0,00	5,31	5,28	0,03	5,29	0,02
P_2O_5	0,83	0,83	0,00	0,83	0,00	0,26	0,27	0,00	0,27	0,00	0,22	0,23	0,00	0,22	0,00
Total	95,27	95,01	0,30			101,13	101,26	0,22			98,57	97,77	0,84		

a) Total Fe as Fe_2O_3. *=standart deviation: in wt% for Si to P.

Table 5.7: XRF-Standards

Chapter 6

Results and discussion

In this chapter an explanation of the formation of Skerin ridge based on the observations presented in the previous chapter is presented. Firstly, general considerations on the emplacement processes for the silicic ridge with surface and internal structural analysis. Secondly, distinct products connected to the ridge are discussed and their emplacement chronology. The final part of this chapter will be dedicated to hazard assessment were a simple model was used for calculating the rates of ice melting and meltwater production.

6.1 Skerin ridge: general considerations

The silicic lavas of Skerin have a volume of ≈0.043 km^3 comparable in size and volume to several other silicic lava flows on the slopes of stratovolcanoes (e.g. Harris et al., 2004). In spite of its elongated structure Skerin ridge does not fall into a conventional silicic lava flow field that typically has a narrow channel extending to a broad flow front (e.g. Harris et al., 2004). Skerin has been classified as a ridge formed in a fissure eruption (e.g. Jónsson, 1998) although little research had been done on the ridge itself. Observations presented in this thesis that support a fissure origin for the Skerin lavas are: 1) Skerin belongs to a series of ridges on Eyjafjallajökull with a predominant W-E trend that extend semi-radially out of the main crater (Figure 3.2) 2) regular lateral distribution of the central lava segments with few structural differences and tapering on both ends is more expressive for lavas erupted from a volcanic fissure crack or a system of fissures with higher effusion rates mainly confined to the central area 3) linear scoria deposits form on top of the main silicic lavas reveal a sequence of dikes intersecting the ridge (Figure 5.1) 4) the lavas are emplaced in a rather improbable position considering normal flow dynamics and would most likely have been

directed to the steep northern slopes or south slopes instead of following a NW divide.

Another aspect of Skerin ridge that is peculiar are the steep marginal sides and a flat top (high aspect ratios ranging from 0.3-3, see Table 5.2) indicating some sort of confinement. Glassy columnar margins appear to suggest cooling by waters which is in agreement for lava flows confined to open channels or vaults in a thin glacier (See Figures 2.1)Lescinsky and Sisson (1998); Tuffen et al. (2002b); McGarvie (2009).

6.2 The structure of the silicic ridge and emplacement processes

6.2.1 Surface structures and volcanic architecture

The silicic lavas of Skerin ridge present lobate character with hemispherical to elongated lobes displaying lengths of 10-1450 m, widths of 17-335 m and thicknesses 20-100 m exhibiting aspect ratios of 0.3 to 3 (av. 1, Table 5.2). The more voluminous central part represents about 80% of the ridge while the remainig mounds of the tapering ends represent approx. 20% (10% in each end). Each lobe indicates a single sustained intrusive event with more prolonged and efficient outflow of lava at the central part which resulted in broader lateral and downward lobe expansion while lower outflow at the tapering ends resulted in smaller mounds. Two surface structures are descriptive for Skerin: 1) the massive central region of the ridge composed of long and broad lobes with lateral cooling margins and a brecciated flow top; 2) hemispherical less voluminous mounds at the NW end completely covered by a carapace of glassy columns.

Effusive eruption is interpreted to be the dominating style forming the lavas at the Skerin ridge, with each lobe being representative for a vent in the fissure. The total length of a segment may not conform to the total length of the vent where lavas may have flowed down the slopes until colliding with adjacent lava segments or confined by ice. In other instances a breakout may have produced an adjacent lobe resembling singular vent lobe. The term referred to breakouts describes a rupture with consequent outflow of new lava a result of increase hydrostatic pressure in the flow which has developed a thick insulated crust. Thus further flow into the newly formed breakout and inflation will expand the breakout into a fully formed lobe which later can rupture forming another breakout and lobe (Hon et al., 1994).

A fraction of the eruption is attributed to an explosive phase as revealed by the pumice deposit at the tephra mound (see Figure 5.1). A basaltic tuff deposit at the same location suggests a mafic phreatomagmatic phase at the initial stage of the eruption which will be discussed later in this chapter. Phreatomagmatism would induce higher melting rates by several orders of magnitude. Only the tephra mound gives evidence of the explosive phase and further observations are hindered by the glacier. Since little of the basal area at the SE part is exposed it is difficult to assess the importance of this style of eruption in the upper part of the ridge.

As seen in segment S5, large subvertical walls of glassy columnar joints with no evidence of basal or marginal breccia characterize the segment on both south and north margins indicating areas cooled by quenching (Figures 5.10B and D). This pattern is interpreted to be representative for all the ridge although much of this carapace is still largely covered by the glacier or eroded away. Extensive jointing and glassy margins have been widely attributed to thermal contraction due to high temperature gradients associated with lava interacting with colder media (e.g. Peacock and Fuller, 1928; Long and Wood, 1986; Lescinsky and Fink, 2000; Tuffen et al., 2002a). Close-spaced elongated columns in Skerin ridge suggest the role of water and steam circulating through the network of cracks generated with cooling. High subvertical walls on the lateral margins of the lobes suggest confinement and the ice walls of the canyon are reasonable means providing this confinement with meltwaters percolating in between interacting with the lava body (see Figure 6.7). The high aspect ratio of the segment supports enhanced cooling and also confinement which is attributed to meltwaters interacting with the effused products therefore strengthening the viscous zone of the crust enabling it to support vertical growth of magmas of this type (Figure 6.1). Lavas confined by near-vertical ice walls and meltwater explain the large coverage of the glassy carapace (in this case >60 m) rather than some other form of cooling e.g. river banks, etc. Thus segment S5 is strongly linked to the surrounding glacier as the cooling and confiner agent suggesting this is plausible.

Long parallel cracks on S7 (Figure 5.1) may suggest gravity collapse due to the weight of the crust shortly after emplacement, pressure relief as the glacier retreated if the segment was partly being supported by the glacial walls that slowly migrated outwards due to ice melting or later forces exerted by the moving glacier.

The surface breccia and flow-related structures such as ogives on top of the central part of the ridge are interpreted to be of subaerial origin. This is consistent

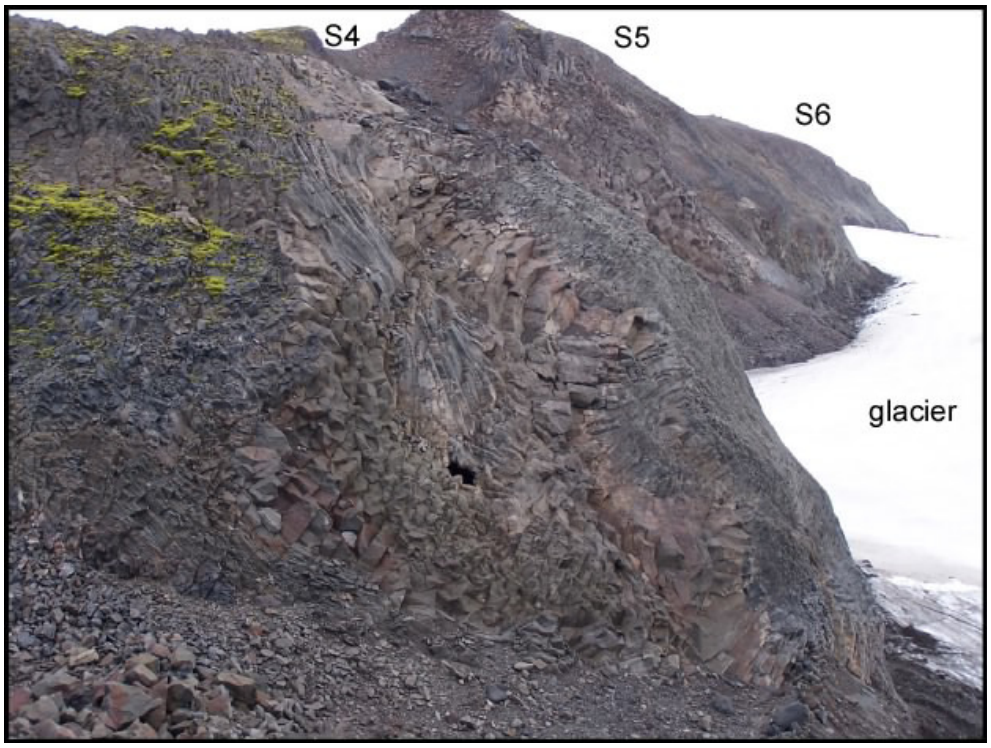

Figure 6.1: Segments S4, S5 and S6 as they are seen from S4. View is toward SE. A carapace with columnar joints forms on the margins of S4 and S5. S6 is highly eroded and lacks marginal structures only showing the flow interior. The large relative hight of the segments are explained by ice confinement. Segment S5 is approximately 80 m high.

with the lavas at that location being able to melt their way through the glacier to form a canyon and flow partly subaerially in the confines of the canyon. Scoria deposits on top of the silicic lavas formed in a dry strombolian eruption are further support for the post-emplacement subaerial condition of these lavas.

The brecciated flow top (Figure 5.10C) is composed of wedge shaped in average 0.3-0.5 m sized blocks being bluish and vesicular. Coarse light colored and glassy breccia is found in a few locations. This breccia originated as the brittle crust of the lava was disrupted and fragmented by viscous tearing induced by the friction along the margins and the pull of the faster moving liquid core (Rowland and Walker, 1990). Endogenous growth has been shown to cause fracturing and brecciation as well (Oskarsson, 2005) and may be the leading process in the formation of the surface breccia at Skerin ridge due to the limited horizontal advancement and shearing. Breccias with coarser texture suggest a lava crust that cooled subaerially and a glassy breccia may as well be a product of subaerial cooling although it may represent dislodged crust from ice-contact areas. The rather small average size of the breccia in comparison to other silicic flow fields (e.g. Harris et al., 2004) is indicative of a passive flow with short propagation and little crustal transportation and shearing.

Other surface flow expressions as the ogives and breccia piles (See Figures 5.14 and 5.13) are relatively weak due to restrict movement of the lava segments and the pattern cannot be compared to patterns of other flow fields in general with folds of well defined wavelengths and amplitudes (e.g. Harris et al., 2004). Breccia pile lineations are scarce and resemble ramp structures interpreted to be pressure ridges formed by internal shearing due to injection of new lava into the lobe (Maeno and Taniguchi, 2006). Ogives are expressions of stretching and thrusting of the rigid crust as new lavas are injected into the flow pressurizing the system. In defined channels ogives form folds perpendicular to the flow direction (not unlike pahoehoe ropes) with wavelength and amplitude that are controlled by cooling rate, strain rate, and composition. Similar structures have been named wrinkles in the literature and may be descriptive for the same structure or a slightly weaker expression of the same. Ogives at Skerin as mentioned above are not aligned into ridges and form independent blocks of massive lava ripped from the ground, dipping into the breccia with a steep face lining upwards. Larger blocks of breccia surround these structures. These can be interpreted as localized thrust zones in the flowing viscous crust induced by incremental lavas injected from the fissure into the interior of the lobe causing shearing in the core and squeeze of older surface increments (See Figure 5.13).

Larger, subrounded breccia (av. 0.5-1.5 m) (Figure 5.15C) arranged into steep hills on the margins of segments S7 and S8 show a more fragmented lithology and high-energy disruption, tearing and fragmentation. This corresponds to ramping induced by thrusting and shearing with consequent tearing and brecciation of the ductile crust with progressive increments of new lava into the lobe in a more voluminous subaerial expansion.

A narrow fissure at the tapering ends of the volcanic fissure crack is compatible with the less voluminous lavas at these locations. At the NW end, lava mounds of hemispherical shape completely covered with a glassy carapace with joints radiating prismatically support again the fact that the lavas were erupted under glacial confinement (the mounds at the tapering SE end are located on a glacial divide and subject to high erosion rates preventing the preservation of possible signatures of cooling margins). Here although, the lavas did not grow to advance subaerially and where more likely confined into wet cavities in the glacier forming a pattern of prismatic cooling joints. This structure can be compared to silicic lava flows at Bláhnúkur in Iceland attributed to lavas that rose into cavities with advance rates higher than the cavities growth and were molded and chilled against the ice (Tuffen et al., 2002a). It is assumed that melting rates do not increase with

the formation of a thick insulating crust and the lava will solidify after coming to halt against the near-stationary ice wall (Lescinsky and Sisson, 1998; Vinogradov and Murav'ev, 1985; Tuffen et al., 2002a).

6.2.2 Internal structures

The internal structure of the silicic lavas of Skerin form a three-part pattern differentiated by structural and textural morphology: the flow margin, the flow interior and the brecciated flow top (Figure 6.2). All three zones are gradational where the flow interior changes gradually to the marginal crust and flow top breccia. Joints also propagate from the margins to the interior suggesting that the isotherms of cooling were concentric (Spry, 1962) and phenocrysts are evenly distributed in size and abundance throughout the lobe. This pattern is in agreement with other intraglacial silicic and intermediate lava flows that are interpreted to have been confined to glacial canyons (Lescinsky and Sisson, 1998). This pattern suggest also that each lobe segment grew by endogenous processes meaning continuous injection of lava into the lobes interior causing uplift and stretching of the outer crust with inflation. Exogenous growth of multiple discrete injections would have produced highly variable isotherms and more complicated joint patterns (Goto and Tsuchiya, 2004).

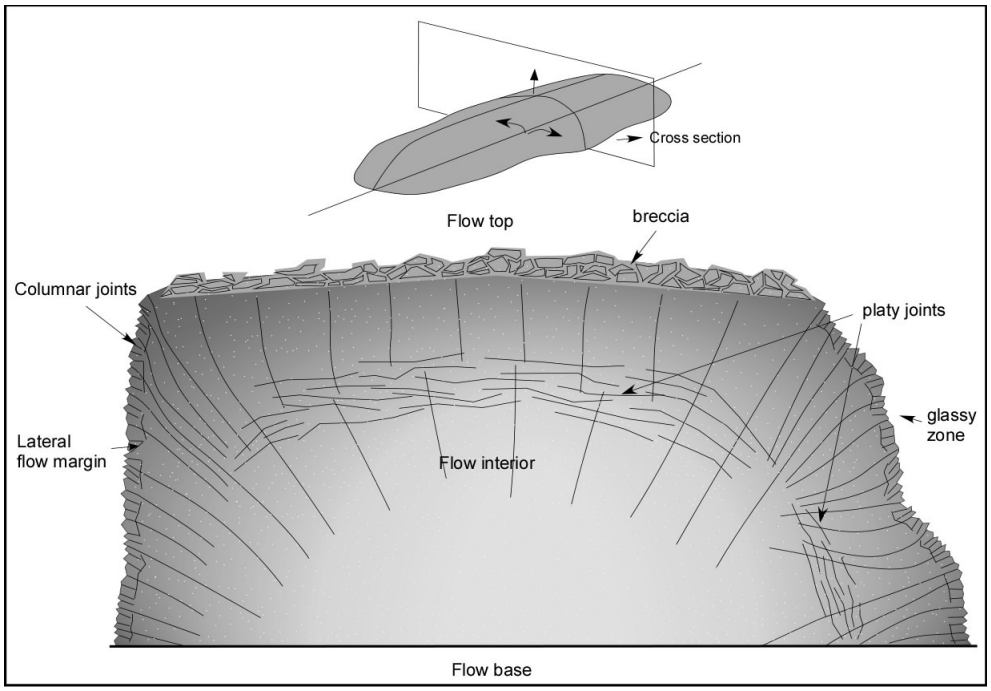

Figure 6.2: A schematic cross-section showing the internal structure representative for the lavas of Skerin.

The flow margins are characterized by subvertical to vertical walls with a cara-

pace of porphyric, non vesicular small glassy columnar joints (hypohyaline)(Figure 6.3). The columns grow prismatically/concentrically inwards to form larger columns (hypocrystalline) that form approx. 12% of the lobe. Thus the total volume of the flow margin is approx. 10-15% (for a lobe with width ≈50 m). A highly brecciated carapace has been diagnostic for silicic lava flows and domes in general and reflect tearing and autobrecciation of the brittle crust. A crustal margin absent from breccia suggests that the lavas expanded without brecciation to be directly molded and chilled by the running meltwaters or ponded waters confined in the ice canyons. Later as the lobe grew vertically and expanded to an open space within the ice canyon these flows developed breccia on the top as the flow cooled and crept subaerially. Chilled margins absent of breccia are also observed and described by Lescinsky and Sisson (1998) for lavas (SiO_2 content ranging from 61.3 to 64.1 wt%) interpreted to have advanced into an ice canyon and cooled by running meltwaters.

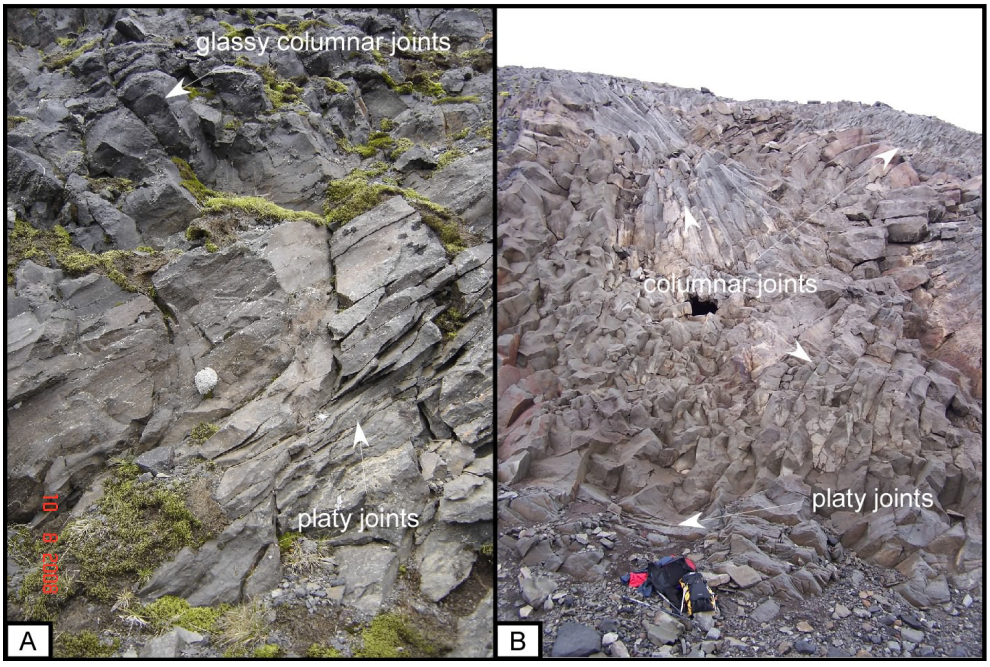

Figure 6.3: Joint pattern in segments S1 and S4. a) Lava lobe S1 has a crust formed by glassy columnar joints that grade inwards to platy jointing and further into larger columns. Cooling of the crust formed a crust that supported insulated flow within. Platy jointing is a result of creep at the brittle-ductile boundary at the last stage of emplacement and cooling. b) Small glassy columns of the margins grade toward larger prismatic columns in the center, a pattern attributed to enhanced cooling induced by steam or water with decreasing cooling rates in the interior.

The boundary between the flow margin and the flow interior is marked by alternating dark and light colored bands and in some locations platy jointing (Figures 5.7B and 5.5). Both structures are diagnostic for plastic strain at the

brittle-liquid boundary as the lavas are deformed with weight collapse or with creeping (e.g. Smith, 2002; Gonnermann and Manga, 2005). Banding develops soon as cooling and crystallization begins at the propagating boundary activated with shearing forming planar zones of crystalline and glassy texture. Thus well defined bands of alternating colors are likely to form in locations with faster rates of cooling. Platy joints are interpreted to form close to the brittle phase at the final stage of flow emplacement and cooling when creep activates shearing and fracturing of the strain zones into wedge-shaped plates.

The flow interior forms approx. 80-90% of the total volume of the lobe and is composed of a microcrystalline porphyric light colored non-vesicular rock with hypocrystalline texture (crystallinity 50-90%). Homogenous flow bands with a spacing of 1.0-2.5 cm parallel to the margins characterize the massive interior and large columns expand perpendicular to the flow margins, concentrically or subvertically relative to the flow core (Figure 5.12B). This pattern in the flow interior testifies to slower rates of cooling and the insulating properties of the crust are crucial for this pattern to develop. This is well documented for both subaerial and subglacial/subaquatic lava flows having large columns and crystalline texture in the core that grade outwards into smaller columns at the chilled more glassy crust (Goto and McPhie, 1998; Thordarson and Self, 1998; Lescinsky and Sisson, 1998). Hypocrystalline texture in the flow interior is also an expression of slower rates of cooling indicating more prolonged time for the melt to crystallize in the thermally stable environment provided by the crust.

Flow bands with homogeneous texture reflect higher crystallinity forming larger planar alignment of crystal segregations interlayered with smaller bands of glassy texture which in this case are almost invisible to a baren eye. Induced by stretching and shearing of the ductile body in a highly viscous flow these planar alignments are manifested as bands. Evenly distributed phenocrysts support again a viscous lava body with sufficient strength and density to uphold the crystals without segregation and gravity settlement.

Silicic flows can develop an insulating crust and hold moving liquid lavas in the interior, a process seen in the cave of segment S4 (Figure 5.6). In Skerin, rapid cooling induced by the water/steam enhanced the cooling rates and the speed of formation of the glassy crust inducing also the formation of a thicker and stronger viscous layer beneath the fractured zone of the glassy crust. The crust is measured to be 3-10 m thick. Due to a dynamic in the fissure, a draw down of magma column due to decrease in magma discharge or possibly a breakout causing a pressure drop, the insulated lava detached from the brittle crust subsiding about

10 m leaving an empty compartment in the mound. Flow lines and small lava drops or stalactites on the ceiling are evidence of this subsidence and the mound of lava on the floor may represent the product of it or lava that expanded in the interior as a later flow pulse. A concave ledge on the margin of the mound is interpreted to mark a later detachment in a second lava drop or a pulse of lava rise and drop inside the insulating environment. Lavas in the interior have low density, coarse-crunchy texture reflecting cooling in the hot insulated environment of the cave.

Breccia constitutes the upper flow top grading inwards to the massive core. The brecciated flow top represents the area of the flow that cooled under subaerial conditions forming the conventional structural morphology of silicic lavas which is the brecciated crust. The-wedge shaped breccia characterizes a crust that has reached temperature of brittle behaviour that is disrupted by shearing and tearing, induced by the viscous inner core and margins. Cooling by radiation is increased at this stage leading to further disruption and brecciation.

A slightly different inner pattern is observed in a thin low-voluminous lobe from segment S1 that appears to have flowed 200-300 m down from the fissure into the mafic scoria cone Rauðhyrna (Figure 6.3). Two vertical cross sections were logged (Figure 5.5). The lavas at this location where depleted in SiO_2 ranging form 63.11 to 64.76 wt%. In the cross section three zones are predominant, the upper glassy crust, the platy zone and the inner vesicular folded zone. This pattern is most likely representative for the entire segment. The basal area of the cross section could not be identified but was exposed in another sector showing the lava being directly emplaced on the underlying scoria with no breccia layer with a vesicles zone less than 10 cm thick. All zones are gradational.

The glassy upper crust is formed by non-brecciated closely-spaced cooling joints as described for other segments. Jointing fades into the lobe and may bear signature of subaerial cooling although cooling by meltwater is plausible and in agreement with other locations showing clear evidence for enhanced cooling by water/steam.

Flow banding is a characteristic for the glassy-crystalline boundary formed with same mode as explained above and thick zone of platy jointing at the banded zone and below indicates a high-intensity creep right before the lavas came to complete stagnation.

The flow interior with a vesicular folded pattern is peculiar for segment S1 and can be used to track dynamics in the flow interior and the emplacement mechanism for that segment. For basaltic lavas, the vesicular horizons are characteristic

for the crustal and basal zone, being the upper vesicular crust representative for half to one third of the normalized height (H/L height divided by lobe thickness) of the lobe and the basal zone only H/L ≈0.1-0.2 (Thordarson and Self, 1998; Oskarsson, 2005). This vesicle distribution accompanies the columnar pattern (smaller columns at the crust and larger at the core) that the lavas present showing that gas-bubbles rise by buoyancy to be trapped and preserved at the cooling brittle-ductile boundary that grows inwards as the thermal cooling propagates into the interior. Thus the basal vesicular zone is very limited in size due to the hot lava bulk above that slows the inwards growth of that horizon and in long-lived flows the growth is impeded by thermal erosion promoted by the moving liquid core. The core is usually depleted in vesicles although the more viscous a'a lavas have moderately larger amount of vesicles in the core.

As observed in the flow lobe of S1, vesicles form in the flow interior and arrange into horizons or bands (Figure 5.5). These bands are highly folded with a hinge lining toward the flow direction (NW) and are compressed on the upper region beneath the platy zone (Figure 6.4). The mechanism of emplacement for these bands is interpreted to be the same as for basaltic lavas. Horizons or vesicular bands in the upper crust are interpreted to form when a drop in the hydrostatic pressure of the lavas flowing through the interior occurs with pressure relief and gas accumulation. These gas-filled horizons will eventually trap in the ductile zone and stagnate to be pressed with the accretion of new lava in a subsequent pulse. Vesicles may segregate to form larger pockets of vesicles or megavesicles. This mechanism of accretion and cooling of new lava to the lower part of the crust thickening the crust enables it to retain incoming lava and grow by endogenous growth. With shearing at the brittle-ductile boundary these vesicles were stretched or recycled into the flow. Folding is expected for viscous bodies deforming by the presence of a viscous fluid affected by the different viscous properties of the chilled basal and upper crust, a common structure observed in silicic lavas (Smith, 2002). Thus folding preserved in S1 reflect a secondary process in which the ductile body with the vesicular horizons was deformed under stress applied by the new lavas injected into the lobe at the final stage of emplacement.

In the observed sections of the glassy crustal zone vesicles were absent while being more distributed through the inner core. Vesicles form also in the breccia that is cooled subaerially. This may support that high cooling rates and increase in viscosity for the trachytic lavas prevent vesicles from accreting to the crust whereas their rise is slower than the fast downward propagation of the isotherms. In contrast, vesicles appear to propagate more easily through a body being de-

Figure 6.4: A section of S1 that shows folding in the flow interior attributed to a body of magma creeping between two less viscous zones. Megavesicles which are segregations of vesicles are trapped between the folding. Trekking pole for scale.

gassed and cooled under subaerial conditions.

6.3 Eruption episodes and synchronicity of events

Skerin fissure has delivered intermingled products with compositions that vary from mafic to silicic and all samples plot elegantly at the Hawaiian line of the total alkali versus silica (TAS) diagram (MacDonald and Katsura, 1964)(see Figure 5.18. Note: few samples on the chart are from lava flows found on the vicinity of Skerin ridge (blue dots)).

For better clarity, the ridge is divided into two zones, the upper zone and the lower zone. Lava flows on the vicinity of the ridge will be addressed separately.

The area of interest of the lower zone is concentrated at the Rauðhyrna scoria deposit. Four compositions are representative for this area. Rauðhyrna is composed of basaltic scoria with a lava lobe of same composition: a basaltic lava NW slightly beneath Rauðhyrna and an intermediate highly columnar lava flow N of Rauðhyrna and a trachyandesite lava lobe that stretches NW from segment S1 SE of Rauðhyrna (Figure 5.2).

Compositional properties of the two lavas NW and beneath Rauðhyrna (sam-

ples ESK10-basaltic and ELAVA08-intermediate, see Table 5.4 and 5.5) indicate that these do not represent lavas created from same eruption episode that formed the Skerin ridge, most likely being Pleistocene lavas that are predominant at this part of Eyjafjallajökull.

A puzzling formation encloses the lava lobe of trachyandesite that extends from S1 and is embedded in the basaltic scoria deposit Rauðhyrna as shown in Figures 5.4 and 6.5. The section of S1 that is embedded in Rauðhyrna (sample ESK07A and B) is a lobe that was emplaced gently on the scoria underneath and covered gently by the scoria above. No faults are located in the scoria deposit giving evidence of deformation and possible removal of scoria over the lobe neither did the lavas intrude into the scoria deposit. As described in the previous subchapter the internal structure of the lobe suggests it was emplaced as a sheet-lava flowing down in the direction of Rauðhyrna with no brecciation a result of a breakout and tube-fed lava from the fissure that created S1 (see schematic representation in Figure 6.10). Continuing eruption at Rauðhyrna gradually covered the silicic lobe with scoria. The silicic lobe is depleted in silica comparatively with the main ridge suggesting that S1 derived form a more depleted source. Based on these observations there is compelling evidence that the strombolian eruption that formed Rauðhyrna and the effusive episode that formed the main silicic ridge were synchronous events.

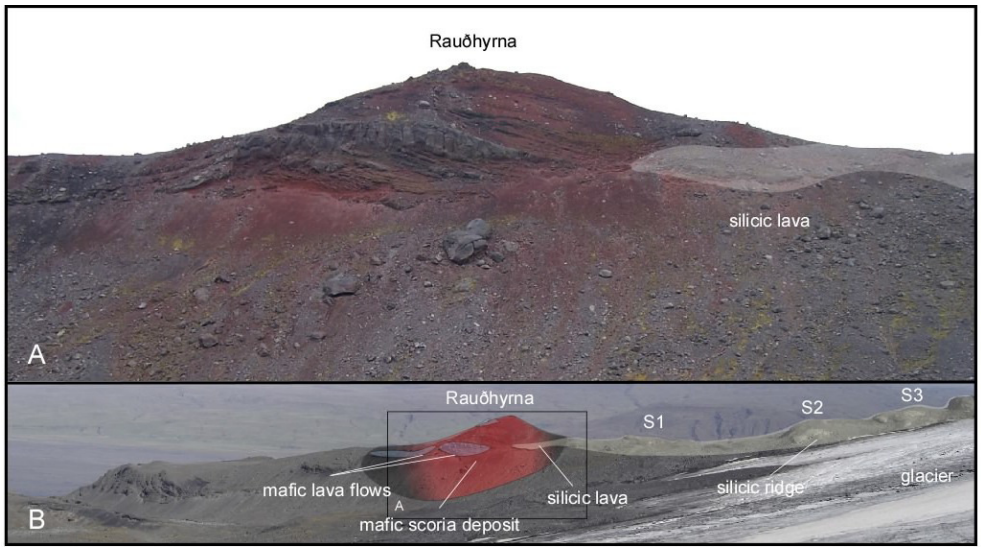

Figure 6.5: The complex Rauðhyrna reveals an unusual event in which a silicic lava lobe (colored for illustration) from the main ridge flows onto the active strombolian eruption (Rauðhyrna) and is covered by it. No marks of a forced intrusion of the lava or structural deformation of the scoria cone are present supporting a synchronous event for the basaltic-silicic eruption. The intermingled multi-component deposit at the tephra mound also suggest a synchronous event for their formation.

Moving to the upper zone of the ridge the area of interest is the scoria deposits on top of S7 to S9 and the tephra mound, a tip on the north end of S8. As represented on the map on Figure 5.1 the lavas that form the main structure of the ridge are of trachyte composition. One sample was analyzed for the scoria deposits (sample ESK08A at S9) and is of intermediate trachyandesite composition. Beginning with the tephra mound formation, this section is formed of several units which are from top to bottom (Figure 5.16): scoria (intermediate) from the ridge; tuff deposit of unknown chemical composition; pumice deposit of trachyte composition with glassy clast; tuff deposit of basaltic composition; basaltic scoria and lava lobes. The tuff and pumice contacts and the overlying scoria are sharp with no unconformities or weathering. The contact between the lower tuff and the lava flow beneath is unclear.

A complex interplay of explosive and phreatomagmatic activity of differing products at this location suggest 1) a watered environment most likely ponded meltwaters formed at the emergent explosive phase of the eruption 2) lavas of distinct composition erupted from that location namely a mafic phreatomagmatic eruption (lower tuff deposit) followed by a silicic explosive eruption and ending with a phreatomagmatic mafic to intermediate explosion (unknown composition). The overlying scoria is most likely of intermediate composition as the adjacent scoria from S9.

It is likely that at about the same time, or shortly after the silicic explosive phase forming the pumice deposit at the tephra mound, silicic lavas were erupted as sheet-lavas from the main propagating fissure to be emplaced and confined within the glacial canyon melted by the rising lavas. The uppermost deposit on top of the silicic lavas is the intermediate scoria that represents the final stage of the eruption. This was a strombolian eruption interpreted to have began shortly after the silicic lavas were emplaced (Figure 6.6).

As described in section 5.5, the lava flow that extends from the northern end of the tephra mound mound connects further downslope to a large lava flow of same composition. The depleted composition of the lava flow in comparison to other eruption phases suggests it formed in an eruption episode preceding the Skerin ridge eruption although the time between them cannot have been long due to the freshness of the lava field. Close inspection of the flow field identified an a'a type lava flow with marginal cooling structures (columns and secondary joints) that suggest the lavas were also confined to a channel in the glacier (see Figure 5.17). Other lavas on the viscinity of Skerin may tell a similar story for lavas erupted from intraglacial ridges into canyons in the ice. This is important

for future paleostructural geology to consider intraglacial "subaerial" lava flows with similar structural morphology as subaerial interglacial flows.

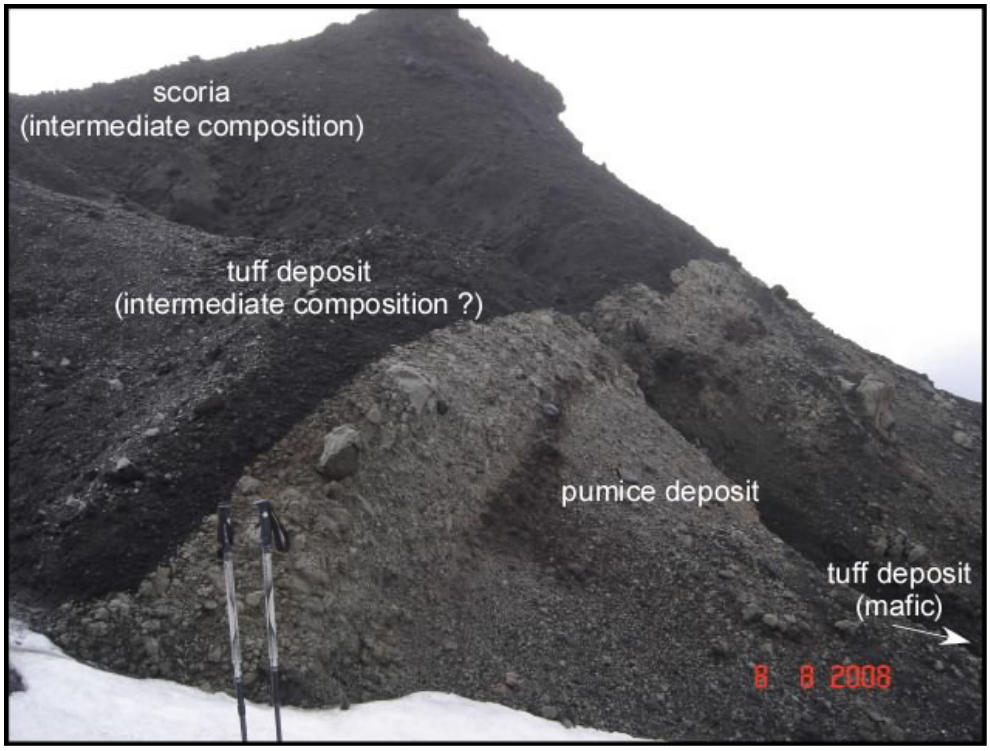

Figure 6.6: Tuff (unknown composition), pumice and mafic tuff deposits on the tephra mound testify of phreatomagmatic-explosive activity of multi-compositional material. Sharp contacts without hiatus confirm the synchronicity of these events.

Petrographic analysis revealed phenocrysts with several degrees of dissolution and zoning many with inclusions suggesting disiquilibrium in the melt most likely attributed to magma mixing (Jakobsson et al., 2008). This is in agreement with the complex structural relations of the products described in the field. Sparks et al. (1977) suggests that silicic volcanism can be triggered by mafic intrusions as interpreted for the plinian eruption at the Icelandic volcano Askja in 1875 and is a likely scenario for the Skerin eruption. Interestingly, mafic dikes appear to have advanced parallel to the silicic magma at the Skerin eruption erupting at the same time.

Based on the observations from the upper and lower zones, mafic lavas were erupted from two locations primarily, at Rauðhyrna creating scoria in a strombolian eruption and at S8 as a phreatomagmatic explosive phase forming a tuff deposit. Following these events was the silicic effusive phase from a sequence of vents in the main fissure that formed segments S1 to S12. At the upper part of S8, water was present leading to explosive interaction and the formation of pumice with glassy clasts. Finally, intermediate lavas erupted from a sequence

of fissures on top of segments S7 to S9, possibly explosively close to the tephra mound forming a tuff layer but mostly in a strombolian eruption forming the scoria deposits.

A conceptual model with a summary of observations will be given at the end of this chapter.

6.4 Paleo ice-thickness considerations and time of eruption

Skerin ridge gives several clues about the ice-thickness at the time of eruption. These are: 1) The cooling features give evidence of the minimum thickness of the ice canyon at the time of eruption (see Figure 6.7); 2) the presence of weak structures on the ridge as scoria deposits, ogives and breccia suggest that the glacier never covered these flow-tops since these features would be easily eroded away; 3) deposits attributed to strombolian eruptions such as the scoria deposits and flow related structures as ogives and flow top breccia of subaerial origin reveal 'dry' areas within the confines of the glacier or the absence of the glacier; 4) glacial till, erratics, striations and erosion faces give evidence of the extent of the surrounding outlet glaciers (illustration in Figure 6.7).

By considering these parameters, the minimum and maximum thickness of the glacier at the time the eruption took place can be estimated. Cooling structures on the margins of S5 are good evidence for the minimum thickness of the glacier when the segment was formed. These give thicknesses of $\approx$ 60-70 m for that location. Breccia on top of same segment indicate that the glacier did not expand to cover the entire segment after emplacement giving a maximum thickness, considering a small depression in the ice (cauldron) of $\approx$ 80-90 m for that location. This thickness can only apply to the immediate surroundings of segment S5 considering that it is located at the lower marginal region of the glacier (950 m a.s.l.) where recession is the most. In spite the fact that thickness of the glacier increases closer to the summit, scoria deposits and flow-structures (ogives and breccia) on top of segments S5 to S9 ($\approx$ 1350 m a.s.l.) confirm that the glacier did not expand to cover these areas. In contrast, both the low volume NW and SE tapering ends show evidence of having been completely covered by ice during the eruption and in periods of glacial advancement. NW segments (S2-S4) have a roof that is striated and are also covered with a thin layer of till. These features are in agreement with glacial propagation shown in older geological maps from that region and photographs (see Figure 4.1, Jónsson (1998)). SE segments

(S10-S12) are highly eroded being located at a glacial divide between the north propagating outlet glacier heading to Smjörgil and the south-west propagating glaciers. Based on these information and radio-echo sounding measurements a reconstruction of the ice thickness at the time of eruption is possible as illustrated in Figure 6.8.

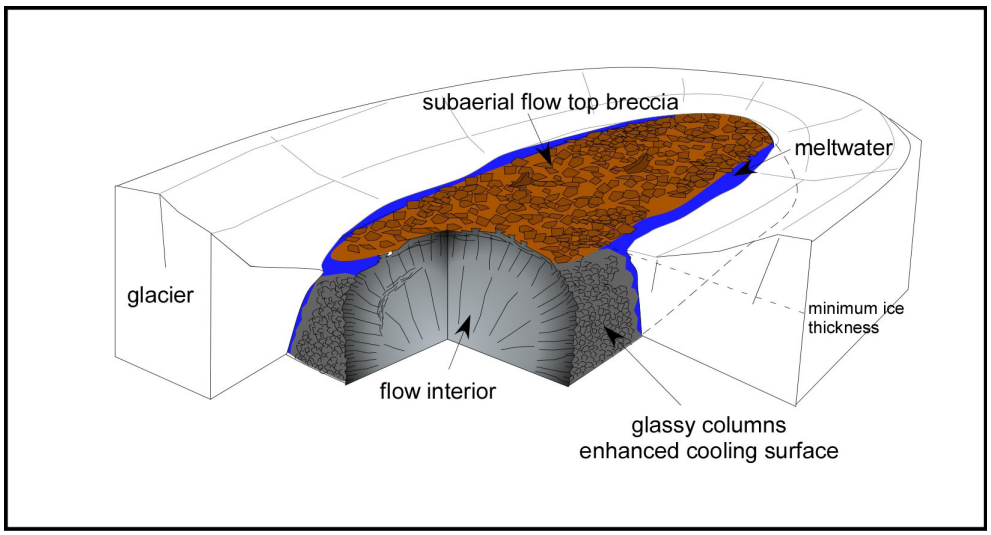

Figure 6.7: Sketch illustrating the paleo-ice thickness constrains applied for Skerin ridge. Structures showing enhanced cooling (glassy columnar joints) give evidence for the minimum ice-thickness and the flow top breccia suggest open ice cauldrons, that is dry areas not covered by the glacier.

The scoria deposit at Rauðhyrna implies it was formed under subaerial conditions on the absence of a glacier (perhaps at a glacier margin) or in a melted area within the confines of the glacier. The fact that the silicic lobe from S1 expanded over dry ground as it was extruded from a segment (S1) located close to other segments that erupted subglacially (segments S2-S4), indicates that the dry setting might represent a combination of both marginal position and dry places within melted areas around the vent.

Post-eruption erosion of the ridge is ascribed to frictional erosion on the margins by the propagating outlet glacier Akstaðajökull that expands NW parallel to the ridge down the Akstaðaheiði valley. The glacier eroded a large part of Rauðhyrna leaving striations on the south margins of the lavas embedded in the scoria and erratics to elevations down to 840 m a.s.l. (Figure 5.4). Silicic segments, especially S6 show glacial erosion on the south margin. A small finger of the glacier propagated over segments S1-S4 leaving striations and till on top of these segments and eroding the NW side of S5 (see Figure 4.1).

No historical documented evidence exists on the time of the eruption that formed the Skerin ridge. A volcanic eruption has been proposed at the NW side

of Eyjafjallajökull close to 920 AD (maximum age) (Dugmore and Larsen, 2009, in prep.) based on flood deposits (jökulhlaup) derived from Eyjafjallajökull. These deposits occupy a stratigraphical position equivalent to a known tephra layer (Katla K 920) on the margins of Markarfljót river in the Langanes area. A series of box-gullies cut into the fans of Langanes and lava surfaces where the soil has been flushed away on the plains of Litlaheiði indicate recent flood episodes which may coincide with this event. No other eruption is documented for the NW area in postglacial times thus making Skerin ridge a likely candidate. The soil and tephra profile is complete after 1341 with no gravel attributed to glacial flood episodes (tephra layer H 1341) (Dugmore and Larsen, 2009, in prep.). Other features that may indicate recent volcanism for Skerin ridge are fresh rock samples and the presence of weak structures in the ridge easily affected by erosion such as scoria, tuff and pumice deposits.

As suggested by Kirkbride and Dugmore (2008), based on fluctuations recorded at the outlet glaciers of Gígjökull and Steinsholsjökull, the ice cap of Eyjafjallajökull advanced before the 3rd century AD, in the 9th and 12th centuries, and with five groups of advances within the Little Ice Age (1700-1930 AD). These observations do conform in general with other glacier advances identified in Iceland and climate proxies although the advances between the 9th and 13th centuries do challenge the view of a prolonged Medieval Warm Period supporting medieval episodes of cooler and wetter conditions in Iceland (Kirkbride and Dugmore, 2008). The data gathered from Skerin ridge supports a larger ice cap at the time of its formation. If this eruption occurred around 920 AD, the findings are in agreement with the observations made by Kirkbride and Dugmore. Considering that the topography was altered with the formation of the ridge and that glacial mass distribution changed, it is difficult to address with certainty the actual size and volume of the glacier at the time the eruption occurred except it was larger than at present day.

Skerin ridge forms an ice divide. As previously described, prior to the eruption the mass distribution of the glacier, flow and bed topography was likely different. With the formation of the ridge, the glacier that expanded to the N was diverted by the ridge toward NW and the glacier N of the ridge has been limited in size. Today a substantial flow concentrates on the SW side with thicknesses ranging from 80-120 m (see ice-radar measurements in Figure B.1 and B.2 in the Appendix) flowing toward Akstaðaheiði deepening the valley and eroding the margins of the ridge.

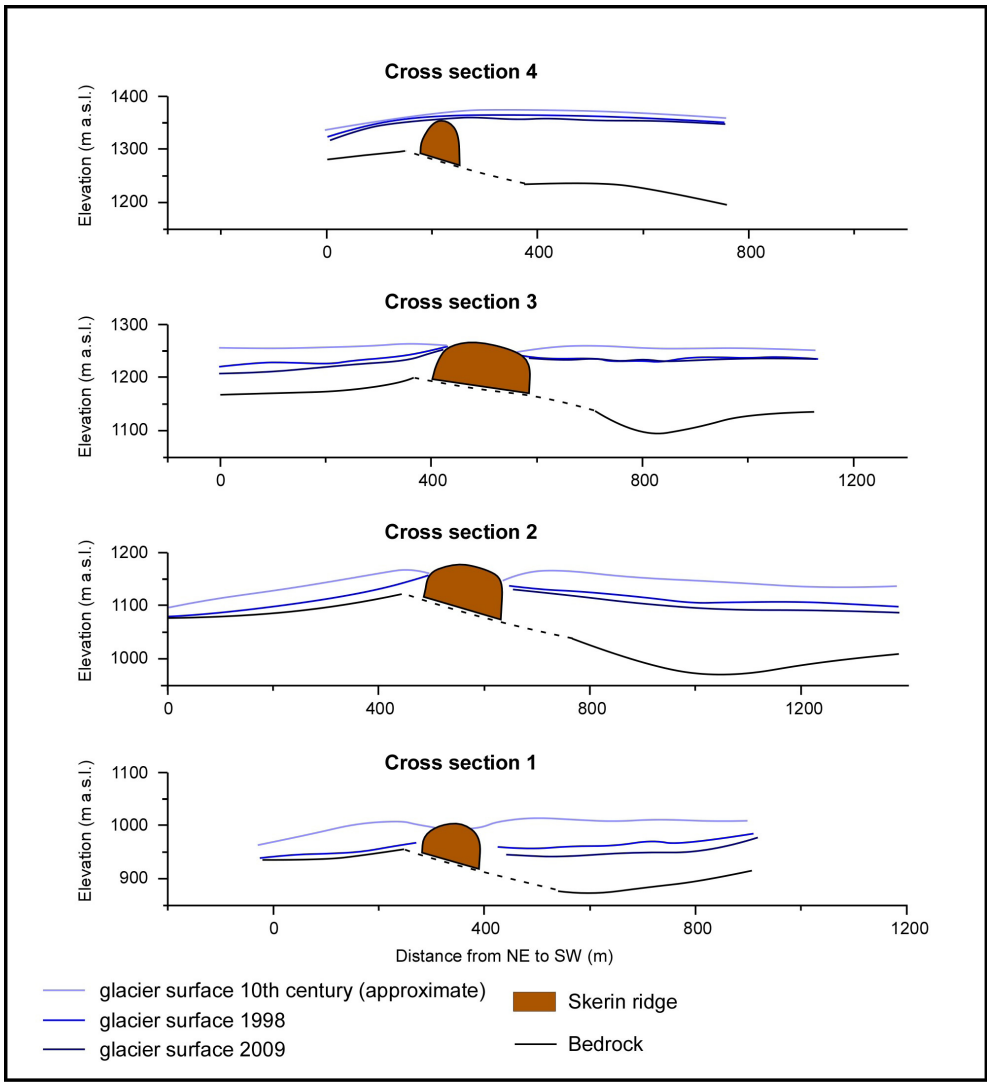

Figure 6.8: Based on the morphological structures (cooling features) revealed in Skerin ridge the paleo-ice thickness can be estimated. Four cross sections were measured with radio-echo sounding which showed the bedrock topography and present ice thickness. The location of the profiles are depicted in Figure B.1 in the Appendix. The assumed glacial surface at the time of eruption (possibly 10th century AD) is sketched with a small depression (cauldron) on the vicinity of the ridge. For cross section 1 (around S5) the inferred ice-thickness at the time of eruption is estimated to be 70-90 m above present thickness. Higher in the ridge melting is less predominant and the inferred ice thicknesses ranges from 10-40 m. The data processing and calculations related (including the glacier surface for the year 1998 and 2009) were kindly provided by Eyjólfur Magnússon at the University of Iceland (pers.com).

6.5 Volume of meltwater created in the eruption and hazard assessment

The space occupied by the ridge represents the minimum volume of ice melted during the eruption. Two eruption styles should be considered for calculating rates of meltwater production in time, effusive lava episodes and phreatomagmatic

explosive episodes. Both styles are visible in the Skerin ridge and will be discussed here.

Fissure segments of Skerin which erupted lavas during relatively quiet low magma flux, are interpreted to have melting rates proportional to the lava eruption rates. Lavas reaching the base of the glacier would melt the ice forming a thin-layer of water between the lava crust and the ice. This water layer is an effective medium transferring heat by convection to the adjacent ice and therefore continued melting (Hoskuldsson and Sparks, 1997). As the lavas advanced with faster rates than the wall meltback, they collided and banked to be molded and shaped against the nearly stationary cavity or canyon.

Subaerial opening in the glacier possibly developed with melting and collapse of ice with the rising lavas. As described above, segments S5 to S8 grew to expand under subaerial settings. On the other hand low voluminous fissures as those located at the tapering ends formed cavities that did not evolve to subaerial openings. Only S1 interpreted to have been at the margins of the glacier expanded subaerially.

Segments holding a glassy carapace of columnar joints oriented perpendicular to the margin show close vicinity of the confining glacial margin (DeGraff and Aydin, 1993) and models suggest that the ice wall or cavity will not grow significantly larger after the lavas have chilled against the ice (Vinogradov and Murav'ev, 1985; Lescinsky and Sisson, 1998). Thus the glassy margins provide good boundaries for estimating the close location of the ice-wall of the canyon or cavity.

Phreatomagmatic explosive activity is very effective melting ice. The eruption in Gjálp in 1996 showed to have melting rates of 10^{-3} m s^{-1} attributed to high heat transfer with turbulent mixing of quenched ash fragments and meltwater (Gudmundsson et al., 1997; Gudmundsson, 2003). In a thin glacier, phreatomagmatic eruptions will work their way through the glacier in minutes to hours with high meltwater production that will drain in large floods (jökulhlaups) (Gudmundsson et al., 1997; Smellie, 2002; Gudmundsson and Högnadóttir, 2005).

The area around S8 experienced phreatomagmatic activity which produced a tuff layer, silicic pumice with glassy clast ending with another tuff layer most likely prior to the strombolian episode. Such activity indicates watered environment attributed to meltwater presence in small depressions promoted by a thicker glacial setting. Melting rates at that location are expected to have been fast and the volume of melted ice larger. Meltwater from these depressions drained into tunnels and channels and likely through surface flow both north and south of the

ridge or followed the ridge enlarging the canyon.

Based on the observations in this chapter of lava confinement and minimum and maximum ice thicknesses a simple model was used to estimate the ice melting rates considering different effusion rates with respect to varying viscosities and emplacement processes (Table 6.1) (Gudmundsson and Högnadóttir, 2005). Trachyte lavas have been estimated to hold viscosities from 10^4 to 10^{12} Pa s (LaMoreaux, 2008) with several factors affecting their rheology. Giving viscosities in the range of 10^4 to 10^7 Pa s for the Skerin lavas, considering the alkalinity and possibly higher bulk temperatures (900-950 °C) stimulated by a mafic intrusion, the order of magnitude for effusion rates and timescales can be explored using equation 4.2 (Hoskuldsson and Sparks, 1997; Tuffen and Castro, 2008) (Table 6.1 and 4.1). According to equation 4.2, using an average size dike sizing 5 m (2h=2.5 m) and an average aspect ratio η=500 for silicic dikes in Iceland with the lower range of viscosities above, will yield effusion rates of 1000 to 1 m^3/s respectively. With respect to these effusion rates, a ridge with volume ≈0.043 km^3 gives eruption timescales between 4.3x10^4 to 4.3x10^7 s (half a day to about 500 days).

Using parameters given in Table 6.1 (estimated ice length, width and thickness) and equation 4.1 from Gudmundsson and Högnadóttir (2005), the range of possible melting rates can be explored. Effusion rates of 1, 10, 100 and 1000 m^3/s are used as input, and the emplacement time of each segment calculated. The obtained emplacement times and the width of the segment are used as input for Δt and Δb in equation 4.1. The ice thickness (h in equation 4.1) is estimated as segment height (Table 5.2) plus 10 meters, to take into account that water levels will always be substantially below original ice thickness (e.g Gudmundsson et al., 2004). Considering phreatomagmatic activity, an ice canyon slightly larger that Skerin (thickness +10 m) formed completely under this style of eruption in about 2 hours, would create meltwaters at an average rate of 6200 m^3/s. Knowing that most of the ridge is made of lava, this meltwater production rate must be an overestimate although a short-lived phreatomagmatic phase may for a brief period cause substantial melting.

Segment	Approx. length (m)	Approx. width (m)[a]	Approx. thickness (m)[a]	Ice volume (10^6 m^3)	Q (Δt1) m^3/s [b]	Q (Δt2) m^3/s [b]	Q (Δt3) m^3/s [b]	Q (Δt4) m^3/s [b]	2 hrs Phreat. [c]
S1	410	50	30	0,62	0,0131	0,13	1,31	13,1	78,4
S2	90	110	60	0,59	0,0127	0,13	1,27	12,7	75,7
S3	90	50	60	0,27	0,0058	0,06	0,58	5,8	34,4
S4	80	50	40	0,16	0,0034	0,03	0,34	3,4	20,4
S5	350	140	100	4,90	0,1046	1,05	10,46	104,6	624,8
S6	410	340	100	13,94	0,2976	2,98	29,76	297,6	1777,4
S7a	70	50	100	0,35	0,0075	0,07	0,75	7,5	44,6
S7b	80	100	90	0,72	0,0154	0,15	1,54	15,4	91,8
S7c	500	170	80	6,80	0,1452	1,45	14,52	145,2	867,0
S7d	790	200	80	12,64	0,2698	2,70	26,98	269,8	1611,6
S8	710	140	70	6,96	0,1485	1,49	14,85	148,5	887,1
S9	90	90	70	0,57	0,0121	0,12	1,21	12,1	72,3
S10	90	30	70	0,19	0,0040	0,04	0,40	4,0	24,1
S11	20	20	70	0,03	0,0006	0,01	0,06	0,6	3,6
S12	10	20	70	0,01	0,0003	0,00	0,03	0,3	1,8
Total	**3790**			**48,7**	**1,04**	**10,41**	**104**	**1041**	**6215**

a) Ice thickness (Table 5.2) +10 m given that the glacier was slightly thicker than the ridge.

b) Ice melting rates estimated for different effusion rates (e.r.) . Δt1 (e.r. 1 m^3/s) = $4.3x10^7$s, Δt2 (e.r. 10 m^3/s) = $4.3x10^6$s, Δt3 (e.r. 100 m^3/s) = $4.3x10^5$s, Δt4 (e.r. 1000 m^3/s) = $4.3x10^4$s.

c) 2 hrs phreatomagmatic eruption t= 7200 s

Table 6.1: Ice melting rates for Skerin eruption. Effusion rates (e.r.) are acquired from equation 4.2 and melting rates from equation 4.1 in chapter 4.

Combining minimum and maximum melting rates, meltwaters were most likely in peak at the initial effusive and phreatomagmatic stage of the eruption as lavas broke through the thin glacier (first hours 500-2500 m^3/s for the SE part of S7 and S8)(Figure 6.9 and Table 6.9). As lavas were erupted into the canyon more passively lower melting rates between 10-100 m^3/s are reasonable in a period of 5 to 50 days. The likelihood of meltwater accumulation within glacial canyons is small due to the steep setting of the ridge on Eyjafjallajökull. It is more consistent with the topography to assume short-time localized pools which burst to create a number of small jökulhlaups during the eruption. The meltwater is believed to have flowed parallel to the ridge and then used two main gorges (Akstaðaá and Miðtunga) and also flowed over the north plain Litlaheiði (Figure 6.9). Direct surface runoff on the glacier is believed to have accompanied the pheratomagmatic explosions in the beginning although significant part of the meltwaters appear to have drained following the ridge NW over the Litlaheiði area and also drained through glacial tunnels or channels primarily on the north side of the glacier. These jökulhlaups eventually connected to the flood plain of Markarfljót and drained to the ocean.

6.6 Summary of observations - a conceptual lava emplacement model

On the basis of the observations made in this study, the following conceptual model of the formation for Skerin ridge is proposed: Magma effusion began at two localities erupting mafic products, at the NW margin of the glacier as a strombolian style eruption forming scoria deposits and at the SE end in a phreatomagmatic explosive style forming a tuff deposit (Figure 6.10A). Silicic lavas rised effusively, most likely triggered by the mafic intrusion and melted cavities in the ice. These lavas formed canyons in the ice or erupted into pre-formed canyons created by the preceding explosive activity in the ice or expanded into cavities in the bed of the glacier to bank against the glacial walls. Silicic magmas erupted explosively at the SE end to form pumice deposits (Figure 6.10B). Effusive lava lobes expanded as balloons by continuous injection of magma into the interior (endogenous growth) to interact with the glacio-confined meltwaters quenching and chilling forming a glassy carapace of columnar joints. Lavas developed a thick insulating crust and grew vertically and horizontally to collide with the adjacent lobes. Lobes that advanced in an open channel formed subaerial flow-related structures as breccia and ogives attributed to a brittle crust being fragmented

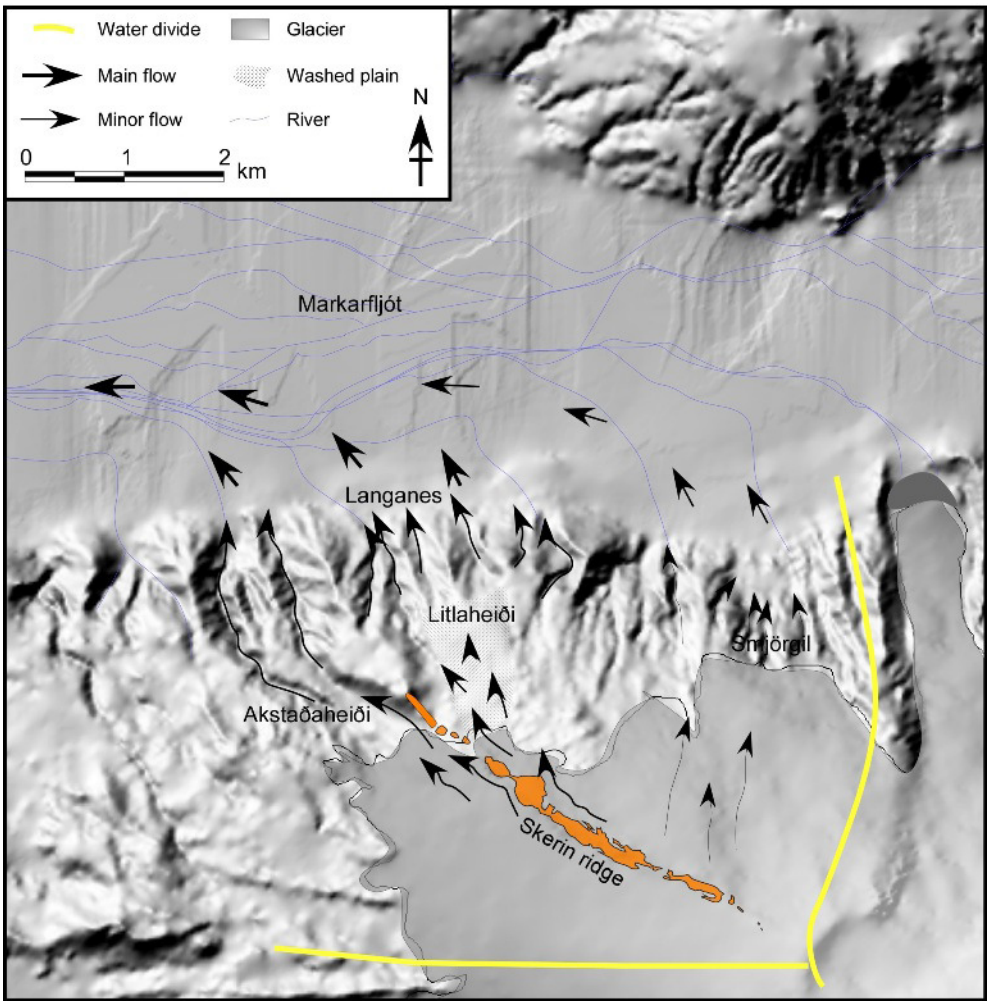

Figure 6.9: Glacial flooding model based on the local topography, water dynamics and evidences from the field. An eruption at Skerin ridge has flood waters directed within the water divides to either W through Akstaðaheiði or N from Litlaheiði and from the uppermost part directly to Smjörgil. Meltwater either flooded on the surface or through channels in the ice. These floods eventually reached the Markarfljót flood plain and drained to the ocean.

and teared by inner growth and shearing at the brittle-ductile boundary induced by the moving core. Thus a result of this intraglacial eruption were lavas with a three-part structure, the columnar glassy margins, the insulated flow interior and the subaerial flow top breccia. A draw down of magma column due to decrease in magma discharge or possibly a breakout formed the cave in segment S4 (Figure 6.10B and C).

Dry strombolian activity from a fissure on top of the silicic ridge marks the last stage of the eruption. This last stage produced deposits of scoria with intermediate composition draping the SE-part of the ridge (Figure 6.10C). A small explosive event took place at same locality as the prior explosive episodes adding a tuff layer to the deposit. The north lava flow is attributed to an eruption from a vent close to segment S8 that took place prior to the eruption of Skerin ridge.

These flows melted canyons and flowed confined by the ice walls to the north margins of Eyjafjallajökull.

Meltwater production is likely to have peaked during the initial phreatomagmatic explosive activity (likely water discharge 500-2500 m^3/s) while much lower meltwater generation is likely associated with the formation of the silicic lavas (10-100 m^3/s). Minimal water accumulation is expected to have occurred due to the steep and marginal settings of the ridge. Washed plains at Litlaheiði, coarse gravel and box-gullies in the fans of Langanes and deep canyons at Akstaðaheiði and Miðtunga are the visible impressions of large floods running from the hillsides of Skerin providing further evidence for this high-energy event.

Post-eruption glacial advancement is particularly evident on the south side of the ridge where the outlet glacier Akstaðajökull has eroded the margins of the silicic lobes, the scoria deposit Rauðhyrna and deepened the valley south of Skerin (Figure 6.10D).

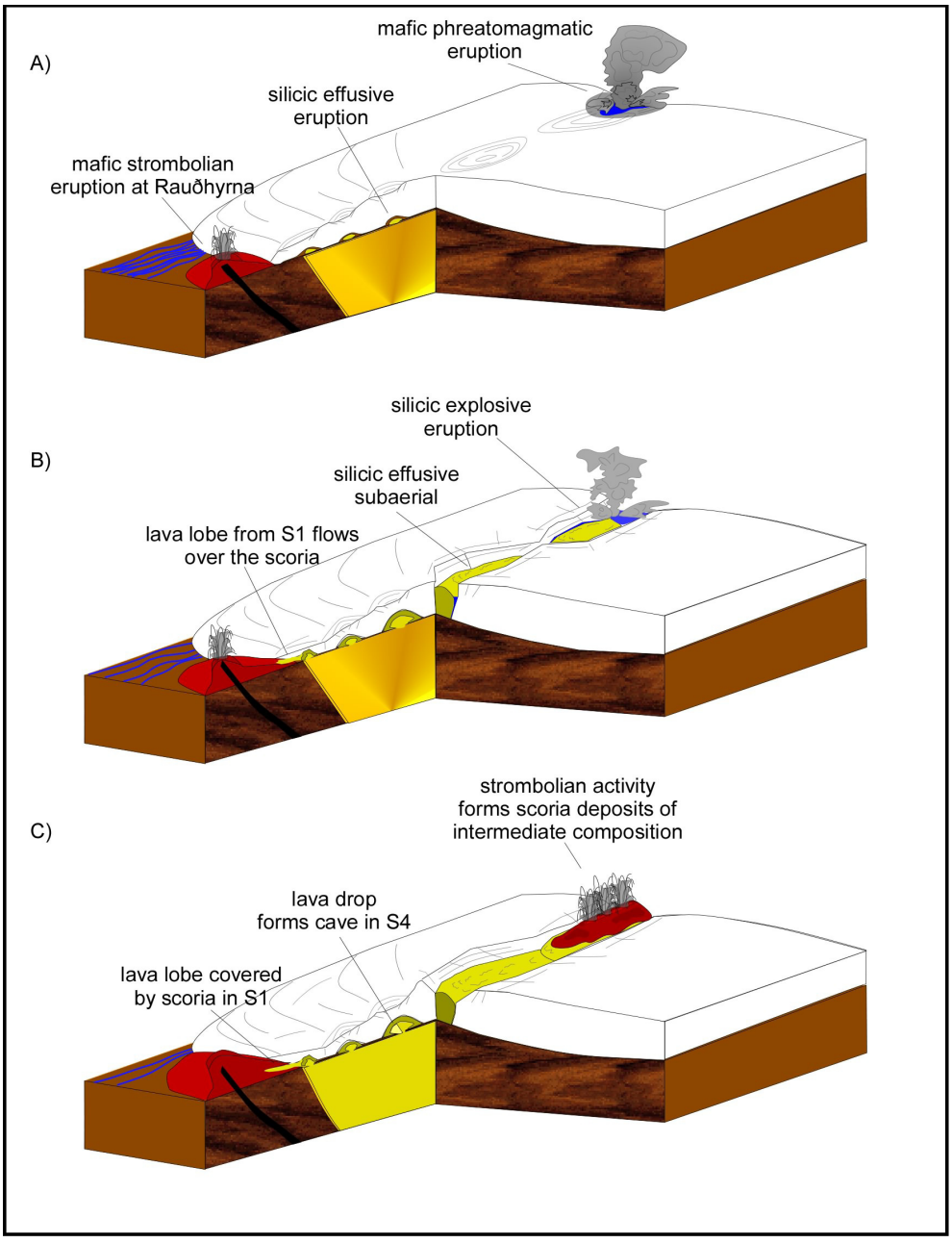
A)
mafic phreatomagmatic eruption
silicic effusive eruption
mafic strombolian eruption at Rauðhyrna
B)
silicic explosive eruption
silicic effusive subaerial
lava lobe from S1 flows over the scoria
C)
strombolian activity forms scoria deposits of intermediate composition
lava drop forms cave in S4
lava lobe covered by scoria in S1

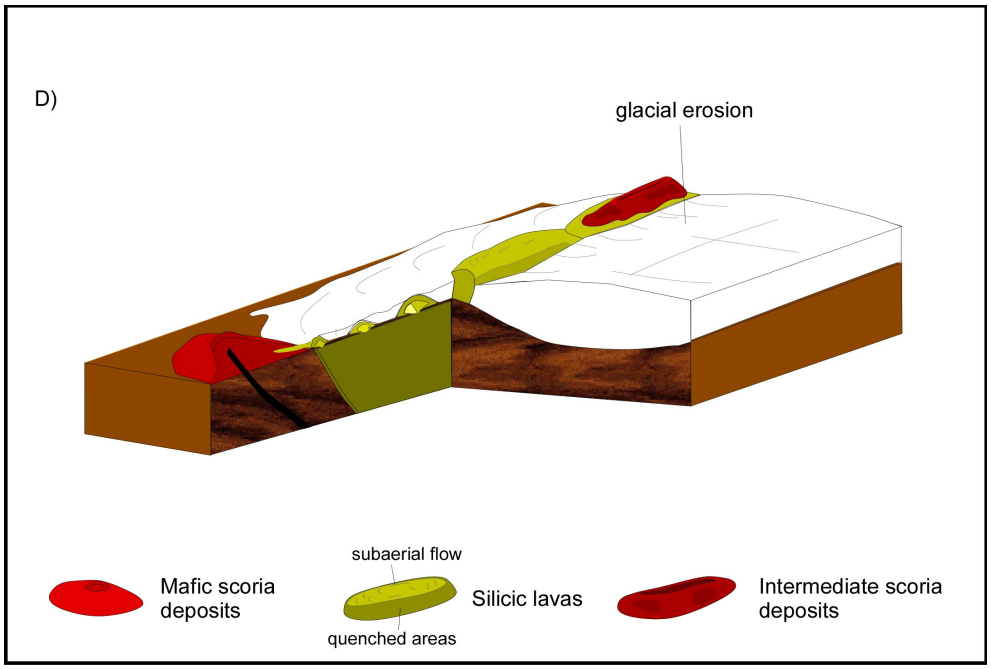

Figure 6.10: The sequence of events during the formation of Skerin ridge. a) Mafic dry strombolian eruption begins at the margins of the glacier forming Rauðhyrna (red cone) and a mafic dike reaches the glacier at the other end of the volcanic fissure causing phreatomagmatic explosions with high melting rates. Shortly after or at the same time silicic lavas begin erupting from the fissure. b) Silicic lava expand subglacially melting cavities which later evolve to larger canyons. The lava interacts with the meltwaters chilling and quenching while segments that expand subaerially form a brecciated crust with flow-related structures. At a few locations the eruption was explosive forming pumice deposits. A small lava lobe at the end of the fissure flowed towards Rauðhyrna scoria deposit and was embedded in the scoria. c) A pressure drop in the dike leaves a cave in segment S4. Eruption changes from effusive silicic to strombolian intermediate eruptions that formed scoria deposits on top of the SE segments of Skerin. d) Post-eruption. The glacier is diverted by the new ridge and the ice flow is concentrated along the south side leading to glacial erosion. Smaller segments are completely covered by the moving outlet glacier while larger segments stand above the reach of the glacier with preserved surface flow structures.

Chapter 7

Conclusions

Skerin ridge on the flanks of the central volcano Eyjafjallajökull, largely embedded in the local ice cap, holds complex multi-composition and intraglacil facies formed by a dynamic magma mixing process. The ridge is about 4.5 km in length formed from a radial trending fissure being large in the center and tapering at the ends with volumes of about 0.043 km^3. The lavas are mainly of trachyte composition that erupted from a system of fissural vents forming lobate segments that present a surface structural morphology attributed to emplacement within glacial canyons with a marginal carapace of glassy polygonal columns representing the surface cooled by the glacio-confined meltwaters and a brecciated flow top of subaerial origin. Besides these two facies, the internal structure shows a pattern that expresses radiative/concentric cooling from the margins to the core and flow dynamics related to the creep of viscous magma in a ductile body.

Flow emplacement and structural comparisons require that the lavas erupted in a single intrusive event and grew by continuous injection of lava into the interior by inflation. Sheet-lava lobes effused primarily to interact with the glacier melting the ice and areas of high volumetric flow emerged through the cauldrons to flow subaerially radially and horizontally confined by the openings in the glacier. The formation of a stronger marginal crust enhanced by the rapid cooling at the lava-meltwater contact may have promoted vertical growth forming lobes with high aspect ratios. In the process, areas under subaerial conditions developed surface flow-related structures as ogives and breccia ridges although being weakly expressed due to the limited expansion of the lobes. The insulating property of the crust is demonstrated in a cave formed by a pressure drop in the dike with the lava detaching from the brittle crust leaving an open space with a volume 15x33x10 m^3 (length x width x height).

Products in the field exhibited deposits of variable compositions. Two loca-

tions showed mafic and silicic products sharply intermingled suggesting a synchronous event for these formations. The final phase of the eruption was a dry strombolian eruption on top of the silicic lavas forming scoria deposits of intermediate composition. Supported by petrographic analysis, a magma mixing event is suggested with a silicic eruption being triggered by a mafic intrusion, both erupting at synchronous time with intermediate lavas erupting at the final stage. Studies based on deposits that are stratigraphy equivalent, a gravel deposit from a glacial flood and a known tephra layer suggest the eruption took place in the 10th century AD.

Considering structural parameters of the silicic ridge as cooling-features and mafic tuff deposits at one location indicating phreatomagmatic eruption, some bounds on melting rates and intensity of flooding can be obtained. Melting rates of 500-2500 m^3/s are estimated for the first 2 hours of phreatomagmatic activity while 10-100 m^3/s are reasonable for the longer silicic effusive event (5-50 days) considering lavas with viscosities between 10^{5-6} Pa s. Studies of intraglacial volcanism have shown to be important for our understanding of emplacement processes within glacial settings, paleoenvironmental reconstruction and hazard assessment. Future work is needed for constrains that regard cooling dynamics of silicic and basaltic rocks induced by water and rheology parameters of trachyte lavas for more precise evaluation of the melting rates in volcanic eruptions of this type. Further petrological work is also important for improving our understanding of the processes that created the complex interplay of volcanic materials in Skerin ridge.

Bibliography

Allen, C. C., Jerecinovic, M. J., Allen, J. S. B., 1982. Subglacial volcanism in north-central British Columbia and Iceland. Journal of Geology 90, 699–715.

Anderson, S., Fink, J., Rose, W., 1995. Mount St. Helens and Santiguito lava domes: the effect of short-term eruption rate on surface texture and degassing processes. J. Volcanol. Geotherm. Res. 69, 105–116.

Björnsson, H., 1988. Hydrology of ice caps in volcanic regions. Soc. Sci. Isl., Reykjavik 45, 139.

Björnsson, H., Pálsson, F., Gudmundsson, M., 1992. Vatnajökull, northwestern part, 1:100,000, subglacial surface. National Power Company and Science Institute.

Branney, M., Kokelaar, P., 2002. Pyroclastic density currents and the sedimentation og ignimbrites. Geological Society, London Memoirs, 27.

Bridges, N., Fink, J., Griffiths, R., 1991. The effects of cooling on lava dome morphology. LPSC XXII, 137–138.

Cordonnier, B., Hess, K.-U., Lavallee, Y., Dingwell, D., 2009. Rheological properties of dome lavas: Case study of Unzen volcano. Earth and Planetary Science Letters 279 (3-4), 263–272.

DeGraff, J., Aydin, A., 1993. Effect of thermal regime on growth increment and spacing of contraction joints in basaltic lava. J. Geophys. Res. 98, 6411–6430.

De Rosen-Spence, A. F., Provost, G., Dimroth, E., Gochanauer, K., Owen, V., 1980. Archean subaqueous felsic flows, Rouyn–Noranda, Quebec, Canada, and their Quaternary equivalents. Precambrian Res. 12, 43–77.

Dingwell, D., Virgo, D., 1988. Viscosities of melts in the Na_2 O-FeO-Fe_2 O $_3$ -SiO_2 system and factors controlling relative viscosities of fully polymerized silicate melts. Geochimica et Cosmochimica Acta 52, 395–403.

Dugmore, A., Larsen, G., 2009. Tephrochronology, hazards and settlement; 6^{th}-10^{th} century AD volcanogenic flooding, Eyjafjallajökull, Iceland. (in prep.).

Edwards, B., Russell, J., Anderson, R., 2002. Subglacial, phonolitic volcanism at Hoodoo Mountain volcano, northern Canadian Cordillera. Bulletin of Volcanology 64 (3), 254–272.
URL http://dx.doi.org/10.1007/s00445-002-0202-9

Einarsson, S., Jóhannesson, H., Sveinbjörnsdóttir, A. E., 1991. Kapelluhraun og gátan um aldur Hellnahrauns (the Krísuvík fires.II . age of the Kapelluhraun and Hellnahraun lava flows, Reykjanes peninsula, Southwest Iceland). Jökull 41, 61–80.

Fink, J., 1980. Surface folding and viscosity of rhyolite flows. Geology 8, 250–254.

Fink, J., 1983. Structure and emplacement of a rhyolitic obsidian flow: Little Glass Mountain, Medicine Lake Highland, northern California. Geol Soc Am Bull 94, 362–380.

Fink, J., 1993. Active Lavas. University College London Press, Ch. The emplacement of silicic lava flows and associated hazards, pp. 5–24.

Fink, J., Bridges, N., 1995. Effects of eruption history and cooling rate on lava dome growth. Bull Volcanol 57, 229–239.

Fink, J. H., Griffiths, R. W., 1998. Morphology, eruption rates, and rheology of lava domes: Insights from laboratory models. J. Geophys. Res. 103, 527–745.
URL http://dx.doi.org/10.1029/97JB02838

Francis, P., Oppenheimer, C., 2004. Volcanoes. Oxford University Press Second Edition, 93–106.

Fuller, R. E., 1931. The aqueous chilling of basaltic lava on the Columbia River Plateau. American Journal of Science 5th series 21(124), 281–300.

Fuller, R. E., 1934. Structural features in the Columbia River lavas of central Washington (a criticism and reply to a paper by M. G. Hoffman). Jour. Geol. 42 (3), 311–328.

Gonnermann, H. M., Manga, M., 2005. Flow banding in obsidian: A record of evolving textural heterogeneity during magma deformation. Earth and Planetary Science Letters 236 (1-2), 135–147.

Goto, Y., McPhie, J., 1998. Endogenous growth of a Miocene submarine dacite cryptodome, Rebun Island, Hokkaido, Japan. Journal of Volcanology and Geothermal Research 84 (3-4), 273–286.

Goto, Y., Tsuchiya, N., 2004. Morphology and growth style of a Miocene submarine dacite lava dome at Atsumi, northeast Japan. Journal of Volcanology and Geothermal Research 134 (4), 255–275.

Govindaraju, K., 1994. 1994 compilation of working values and sample description for 383 geostandards. Geostand. Newsl. 18 (spec.iss.).

Gregg, T., Fink, J., 1996. Quantification of extraterrestrial lava flow effusion rates through laboratory simulation. J. Geophys. Res. 101, 16,891–16,900.

Gudmundsson, A., 1983. Form and dimensions of dikes in eastern Iceland. Tectonophysics 95, 295–307.

Gudmundsson, A., 1995. Infrastructure and mechanics of volcanic systems in Iceland. Journal of Volcanology and Geothermal Research 64 (1-2), 1–22.

Gudmundsson, M., 2003. Melting of ice by magma-ice-water interactions during subglacial eruptions as an indicator of heat transfer in subaqueous eruptions. In: White, J.D.L., S. J., Clague, D. (Eds.), Explosive Subaqueous Volcanism. Vol. 140. AGU, pp. 61–72.

Gudmundsson, M., 2005. Chapter 6: Subglacial volcanic activity in Iceland. In: Caseldine, C.J., R. A. H. J., Knudsen, . (Eds.), Iceland: Modern processes, Past Environments. Elsevier, pp. 127–151.

Gudmundsson, M., Björnsson, H., 1991. Eruptions in Grímsvötn 1934-1991. Jökull 41, 21–46.

Gudmundsson, M., Högnadóttir, T., 2005. Kafli X. Ísbráðnun og upptakarennsli jökulhlaupa vegna efldgosa í Eyjafjallajökli og vestanverðum Mýrdalsjökli. Hættumat vegna eldgosa og hlaupa frá vestanverðum Mýrdalsjökli og Eyjafjallajökli, 160–179.

Gudmundsson, M., Larsen, G., Höskuldsson, A., Gylfason, . G., 2008. Volcanic hazards in Iceland. Jökull 58, 251–268.

Gudmundsson, M., Pálsson, F., Björnsson, H., Högnadóttir, T., 2002. The hyaloclastite ridge formed in the subglacial 1996 eruption in Gjálp, Vatnajökull, Iceland: present day shape and future preservation. In: Smellie, J., Chapman,

M. (Eds.), Ice-volcano interaction on Earth and Mars. No. 202. Geol. Society London, Spec.Publication, pp. 319–335.

Gudmundsson, M., Sigmundsson, F., Björnsson, H., 1997. Ice-volcano interactions of the Gjálp subglacial eruption, Vatnajökull, Iceland. Nature 389, 954–957.

Gudmundsson, M. T., Sigmundsson, F., Björnsson, H., Högnadóttir, T., 2004. The 1996 eruption at Gjálp, Vatnajökull ice cap, Iceland: efficiency of heat transfer, ice deformation and subglacial water pressure. Bulletin of Volcanology 66 (1), 46–65.
URL http://dx.doi.org/10.1007/s00445-003-0295-9

Harris, A., Rowland, S., 2001. Flowgo: a kinematic thermo-rheological model for lava flowing in a channel. Bull. Volcanol 63, 20–44.

Harris, A. J. L., Flynn, L. P., Matias, O., Rose, W. I., Cornejo, J., 2004. The evolution of an active silicic lava flow field: an ETM+ perspective. Journal of Volcanology and Geothermal Research 135 (1-2 SPECIAL ISSUE), 147–168.

Hon, K., Kauahikaua, J., Denlinger, R., Mackay, K., 1994. Emplacement and inflation of pahoehoe sheet flows: Observation and measurements of active lava flows on Kilauea Volcano, Hawaii. Geological Society of America Bulletin 106, 351–370.

Hoskuldsson, A., Sparks, R. S. J., 1997. Thermodynamics and fluid dynamics of effusive subglacial eruptions. Bulletin of Volcanology 59 (3), 219–230.
URL http://dx.doi.org/10.1007/s004450050187

Houghton, B., Nairn, I., 1991. The 1976-1982 Strombolian and phreatomagmatic eruptions of White Island, New Zealand: eruptive and depositional mechanisms at a 'wet' volcano. Bull Volcanol 54, 25–49.

Houghton, B., Wilson, C., 1989. A vesicularity index for pyroclastic deposits. Bull. Volcanol. 51, 451–62.

Hull, D., Caddock, D., 1999. Simulation of prismatic cracking of cooling basalt lava flows by the drying of sol-gels. Journal of Materials Science 34, 5707–5720.

Jakobsson, S., 1979a. Petrology of recent basalts of the Eastern Volcanic Zone, Iceland. Acta Nat. Isl. 26, 1–103.

Jakobsson, S., Gudmundsson, M., submitted december 2007. Subglacial and intraglacial volcanic formations in Iceland. Jökull.

Jakobsson, S., Jónasson, K., Sigurdsson, I., 2008. The three igneous rock series of Iceland. Jökull 58, 117–138.

Jóhannesson, H., Sæmundsson, K., 1998. Geological map of Iceland, 1:500,000. Bedrock Geology, Icelandic Institute of Natural History and Iceland Geodetic Survey, Reykjavík.

Jónasson, K., 2007. Silicic volcanism in Iceland: composition and distribution within the active volcanic zones. Journal of Geodynamics 43 (1), 101–117.

Jónsson, J., 1998. Geological map of Eyjafjöll. Research Institute Neðri ás Hveragerði, Hveragerði.

Jochum, K., Seufert, H., Thirlwall, M., 1990. High-sensitivity Nb analysis by spark-source mass spectrometry (SSMS) and calibration of XRF Nb and Zr. Chem. Geol. 81, 1–16.

Jones, J., 1969. Intraglacial volcanoes of the Laugarvatn region, south-west Iceland - I. Quarterly Journal of the Geological Society 124, 197–211.

Jones, J., 1970. Intraglacial volcanoes of the Laugarvatn region, southwest Iceland, II. Journal of Geology 78, 127–140.

Kirkbride, M. P., Dugmore, A. J., 2008. Two millennia of glacier advances from southern Iceland dated by tephrochronology. Quaternary Research 70 (3), 398–411.

Kjartansson, G., 1943. Árnesingasaga. [The geology of Árnessýsla]. Árnesingafélagið, Reykjavík, 268 pp.

Kristjánsson, L., Jóhannesson, H., Eiríksson, J., Gudmundsson, A. I., 1988. Brunhes-Matuyama paleomagnetism in three lava sections in Iceland. Can. J. Earth Sci. 25, 215–225.

LaMoreaux, K. A., 2008. Recognizing ice-contact trachyte-phonolite lavas at the Mount Edziza volcanic complex, British Columbia, Canada. Master's thesis, University of Pittsburgh.

Landmælingar Íslands, 1990. Icelandic Museum of Natural History, Iceland Geodetic Survey, Geological map of Iceland, Sheet 6, South Iceland.

Larsen, G., 1999. Gosið í Eyjafjallajökli 1821-1823 - stutt samantekt á framvindu og áhrifum gossins samkvæmt lýsingum. Rannsóknarskýrsla RH-28-99, Raunvísindastofnun Háskólans, 13 pages.

Larsen, G., 2000. Holocene eruptions within the Katla volcanic system, south Iceland: Characteristics and environmental impact. Jökull 49, 1–28.

Le Maitre, R., 2002. Igneous Rocks, a Classification and Glossary of Terms: Recommendations of the International Union of Geological Sciences Subcomission on the Systematics of Igneous Rocks, 2nd Edition. Cambridge University Press.

Lescinsky, D., Sisson, T., 1998. Ridge-forming, ice-bounded lava flows at Mount Rainier, Washington. Geology 26 (4), 351–354.

Lescinsky, D. T., Fink, J., 2000. Lava and ice interaction at stratovolcanoes: Use of characteristic features to determine past glacial extents and future volcanic hazards. Journal of Geophysical Research 23 (105), 711–23.

Lipman, P., Banks, N., 1987. Aa flow dynamics, Mauna Loa 1984. U.S. Geol. Surv. Prof. Pap. 1350, 1527–1567.

Long, P., Wood, B., 1986. Structures, textures, and cooling histories of Columbia River basalt flows. Geol. Soc. Am. Bull. 97, 114–1155.

Loughlin, S., 2002. Facies analysis of proximal subglacial and proglacial volcaniclastic successions at the Eyjafjallajökull central volcano, southern Iceland. In: Smellie, J., Chapman, M. (Eds.), Ice-volcano interaction on Earth and Mars. No. 202. Geol. Society London, Spec.Publication, pp. 149–178.

MacDonald, G., Katsura, T., 1964. Chemical composition of Hawaiian lavas. J. Petrol. 5, 82–133.

Maeno, F., Taniguchi, H., 2006. Silicic lava dome growth in the 1934–1935 Showa Iwo-jima eruption, Kikai caldera, south of Kyushu, Japan. Bull Volcanol 68, 673–688.

Manley, C. R., 1992. Extended cooling and viscous flow of large, hot rhyolite lavas: implications of numerical modeling results. Journal of Volcanology and Geothermal Research 53 (1-4), 27–46.

Mathews, W., 1947. "Tuya". Flat topped volcanoes in northern British Columbia. American Journal of Science 245, 560–570.

McDougall, I., Kristjá, L., Saemundsson, K., 1984. Magnetostratigraphy and geochronology of northwest Iceland. Journal of Geophysical Research 89, 7029–7060.

McGarvie, D., 1985. Volcanology and Petrology of Mixed Magmas and Rhyolites from the Torfajökull Volcano, Iceland. Unpublished PhD Thesis, University of Lancaster, 255 pp.

McGarvie, D., 2009. Rhyolitic volcano-ice interactions in Iceland. Journal of Volcanology and Geothermal Research In Press, Corrected Proof.

McGarvie, D., Stevenson, J., Burgess, R., Tuffen, H., Tindle, A., 2007. Volcano-ice interactions at Presahnúkur, Iceland: rhyolite eruption during the last interglacial-glacial transition. Annals of Geology 45, 38–47.

Mee, K., Tuffen, H., Gilbert, J., 2006. Snow-contact volcanic facies and their use in determining past eruptive environments at Nevados de Chillán volcano, Chile. Bulletin of Volcanology 68 (4), 363–376.
URL http://dx.doi.org/10.1007/s00445-005-0017-6

Murase, T., McBimey, A., 1973. Properties of some common igneous rocks and their melts at high temperatures. Geol. Sot. Am. Bull. 84, 3563–3592.

Nemat-Nasser, S., Oranratnachai, A., 1979. Minimum spacing of thermally induced cracks in brittle solids. J. Energy Resour. Techol. 101, 34–40.

Oskarsson, B., 2005. Lava-rise structures in pahoehoe and a'a: Examples from the Hrútagjá lava shield and Kapelluhraun a'a flow field on the Reykjanes peninsula. BS thesis unpublished.

Peacock, M. A., Fuller, R. E., 1928. Chlorophaeite, sideromelane and palagonite from the Columbia River Plateau. Am. Min. 13, 360–383.

Pedersen, R., Sigmundsson, F., 2004. InSAR based sill model links spatially offset areas of deformation and seismicity for the 1994 unrest episode at Eyjafjallajökull volcano, Iceland. Geophysical Research Letters 31, L144610.

Pedersen, R., Sigmundsson, F., 2006. Temporal development of the 1999 intrusive episode in the Eyjafjallajökull volcano, Iceland, derived from InSAR images. Bulletin of Volcanology 68 (4), 377–393.
URL http://dx.doi.org/10.1007/s00445-005-0020-y

Pinkerton, H., Norton, G., 1995. Rheological properties of basaltic lavas at sub-liquidus temperatures: laboratory and field measurements on lavas from Mount Etna. Journal of Volcanology and Geothermal Research 68 (4), 307–323.

Rowland, S., Walker, G., 1990. Pahoehoe and aa in Hawaii: volumetric flow rate controls the lava structure. Bull Volcanol 52, 615–628.

Sella, G., Dixon, T., Mao, A., 2001. Revel: A model for recent plate velocities from space geodecy. Journal of Geophysical Research 107(B4).

Sigmundsson, F., 1991. Post-glacial rebound and asthenosphere viscosity in Iceland. Geophysical Research Letters 18, 1131–1134.

Sigmundsson, F., 2006. Iceland Geodynamics - Crustal Deformation and Divergent Plate Tectonics. Praxis Publishing.

Sigvaldason, G., Óskarsson, N., 1986. Fluorine in basalts from Iceland. Contrib. Mineral. Petrol. 94, 263–271.

Skilling, I. P., 1994. Evolution of an englacial volcano: Brown Bluff, Antarctica. Bulletin of Volcanology 56 (6), 573–591.
URL http://dx.doi.org/10.1007/BF00302837

Smellie, J., 2002. The 1969 subglacial eruption on Deception Island (Antarctica): events and processes during an eruption beneath a thin glacier and implications for volcanic hazards. In: Smellie, J., Chapman, M. (Eds.), Ice-volcano interaction on Earth and Mars. No. 202. Geol. Society London, Spec.Publication, pp. 59–80.

Smellie, J., 2006. The relative importance of supraglacial versus subglacial meltwater escape in basaltic subglacial tuya eruptions: An important unresolved conundrum. Earth-Science Reviews 74 (3-4), 241–268.

Smellie, J. L., Skilling, I. P., 1994. Products of subglacial volcanic eruptions under different ice thicknesses: two examples from Antarctica. Sedimentary geology 91 (1-4 (25 ref.)), 115–129.

Smith, J. V., 2002. Structural analysis of flow-related textures in lavas. Earth-Science Reviews 57, 279–297.

Sæmundsson, K., 1970. Interglacial lava flows in the lowlands of southern Iceland and the problem of two-tiered columnar jointing. Jökull 20, 62–76.

Sæmundsson, K., 1979. Outline of the geology of Iceland. Jökull 29, 7–28.

Sparks, R., Sigurðsson, H., Wilson, L., 1977. Magma mixing: a mechanism for triggering acid explosive eruptions. Nature 267, 315–318.

Spera, F., 2000. Physical properties of magma. Encyclopedia of Volcanoes, 171–90.

Spot Image, 2003. Pictures 713_218_8_030716_5_2_nc_3.tif, 713_218_8_030716_5_2_t_3.tif, 714_219_0_030918_5_1_nc_3.tif and 714_219_0_030918_5_1_t_3.tif provided by Landmælingar Íslands.

Spörli, K., Rowland, J., 2006. 'Column on column' structures as indicators of lava/ice interaction, Ruapehu andesite volcano, New Zealand. Journal of Volcanology and Geothermal Research 157 (4), 294–310.

Spry, A., 1962. The origin of columnar jointing, particularly in basalt flows. J. Geol. Soc. 8, 191–216.

Stevenson, J., 2005. Volcano–Ice interaction at Öræfajökull and Kerlingarfjöll, Iceland. Unpublished PhD Thesis, The Open University, Milton Keynes, 330.

Stevenson, J. A., McGarvie, D. W., Smellie, J. L., Gilbert, J. S., 2006. Subglacial and ice-contact volcanism at the Öraefajokull stratovolcano, Iceland. Bulletin of Volcanology 68 (7-8), 737–752.
URL http://dx.doi.org/10.1007/s00445-005-0047-0

Stevenson, J. A., Smellie, J. L., McGarvie, D. W., Gilbert, J. S., Cameron, B. I., 2009. Subglacial intermediate volcanism at Kerlingarfjöll, Iceland: Magma-water interactions beneath thick ice. Journal of Volcanology and Geothermal Research In Press, Corrected Proof.

Strachan, S., 2001. A geophysical investigation of the Eyjafjallajökull glaciovolcanic system, South Iceland, using radio echo sounding. Ph.D. thesis, University of Edinburgh.

Sturkell, E., Sigmundsson, F., Einarsson, P., 2003. Recent unrest of the Eyjafjallajökull and Katla volcanoes, Iceland. Journal of Geophysical Research 108 (B8, 2369).

Sverrisson, M., Jóhannesson, A., Björnsson, H., 1980. Instrument and Methods - radio-echo equipment for depth sounding of temperate glaciers. Journal of Glaciology 25, 477–486.

Thorarinsson, S., 1974. Vötnin Stríð. saga Skeiðaráhlaupa og Grímsvatnagosa (the swift flowing rivers. the history of Grímsvötn jökulhlaups and eruptions). Menningarsjóður, Reykjavík, 254.

Thorarinsson, S., 1975. Katla og ánnáll Kötlugosa. (Katla and an annal of Katla eruptions). Árbók Ferðafélags Íslands, 125–149.

Thordarson, T., Larsen, G., 2007. Volcanism in Iceland in historical time: Volcano types, eruption styles and eruptive history. Journal of Geodynamics 43 (1), 118–152.

Thordarson, T., Self, S., 1998. The Roza Member, Columbia River Basalt Group: A gigantic pahoehoe lava flow field formed by endogenous processes? Journal of Geophysical Research 103, No. B11, 27,411–27,445.

Toramaru, A., Ishiwatari, A., Matsuzawa, M., Nakamura, N., Arai, S., 1996. Vesicle layering in solidified intrusive magma bodies: a newly recognised type of igneous structure. Bull. Volcanol. 58, 393–400.

Tuffen, H., Castro, J. M., 2008. The emplacement of an obsidian dyke through thin ice: Hrafntinnuhryggur, Krafla Iceland. Journal of Volcanology and Geothermal Research.

Tuffen, H., Gilbert, J., McGarvie, D., 2001. Products of an effusive subglacial rhyolite eruption: Bláhnúkur, Torfajökull, Iceland. Bulletin of Volcanology 63 (2), 179–190.
URL http://dx.doi.org/10.1007/s004450100134

Tuffen, H., McGarvie, D., Gilbert, J., Pinkerton, H., 2002b. Physical volcanology of a subglacial-to-emergent rhyolitic tuya at Rauðfossafjöll, Torfajökull, Iceland. Geological Society, London, Special Publications 202, 213–236.

Tuffen, H., Pinkerton, H., McGarvie, D. W., Gilbert, J. S., 2002a. Melting of the glacier base during a small-volume subglacial rhyolite eruption: evidence from Bláhnúkur, Iceland. Sedimentary Geology 149 (1-3), 183–198.

Ventura, G., De Rosa, R., Colletta, E., Mazzuoli, R., 1995. Deformation and patterns in a high-viscosity lava flow inferred from the crystal preferred orientation and imbrications structures: an example from Salina (Aeolian Islands, southern Tyrrhenian Sea, Italy). Bulletin of Volcanology 57, 555–562.

Vinogradov, V., Murav'ev, Y., 1985. Lava-ice interaction during the 1983 Klyuchevskoi eruption. Vulkanol. Seismol. 7, 39–61.

Werner, R., Schmincke, H., 1999. Englacial vs lacustrine origin of volcanic table mountains: evidence from Iceland. Bulletin of Volcanology 60 (5), 335–354. URL http://dx.doi.org/10.1007/s004450050237

Wiese, P., 1993. Geochemistry and geochronology of the Eyjafjöll volcanic system, Iceland. Master's thesis, Oregon State Univ.

Wright, I., Gamble, J., Shane, P., 2003. Submarine silicic volcanism of the Healy caldera, southern Kermadec arc (SW Pacific): I - volcanology and eruption mechanisms. Bulletin of Volcanology 65 (1), 15–29. URL http://dx.doi.org/10.1007/s00445-002-0234-1

Yokoyama, I., 2005. Growth rates of lava domes with respect to viscosity of magmas. Annals of geophysics 48(6), 957–971.

Zimanowski, B., 1998. Phreatomagmatic Explosions. Elsevier, Amsterdam.

Zimanowski, B., Frohlich, G., Lorenz, V., 1991. Quantitative experiments on phreatomagmatic explosions. Journal of Volcanology and Geothermal Research 48, 341–358.

Zimanowski, B., Wohletz, K., Dellino, P., Büttner, R., 2003. The volcanic ash problem. Journal of Volcanology and Geothermal Research 122 (1-2), 1–5.

Appendix A

X-ray Fluorescence (XRF) Analysis

The samples of Skerin ridge and study-related products were analyzed with XRF spectrometry at the University of Edinburgh for both major and trace elements. The sample preparation began with fragmenting the rock samples on a diamond wheel unto coarser grains. Weathering and oxidized surfaces where removed by handpicking and air blown eliminating any possible contamination. The grains were then ground to fine powder in an agate Tema barrel. For major element analysis, the powders were dried for at least 1 hour at 110°C. 0.95 g of the dried sample was precisely weighted and placed in a Pt5% Au crucible. The powdered sample was then mixed with Johnson Matthey Spectroflux 105 with flux ratio 1:5 and fused at 1000°C in a muffle furnace. Loss on ignition was determined in later steps to reduce the likelihood of alkaline loss by volatilization. After the initial fusion the crucible was reweighted and any weight loss made up with extra flux. A second fusion was made over a Meker burner in which the molten mixture was swirled at least 3 times over 30 seconds to ensure homogeneity. The molten sample was then cast onto a graphite mold held at a 220°C hotplate and flattened with an aluminum plunger in to a thin disk. A glass cover was the placed over the sample lowering the temperature gradient at cooling preventing cracking.

Loss on ignition was determined separately by drying the samples and weighting 0.9-1 g into crucible. The crucibles were then fused in a 1000°C muffle furnace. After fusion the crucibles were placed into a dissicator to prevent moisture absorption and weighted precisely giving loss on ignition. In the procedure 16 samples were weighted without being placed in the dissicator. This mistake was corrected by drying the fused samples for at least 2 hours at 110°C and then weighted again.

For trace-element analysis, 8 g of each sample was weighted (+/- 0.1 g) and mixed with 8 drops of the binding agent MOWIOL (2% PVA). The mixture was

placed on a 40 mm dia aluminum cap on lower tungsten carbide disc. A 38 mm internal diameter inner sleeve was placed on top as guide to prevent sample overspilling cap. The inner sleeve was then removed and an upper tungsten carbide disc was placed on top and the sample pressed to 8 tons to form pressed-powder samples.

Samples both fused and pressed were analyzed using a Philips PW2404 automatic X-ray fluorescence spectrometer with a Rh-anode X-ray tube. The spectrometer was calibrated with USGS and CRPG standards, using the value given by Jochum et al. (1990) for Nb and Zr, and Govindaraju (1994) for the other elements.

For precision and accuracy, one sample (ESK06b) was analyzed in duplicate for the major elements calibrated with the USGS and CRG standards mentioned above and five pressed-powder samples were analyzed (ESK03) for the trace elements. The method for sample preparation and analysis was the same. Results are found in table 5.6. In general, the agreement between samples is very good. Sc showed to have very low concentration and was not included in the table.

Location of samples are listed in table 5.3. Analytical results are given in tables 5.4 to 5.5. The products range from basaltic to trachytitc and follow the hawaiian line of the transiotional alkali versus silica diagram (see Figure 5.18) (Le Maitre, 2002).

All samples are very fresh and samples that show oxidation are attributed to deuteric oxidation. Samples with excessive LOI ($>$ 2%, ESK09c, ESK09b and EGODAS) are tuff deposits and pumice deposits. The tuff deposits have less Na due to the palagonization process.

Appendix B

Radio-echo sounding

A mobile radio-echo sounding equipment was utilized measuring 4 profiles perpendicular to the ridge (SW-NE) across the marginal outlet glaciers. The map of the profiles is shown in table B.1 and the results in table B.2. Data processing and calculations related were done by Eyjólfur Magnússson at the University of Iceland.

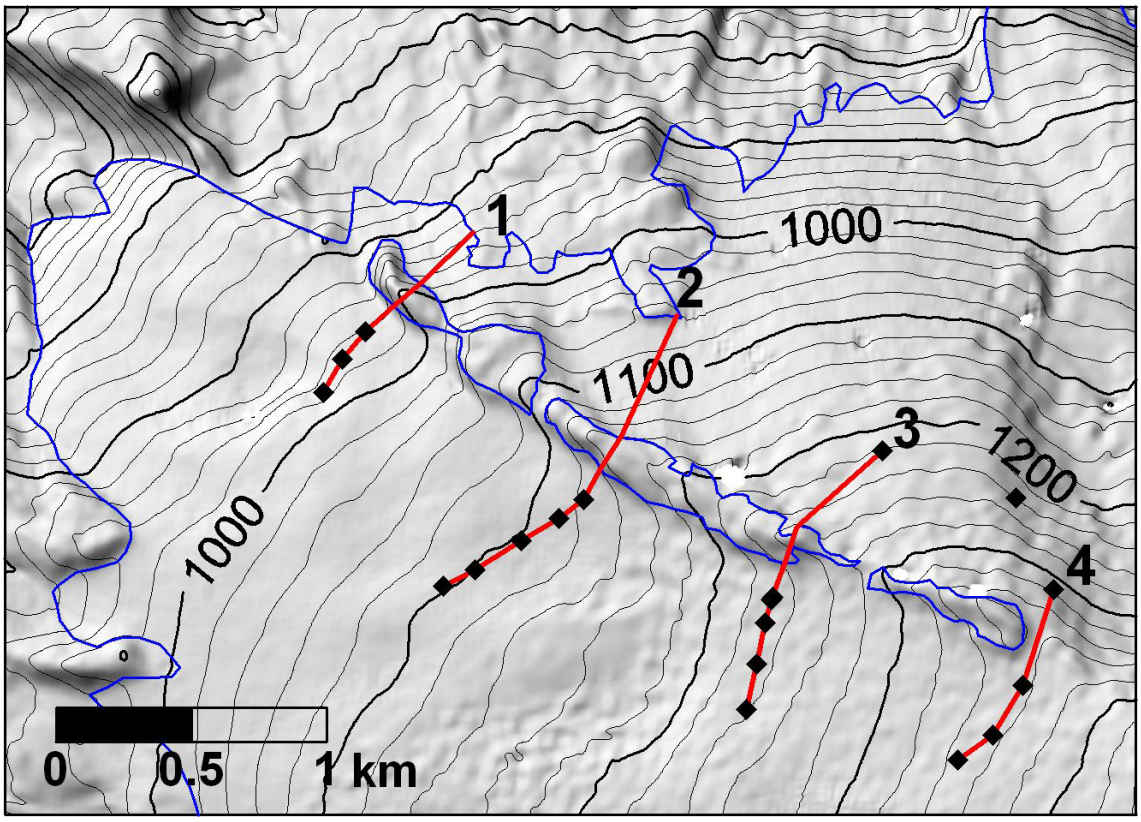

Figure B.1: Profiles measured by foot with the ice-radar (Eyjólfur Magnússon pers.com).

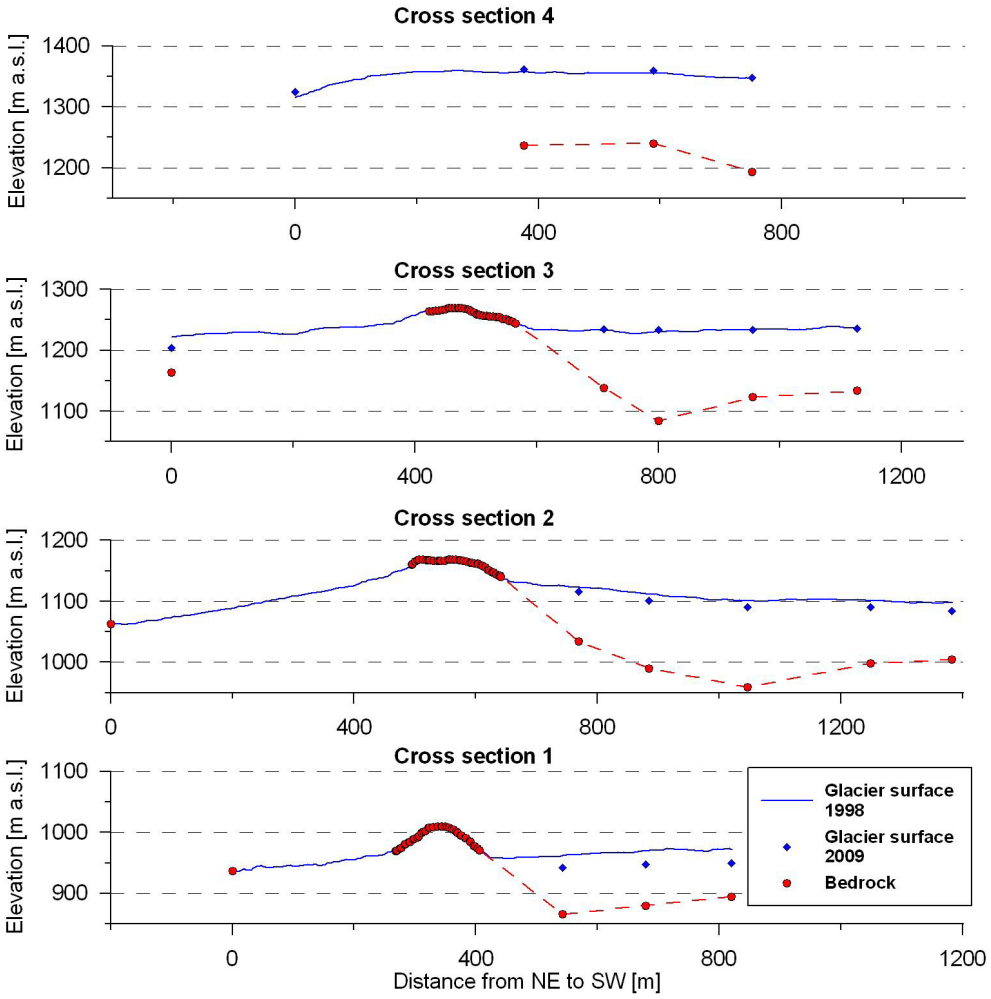

Figure B.2: Cross sections of the profiles measured by the ice-radar. The glacier on the left side of the ridge is less than 40 m thick (Eyjólfur Magnússon pers.com).